
Design and implementation of a test environment to study late-breakdowns in high voltage vacuum circuit breakers

Entwurf und Aufbau einer Prüfumgebung zur Untersuchung von Spätversagern in Hochspannungs-Vakuumleistungsschaltern

Zur Erlangung des akademischen Grades Doktor-Ingenieur (Dr.-Ing.)

genehmigte Dissertation von Dipl.-Ing. Benjamin Baum aus Wetzlar

Tag der Einreichung: 05. Mai 2017, Tag der Prüfung: 11. Oktober 2017

Darmstadt 2017 – D 17

1. Gutachten: Prof. Dr.-Ing. Volker Hinrichsen
2. Gutachten: Prof. Dr. René Smeets



TECHNISCHE
UNIVERSITÄT
DARMSTADT

Fachbereich Elektrotechnik
und Informationstechnik

Institut für Elektrische Energiesysteme
Fachgebiet Hochspannungstechnik

Design and implementation of a test environment to study late-breakdowns in high voltage vacuum circuit breakers

Entwurf und Aufbau einer Prüfumgebung zur Untersuchung von Spätversagern in Hochspannungs-Vakuumleistungsschaltern

Genehmigte Dissertation von Dipl.-Ing. Benjamin Baum aus Wetzlar

1. Gutachten: Prof. Dr.-Ing. Volker Hinrichsen

2. Gutachten: Prof. Dr. René Smeets

Tag der Einreichung: 05. Mai 2017

Tag der Prüfung: 11. Oktober 2017

Darmstadt – D 17

Erklärung zur Dissertation

Hiermit versichere ich, die vorliegende Dissertation ohne Hilfe Dritter nur mit den angegebenen Quellen und Hilfsmitteln angefertigt zu haben. Alle Stellen, die aus Quellen entnommen wurden, sind als solche kenntlich gemacht. Diese Arbeit hat in gleicher oder ähnlicher Form noch keiner Prüfungsbehörde vorgelegen.

Darmstadt, den 05. Mai 2017

(Benjamin Baum)



Inhaltsverzeichnis

Erklärung laut § 9 PromO	ii
List of symbols, abbreviations and chemical formulas	v
Abstract	ix
Kurzfassung	xi
1 Introduction	1
2 Fundamentals	3
2.1 Vacuum circuit breakers	3
2.2 Dielectric breakdown in vacuum	6
2.2.1 Pre-breakdown effects	6
2.2.2 Transition to breakdown	10
2.2.3 Special case of an insulator flashover	11
2.3 Electric arcs in a vacuum environment	11
2.3.1 Arcing during opening operation	12
2.3.2 Arcing during closing operation	14
2.4 Switching of capacitive loads	15
2.4.1 Mathematical and physical basics	15
2.4.2 Making operations	16
2.4.3 Breaking operations	18
2.4.4 Dielectric failures after a successful breaking operation	20
3 Experimental investigations of late-breakdowns above the medium voltage level	23
3.1 Experiences with synthetic test circuits for capacitive load switching	23
3.2 Established research findings	26
3.3 Test circuit parameters according to the standards	27
3.4 Identified challenges of future investigations	28
3.4.1 Handling of (low power) synthetic test circuits	28
3.4.2 Measurement of field-emission currents	31
3.4.3 Additional detection of micro-particles	31
4 Goal of this work	33

5	Test circuit	35
5.1	Requirements	35
5.2	Basic layout	36
5.3	Overview of the measurement systems and data acquisition	37
5.4	Test object	39
5.5	High current sub-circuit	40
5.5.1	Inrush current source	41
5.5.2	Breaking current source	43
5.6	High voltage sub-circuit	43
5.6.1	Alternating voltage source	45
5.6.2	Direct voltage source	45
5.6.3	Voltage making switch	46
5.7	Deviations to a direct test	48
5.7.1	Initial phase of the recovery voltage	48
5.7.2	Characteristics of late-breakdowns	49
6	Simultaneous detection of field-emission currents and charged micro-particles	51
6.1	Basic principle	51
6.2	Field-emission current measurement	52
6.2.1	Discharge current protection	53
6.2.2	Operating current protection	55
6.2.3	Impact of a power diode based protection	56
6.2.4	Data analysis	58
6.3	Charged micro-particle detection	61
6.3.1	Similarities to partial discharges	62
6.3.2	Description of the measurement principle	63
6.3.3	Procedure to verify the absence of disturbances	66
6.4	Preliminary results	68
7	Discussion and conclusion	73
7.1	Summary of the realized test circuit	73
7.2	Discussion of the pre-breakdown current measurement	74
	Appendix	77
	Bibliography	88
	Own publications	89
	Supervised student research projects and diploma theses	91
	Curriculum Vitae	93

List of symbols, abbreviations and chemical formulas

List of symbols

A_e	m^2	emission area
$A_{e,est}$	m^2	estimated emission area
b_{FNP}	–	ordinate-intersection of a Fowler-Nordheim plot
C	F	capacitance
C_b	F	capacitance of the breaking current source
C_{cc}	F	coupling capacitor
C_{dc}	F	capacitance of the direct voltage source
C_l	F	capacitive load
C_{lf}	F	capacitance of the field-emission current measurement system
C_m	F	capacitance of the making current source
C_{par}	F	high voltage stray capacitance of the test object
$C_{par'}$	F	low voltage stray capacitance of the test object
C_{vac}	F	capacitance of the test object
\hat{C}_{vac}	F	acting capacitance of the test object
C_{Vvac}	F	capacitance of the voltage divider
d_{uon}	m	gap distance of the voltage making switch
d_{vac}	m	gap distance of the test object
e	As	elementary charge: 1.6×10^{-19} As
E_c	$V m^{-1}$	contact surface electric field strength
E_{cap}	J	energy stored in a capacitor
E_{uon}	$V m^{-1}$	electric field strength of the voltage making switch
E_{vac}	$V m^{-1}$	homogeneous electric field strength
H_{lf}	–	transfer function of the field-emission current measurement
i_b	A	capacitive breaking current
i_{bd}	A	capacitive discharge current
i_c	A	capacitive displacement current of a vacuum circuit breaker
i_{cc}	A	capacitive displacement current of the coupling capacitor
i_d	A	current of a diode
i_{fe}	A	field-emission current
$i_{fe,d}$	A	alternatively measured field-emission current
i_{hf}	A	current of a charged micro-particle

$i_{hf,cc}$	A	decoupled current of a charged micro-particle
i_{iso}	A	resistive leakage current of the test object
i_{lf}	A	low frequent current
$i_{lf,d}$	A	alternatively measured low frequent current
i_m	A	inrush current
i_s	A	source side current
i_{sat}	A	reverse bias saturation current of a diode
j_{fe}	$A m^{-2}$	field-emission current density
k_c	–	capacitive voltage factor
K_{fe1}	$A V^{-2}$	field emission constant
K_{fe2}	$V m^{-1}$	field emission constant
k_{pp}	–	first-pole-to-clear-factor
L_b	H	inductance of the breaking current source
L_l	H	stray inductance of the load
L_{lf}	H	inductance of the field-emission current measurement system
$L_{\sigma m}$	H	extended inductance of the making current source
L_m	H	inductance of the making current source
L_s	H	inductance of the power system
m_{FNP}	–	slope of a Fowler-Nordheim plot
m_p	kg	mass of a micro-particle
n	–	ideality factor
Q_{bd}	C	charge of a discharge current
Q_{cap}	VA	capacitive reactive power
Q_p	C	charge of a micro-particle
R_b	Ω	resistance of the breaking current source
R_{lf}	Ω	resistance of the field-emission current measurement system
R_{bd}	Ω	resistance of the discharge current measurement system
r_p	m	radius of a micro-particle
R_s	Ω	resistance of the power system
t_{arc}	s	arcing time
t_p	s	transit time of a micro-particle
u_0	V	direct source voltage
u_{ac}	V	alternating component of the recovery voltage
u_b	V	voltage of the high current source
u_d	V	voltage across a diode
u_{dc}	V	direct component of the recovery voltage
$u_{hf,cc}$	V	voltage output of the partial discharge measurement impedance
u_l	V	load side voltage
u_{lf}	V	voltage output of the field-emission current measurement system
u_s	V	alternating source voltage
$u_{s'}$	V	voltage at the source side terminal of a switch

U_s	V	highest value of the phase-to-phase operating voltage (r.m.s. value)
u_t	V	thermal voltage
\hat{U}_{test}	V	amplitude single-phase test voltage
u_{uon}	V	voltage across the voltage making switch
u_{vac}	V	voltage across the test object
v_c	m s^{-1}	critical impact velocity
v_i	m s^{-1}	impact velocity of a micro-particle
v_{uon}	m s^{-1}	contact velocity of the voltage making switch
Z_b	Ω	impedance of the breaking current source
Z_{cc}	Ω	partial discharge measurement impedance
Z_{gnd}	Ω	impedance of the return wire
$Z_{\text{ocp,on}}$	Ω	low impedance of the operating current protection system
$Z_{\text{ocp,off}}$	Ω	high impedance of the operating current protection system
Z_{rv}	Ω	impedance of the recovery voltage source
β_g	–	macroscopic (geometric) field enhancement factor
β_m	–	microscopic field enhancement factor
β	–	field enhancement factor
β_{est}	–	estimated field enhancement factor
δ	rad s^{-1}	damping factor of a <i>LRC</i> -resonance circuit
ε_0	F m^{-1}	permittivity of vacuum: $8.854 \times 10^{-12} \text{ F m}^{-1}$
ρ_p	kg m^{-1}	density of a micro-particle
φ_c	eV	work function of the contact material
φ_{cap}	rad	capacitive phase angle
φ_u	rad	phase angle in a three-phase system
ω_0	rad s^{-1}	resonance frequency of a <i>LRC</i> -resonance circuit
ω_e	rad s^{-1}	eigenfrequency of a <i>LRC</i> -resonance circuit

List of abbreviations

AMP	amplifier
AC	alternating current
Cr	chromium
Cu	copper
DC	direct current
DCP	discharge current protection
D_{f}	power diode
EMI	electromagnetic interference
FN	Fowler-Nordheim
FEOC	Circuitry optimized to measure field-emission currents
GC	Greinacher cascade
INV	inverter

L_1	first phase of a three-phase system
L_2	second phase of a three-phase system
L_3	third phase of a three-phase system
MPOC	Circuitry optimized to detect charged micro-particles
N	neutral phase (return wire)
NSDD	non-sustained disruptive discharge
OCP	operating current protection
PRPD	phase-resolved partial discharge
p.u.	per unit
r.m.s.	root mean square
RV	recovery voltage
S, S_1, S_2	normal switch
S_{aux}	auxiliary breaker
S_b	breaking current protection switch
S_{ion}	current making switch
S_m	inrush current protection switch
S_{sel}	current selection switch
S_{uon}	voltage making switch
S_{vac}	test object (vacuum circuit breaker)
SF_6	sulfur hexafluoride
T_{adj}	adjustment transformer
T_{hf}	high frequency transformer
T_{hv}	high voltage test transformer
T_{iso}	adjustment transformer
THD	total harmonic distortion
VCB	vacuum circuit breaker
VI	vacuum interrupter

Notation

Within this work, the following variable notations are used:

- instantaneous value: $x(t)$
- amplitudes: \hat{X}
- root mean square values: X
- variables in general: x

Abstract

In the last decades, the vacuum switching technology has established itself as the standard in the medium voltage level ($U_s \leq 52$ kV). However, at higher voltages, this technology is not yet competitive to the current SF₆ switching technology. Especially during switching of capacitive loads, a high number of restrikes (dielectric breakdowns) occur. This capacitive switching duty is dielectrically the most challenging for a vacuum circuit breaker and tested widely. However, the interpretation of these tests are difficult due to the absence of suitable diagnostic tools. Therefore, the present thesis deals with the development of a suitable test environment to investigate 72.5 kV vacuum circuit breakers.

Based on experiences from the medium voltage level and established research findings in the field of restrikes two main requirements have been derived:

1. The synthetic test circuit needs to be realized using only test transformers. This is necessary to achieve a high number of test series because the use of power transformers is limited and not economical. In case of a capacitive switching duty, this limitation effects the generation of the recovery voltage and how it is applied to the test object. The recovery voltage itself consists in equal parts of a direct and alternating voltage component and must be applied precisely during its voltage zero crossing. This has been realized using two independent voltage sources and a voltage-making switch that has been specially designed for this purpose.
2. A simultaneous detection of field-emission currents and charged micro-particles is needed. Both phenomena can cause restrikes but are not necessarily independent from each other. To measure field-emission currents, a proven concept from the medium voltage level has been adapted towards a high number of capacitive switching operations in rapid succession. This has been achieved by exploiting the separate generation of current and voltage of a synthetic test circuit. Based on their identical interaction with the test circuit, micro-particles have been detected using partial discharge measurement equipment. As a consequence, the whole test environment must have a low partial discharge level to enable this detection.

Within this work, the measurement systems as well as the test circuit have been commissioned and tested. It was possible to demonstrate the simultaneous detection of micro-particles and field-emission currents ($\geq 100 \mu\text{A}$). Furthermore, a best practice has been defined for future investigations. Based on first measurements, micro-particle activity up to a second after a switching operation could be observed. In addition, it has been shown, that the recovery voltage can be applied to the test object precisely ($\pm 100 \mu\text{s}$) at the voltage zero crossing with an additional voltage-making switch. Thus, the main negative aspect in their generation, which arise from the use of test transformers, can be compensated.




Kurzfassung

In den letzten Jahrzehnten hat sich die Vakuumtechnologie als Standard für Leistungsschalter in der Mittelspannung ($U_s \leq 52 \text{ kV}$) etabliert. Allerdings ist diese Technologie bei höheren Spannungen gegenüber der gängigen SF_6 -basierten Schalttechnik noch nicht konkurrenzfähig. Insbesondere beim Schalten von kapazitiven Lasten kommt es vermehrt zu Rückzündungen (dielektrischen Versagern). Diese Schalthandlung ist die dielektrisch kritischste Herausforderung für einen Vakuumleistungsschalter, wodurch sie gezielt experimentell untersucht wird. Allerdings ist die Interpretation dieser Tests durch das Fehlen geeigneter Diagnosewerkzeuge entscheidend behindert. Aus diesem Grund befasst sich die vorliegende Dissertation mit der Entwicklung einer eigens für diese Untersuchung geeigneten Prüfumgebung für 72.5 kV Vakuumleistungsschalter.

Anhand von Erfahrungen aus der Mittelspannung und etablierten Forschungsergebnissen in Bezug auf Rückzündungen konnten zwei Hauptanforderungen für diese Prüfumgebung abgeleitet werden:

1. Der synthetische Prüfkreis muss mit Testtransformatoren realisiert werden. Dies ist notwendig, um eine hohe Anzahl von Messreihen zu erreichen, da die Nutzung von Leistungstransformatoren limitiert und nicht ökonomisch ist. Im Fall des kapazitiven Schaltens beeinflusst dies lediglich auf die Erzeugung und Zuschaltung der Wiederkehrspannung. Diese besteht zu gleichen Teilen aus Wechsel- und Gleichspannung und muss exakt im Spannungsnulldurchgang zugeschaltet werden. Realisiert wurde dies durch die Nutzung unabhängiger Spannungsquellen und einen eigens hierfür entwickelten präzisen Spannungszuschalter.
2. Eine zeitgleiche Detektion von geladenen Mikropartikeln und Feldemissionsströmen ist notwendig. Beides sind Mechanismen, die Rückzündungen verursachen können, aber nicht unbedingt exklusiv voneinander auftreten. Zur Messung von Feldemissionsströmen wurde auf eine bewährte Methode der Mittelspannung zurückgegriffen, die speziell für eine hohe Anzahl von schnell aufeinanderfolgenden kapazitiven Schalthandlungen angepasst wurde. Dies konnte durch Ausnutzung der separaten Strom- und Spannungserzeugung bei synthetischen Prüfkreisen erreicht werden. Auf Grund des physikalisch ähnlichen Erscheinungsbildes wurde die Detektion von Mikropartikeln mit Hilfe von etablierter Teilentladungsmesstechnik realisiert. Als Konsequenz muss die gesamte Prüfumgebung einen geringen Teilentladungspegel aufweisen, um diese Detektion überhaupt zu ermöglichen.

Im Rahmen dieser Arbeit wurden sowohl die Messsysteme als auch der Prüfkreis aufgebaut und erprobt. Es konnte gezeigt werden, dass eine zeitgleiche Detektion von Mikropartikeln und Feldemissionsströmen ($\geq 100 \mu\text{A}$) möglich ist. Des Weiteren konnte für zukünftige Messungen eine geeignete Vorgehensweise abgeleitet werden. Anhand von ersten Messungen konnten mögliche Mikropartikel-Aktivitäten bis zu mehreren Sekundes nach einer Schalthandlung detektiert werden. Darüber hinaus konnte gezeigt werden, dass die präzise Zuschaltung ($\pm 100 \mu\text{s}$) der Wiederkehrspannung im Spannungs-



nulldurchgang möglich ist. Hierdurch kann die negative Hauptauswirkungen eines Testtransformators bei der Erzeugung der Wiederkehrspannung kompensiert werden.

1 Introduction

Today's society strongly depends on the reliable supply of electricity. This is, for the most part, achieved by transnational high voltage integrated networks [OO04]. For example, the *Synchronous grid of Continental Europe* transferred power to customers in 24 countries with an overall power peak of 528 GW in the year 2015 [EE15]. Beside other electrical equipment, switches are needed within these networks to direct the power flow. The actual reasons for a switching operation are diverse and range from normal service operations, maintenance, insulation of network sections to the clearance of fault currents [SvK⁺15]. Based on this, different types of switches are used due to economical and practical aspects [Gre11]. Among these types, the *circuit breaker* is faced with the highest demands regarding the switching capability. These include normal load switching as well as breaking and making of short circuit currents.

In the last decades, especially since the *Kyoto Protocol*, the energy sector is undergoing a fundamental structural change. From the generation to the consumption of electric energy, environmental aspects become more and more important. Consequently, there are new and additional restrictions for future (circuit) breakers. Particularly a green-house gas free design, with low maintenance requirements and a long service life, are the main concern. These requests are already fulfilled in the medium voltage level ($U_s \leq 52$ kV) by vacuum breakers. However, mainly due to dielectric issues, they are not yet established in the high voltage level. Here, breakers, based on the SF₆ switching technology, must be used to guarantee the supply reliability of the power grid. Due to the fact that SF₆ is one of the worst green-house gases¹, a significant amount of the latest research and development efforts are focused on establishing the vacuum switching technology at higher voltage levels [LWX⁺07], [GRRT12], [Sie12a], [YWG⁺16]. [CIG14]

The most demanding dielectric switching stress for a vacuum circuit breaker is the switch off of a capacitive load [CIG14]. This is manifested in an increased occurrence of *late dielectric breakdowns* (sometimes hundreds of milli-seconds after a successful current interruption) which can be initiated by field-emission currents and/or micro-particles [Sla08]. Thus, dielectric tests under these conditions are of great importance. For this purpose, often *synthetic* test circuits (instead of direct ones) are used. These test circuits take advantage of the fact that switches are stressed with high currents and low voltages during a closing, closed or opening² position while the opposite occurs in an open position. Therefore, a single (direct) power source can be replaced by two sources, where one is optimized for high voltage and the other one for high currents. Thus, the power demand of a synthetic test is considerably reduced compared to that of a direct test. [SvK⁺15]

Currently, dielectric investigations of vacuum circuit breakers above the medium voltage level are facing two problems. First, the generation of the special recovery voltage³ of a capacitive load switching is more and more challenging. This is caused by the necessity to use high voltage *test* transformers due to economical and practical reasons. However, these transformers have a significantly reduced rated

¹ global warming potential for 100 years (GWP_{100}): 23900 [SMI97]

² provided that an arc is burning between the contacts

³ consists to equal parts of a direct as well as an alternating voltage component

current (compared to a power transformer) which leads to power limitations and distortions in the output voltage in case of a high current steepness. Second, with the exception of a field-emission current measurement, adequate diagnostic tools are absent, which could be used in a capacitive load switching test. Thus, a detailed analysis of the late-breakdown phenomena is made more difficult.

Within this work, a test environment is presented to investigate the phenomena of late-breakdowns in 72.5 kV vacuum circuit breakers during capacitive load switching. For this purpose, a (low power)⁴ synthetic test circuit is used. Compared to test environments utilized in the medium voltage level [DGK⁺04], [KLKG07], [KHK10], [YGL12], [DYTM14], the following core features are enhanced or newly added. First, the recovery voltage has been improved regarding the decay of its direct voltage component. Second, the existing field-emission current measurement principle has been adapted towards a high number of capacitive switching operations in rapid succession. Third, a measurement system to detect micro-particles has been defined and implemented. Fourth, concepts have been developed and tested to use both measurement systems simultaneously.

⁴ due to the use of a test transformer

2 Fundamentals

This chapter starts with a brief introduction of the basic working principle, the structure and the internal field distribution of a vacuum circuit breaker. This is followed by a discussion about the internal dielectric breakdown of a vacuum circuit breaker. Afterwards, the characteristics of a making and breaking arc in a vacuum environment are presented. The chapter closes with a discussion regarding the issues associated with the switching of capacitive loads in the electrical power grid.

2.1 Vacuum circuit breakers

A *vacuum circuit breaker* (VCB) is a mechanically operated switch. Its working principle is based on the opening and closing of a pair of contacts in a *high-vacuum* environment¹. Due to the physical characteristics of this vacuum environment, no arc quenching and insulation medium is required. Compared to other switching technologies, this makes the design simpler and decreases the drive energy required to operate the contacts [CIG14]. This results in various advantages, e.g. the possibility of frequent switching operations, low life-cycle-costs, excellent arc quenching capabilities and nearly maintenance free operation. Therefore, the vacuum technology is now well established in the medium voltage level. Above this voltage level, for voltages at 72.5 kV and 145 kV, VCBs are available [BGW⁺12], [Sie12a], but, except for Japan and China, they are not widely used. [SvK⁺15], [Lip03], [Fal06], [LWX⁺07], [Sla08]

Abbildung 2.1 shows a typical design of a 72.5 kV live-tank VCB. It is based on two components: the *pole assemblies* and the *operating mechanism box*. The pole assemblies consist of the *vacuum interrupter* (VI), the upper and lower grid terminal, a porcelain enclosure and an insulation gas. The porcelain enclosure provides the mechanical support for the VI and the upper grid terminal. It also serves as a pressure vessel for the external² insulation gas which is needed to ensure a compact design of the VI. The operating mechanism box provides the energy for the switching movement which is transferred to the VI's movable contact via an operation rod. A spring between the VI and the rod is used to provide a contact force at closed position and to reduce the mechanical shocks during switching. For reasons of insulation, the pole assemblies are mechanically fixed to the operation mechanism box by insulators. [Sie10] [Lip03]

In Abbildung 2.2 a typical cross section of a VI³, the switching element of a VCB, is shown. It is based on a vacuum-tight enclosure made of ceramic and metal parts. During the manufacturing process, all parts are hermetically soldered together while the inside is evacuated to a pressure less than 1×10^{-7} mbar. The electric switching is done by a pair of electric contacts inside the enclosure. Usually one of the contacts is fixed and the opposite one is movable. To ensure this movement while maintaining the integrity of the vacuum environment, a metal bellow is used. [SvK⁺15]

¹ hereafter referred to as vacuum

² with respect to the VI

³ also named vacuum bottle or vacuum tube

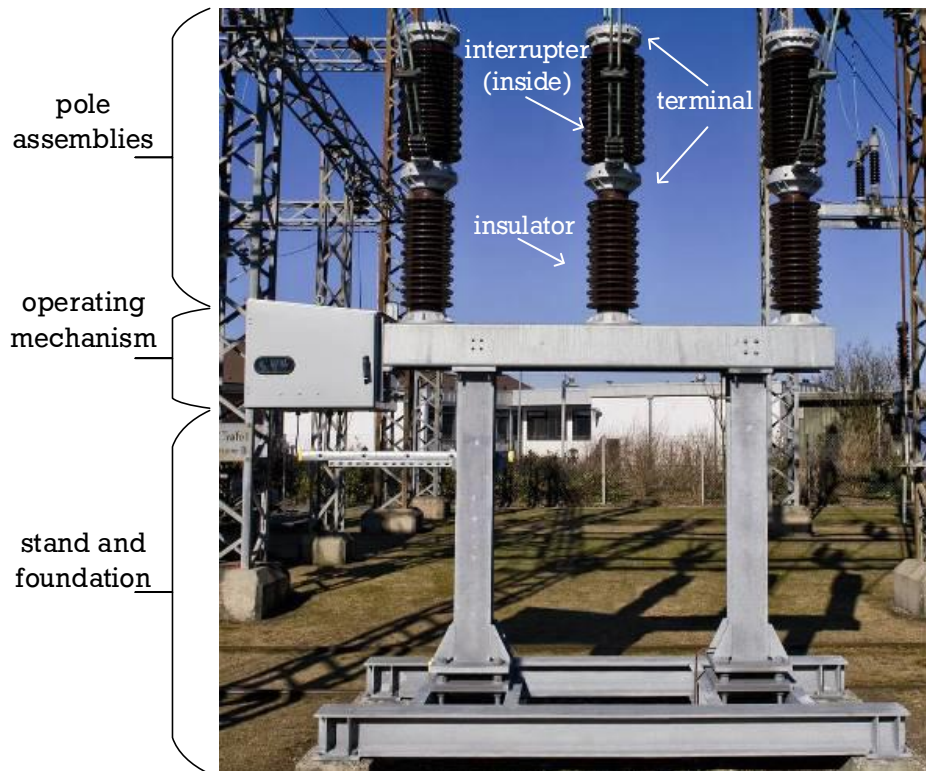


Abbildung 2.1: Example of a 72.5 kV vacuum circuit breaker (live-tank); adapted from [Sie12b]

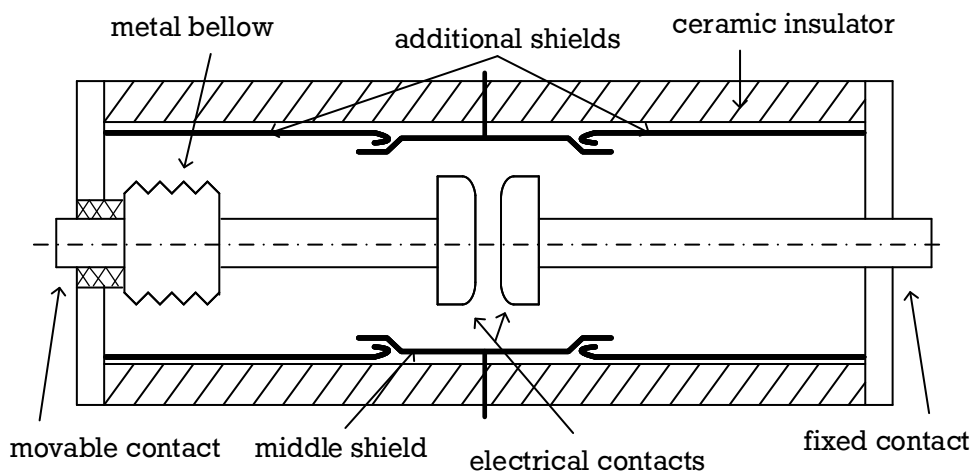


Abbildung 2.2: Simplified cross section of a vacuum interrupter; adapted from [Sla08]

VIs use only one pair of contacts to conduct and interrupt the current as well as to insulate the voltage. To ensure a low resistance when the contacts are closed, larger contact diameters⁴ and certain contact forces are necessary. After contact separation under load, an arc will ignite between the contacts. This arc vaporizes the contact material and thereby damages the surface. To limit this damage, the energy input is distributed over the whole contact surface. This is achieved by using specially designed contact systems. Towards current zero, the energy input to the arc decreases until the vaporization of contact material stops and the arc extinguishes. Within micro-seconds, charge carriers recombine and the dielectric strength of the gap is restored. The remaining metal vapor will condensate at the interior of the enclosure. Therefore, an additional metal shield⁵ is required to protect the ceramic surface from conductive layers of condensed metal vapor. [SvK⁺15] [Kap11] [Sla08]

The electric field distribution of a VI can be compared to that of a plate-plate capacitor [Sla08]. Thus, the homogeneous part of the electric field strength E_{vac} between the contacts is given by

$$E_{\text{vac}} = \frac{u_{\text{vac}}}{d_{\text{vac}}} \quad (2.1)$$

where u_{vac} is the applied voltage and d_{vac} the gap distance [KSW13]. Due to the presence of the vapor shield, the electric field outside and at the edge of the contacts differs. The electric field E_c at the contact surface is further enhanced, for example, by micro protrusions [Lat95]. This can be expressed and linked to the homogeneous field strength with the *total* field enhancement factor β .

$$E_c = \beta \cdot \frac{u_{\text{vac}}}{d_{\text{vac}}} = \beta_g \cdot \beta_m \cdot \frac{u_{\text{vac}}}{d_{\text{vac}}} \quad (2.2)$$

It can be separated into the *macroscopic (geometric) enhancement factor* β_g and the *microscopic enhancement factor* β_m [Sla08].

Macroscopic (geometric) field enhancement

The factor β_g describes the field enhancement on a macroscopic level. It is influenced by the design and the surrounding environment of the VI. The main influence factors are as follows:

- the gap distance
- the distance of the contacts to the vapor shield
- the radius of the contacts
- the edge radius of the contacts
- the type of contact system
- the potential of the vapor shield

The value of the macroscopic enhancement factor can be estimated numerically. A modern VI has a value of β_g below 10. [Sla08]

⁴ compared to other switching technologies

⁵ in addition to the usual field grading methods

Microscopic field enhancement

The factor β_m describes the field enhancement on a microscopic level. It is determined by various factors such as:

- the composition of the electrical contact material, its impurities and contamination
- the structure and the roughness of the electrical contact surface
- the manufacturing process of the VI

In general, the cause of this field enhancement is very sensitive to any electrical, thermal or mechanical stress. Consequently, it changes constantly in a VI. Thus, an exact determination is impossible. However, experiments have observed the range of the microscopic enhancement factor β_m to be 100–300. [Sla08] [Lat95]

2.2 Dielectric breakdown in vacuum

Every dielectric breakdown needs a trigger charge, first to initiate the breakdown, and, second, an electric field to provide the energy during the breakdown. In addition, negative and positive charge carriers (at least electrons and positive ions) have to be created in a self-sustaining process to form a plasma [SBM95]. In order to maintain the quasi-neutrality of the plasma, the amount of negative and positive charge carriers created has to be equal. Compared to an electric breakdown in gas, the physical processes of a dielectric breakdown in vacuum are different, more complex and not yet completely understood. One difference lies in the initiation of the breakdown. While a breakdown in gas can be triggered by a few electrons somewhere in the gas volume [Küc09], a breakdown in vacuum usually requires more energy and is initiated at the contact surface [SvK⁺15]. Another difference is the supply of ionizable gaseous matter. In a gas breakdown, the gas itself can be ionized [Küc09]. In a vacuum breakdown, all this matter has to be released first. Due to the low particle density in vacuum, the only source for this is the vaporization of the contact material [SvK⁺15]. Thus, a breakdown in vacuum is strongly influenced by the electric field at the contact surface, the contact properties, the contact history and the internal pressure. [Sla08]

In general a breakdown in vacuum may be separated into two stages [JS81]:

1. *Ignition state*: various pre-breakdown effects generate a microscopic plasma cloud in the discharge path.
2. *Spark state*: the ignition is further developed and expands throughout the whole discharge path. This leads to an almost complete collapse of the voltage because all available electrical energy, stored in the nearby (parasitic) capacitances, is consumed.

Depending on the external circuit, the spark phase may further evolve to a metal vapor arc with a very small arc voltage [JS81].

2.2.1 Pre-breakdown effects

Pre-breakdown phenomena have many origins and forms. However, they can be separated roughly into an electron source and into a supply of ions and metal vapor.

Supply of electrons

Electrode arrangements in vacuum have only one effective source of electrons which is the cathode. Here, electrons exist, which are usually not able to leave the contact surface because they cannot overcome its potential barrier [Kuc07]. However, in the presence of strong electric fields ($E_c > 1 \text{ GV m}^{-1}$), the potential barrier becomes lower and narrower. Now, based on the quantum mechanical tunneling mechanism, electrons have a finite probability to be emitted into the vacuum⁶. As electrons are emitted at a certain area in a certain time, this results in a current density j_{fe} . For VIs, this *field-emission current density* j_{fe} can be satisfactorily expressed with the *Fowler-Nordheim* (FN) equation

$$j_{fe} = K_{fe1} \cdot E_c^2 \exp\left(\frac{-K_{fe2}}{E_c}\right) \quad (2.3)$$

where K_{fe1} and K_{fe2} are constants. In a first approximation, they depend only on the work function φ_c of the pure metallic contact material⁷. [Sla08]

$$K_{fe1} = \frac{1.54 \times 10^{-6} \cdot 10^{4.52\left(\frac{\varphi_c}{eV}\right)^{-0.5}}}{\frac{\varphi_c}{eV}} \quad (2.4)$$

$$K_{fe2} = 6.53 \times 10^9 \cdot \left(\frac{\varphi_c}{eV}\right)^{1.5} \quad (2.5)$$

Under the assumptions that the emission site has a certain area A_e and that there is only one emission site on the cathode, j_{fe} can be expressed as

$$j_{fe} = \frac{i_{fe}}{A_e} \quad (2.6)$$

With Equation (2.2) and Equation (2.6), the FN equation can be transformed into

$$\frac{i_{fe}}{A_e} = K_{fe1} \cdot \left(\frac{\beta_g \beta_m u_{vac}}{d_{vac}}\right)^2 \exp\left(\frac{-K_{fe2} d_{vac}}{\beta_g \beta_m u_{vac}}\right). \quad (2.7)$$

Thus, with a current, voltage and gap distance measurement, the quality of the contact surface can be evaluated. To interpret the data, it is useful to plot $\frac{1}{E_{vac}}$ against $\log_{10}\left(\frac{i_{fe}}{E_{vac}^2}\right)$. This *FN plot* is shown in Abbildung 2.3a. Here, the non-linear relationship results in a straight line with its slope m_{FNp} and intersection with the ordinate b_{FNp} . These parameters can be used to estimate the emission area $A_{e,est}$ and the field enhancement factor β_{est} with the following equations:

$$\beta_{est} = -\frac{K_{fe2}}{m_{FNp}} \quad (2.8)$$

⁶ Besides this mechanism, electrons can also be released by ions bombarding the cathode [MVG02].

⁷ Within this work, a contamination of the contact surface, for instance with insulation layers [Lat95], is not taken into account.

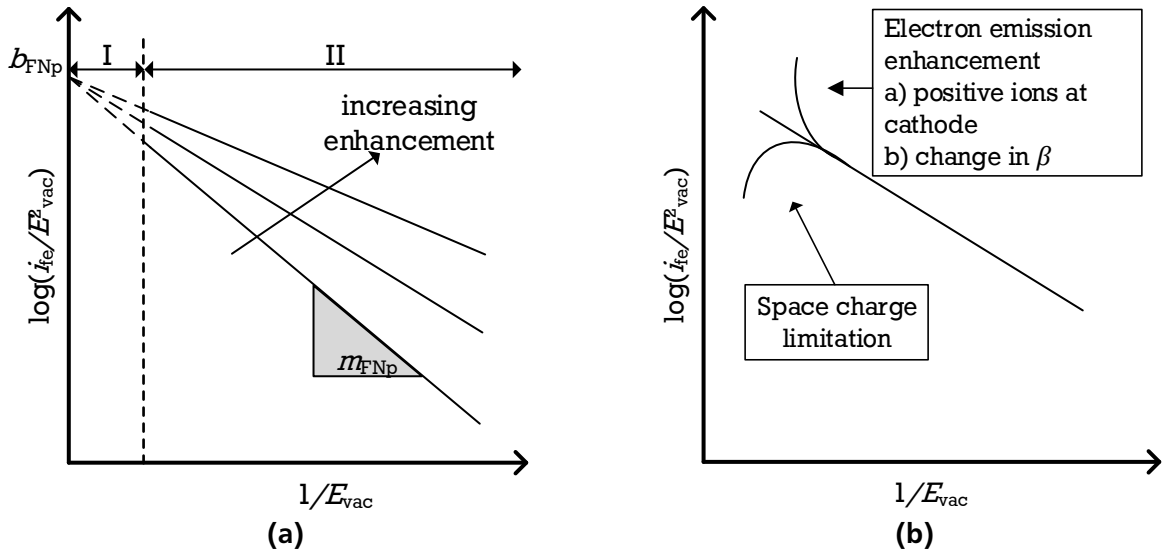


Abbildung 2.3: Fowler-Nordheim plot with general properties (a) and typical influences (b); adapted from [Sla08], [Lat95]

$$A_{e,est} = \frac{e^{b_{FNp}}}{\beta_{est}^2 K_{fe1}} \quad (2.9)$$

Due to the inverse proportionality with the electric field strength E_{vac} , the intersection cannot be measured. As a consequence, it has to be obtained by extrapolating data from section II into section I of Abbildung 2.3a. [Sla08]

A FN plot does not always result in a straight line. Influences, caused by additional phenomena which change the field-emission current density, bend the line. This is shown in Abbildung 2.3b. For instance, an increased slope can be caused by positive ions in the vicinity of the cathode, while a decreased one might be the result of an electron space charge effect. The latter is referring to the Child's law which describes the reduction of the surface field strength E_c caused by the electrons in the field-emission current [HSM07]. Furthermore, a typical emission area, compared to the contact surface of a VI, is extremely small. Thus, usually more than one emission site exists [TS98]. Therefore, estimations of the emission area as well as the field enhancement factor have to be treated as effective values. [Sla08]

Supply of metal vapor and positive ions

The supply of metal vapor is essential for a breakdown in vacuum because its ionization is the only source of positive ions. It can be provided by vaporization of either metallic surfaces or metallic micro-particles⁸. Micro-particles are always present in a VI due to the manufacturing process; but they are also constantly (re-)created by each switching operation. For example, micro-particles with radii up to several tens of micro-meters can be produced by normal operation currents [KSF⁺95]. Usually, they are attached to a surface, but can be released by mechanical, thermal or electrical stress. In the following, the relevant possibilities leading to the generation of an initial plasma cloud are described. [Sla08]

⁸ The influence of non-metallic micro-particles is not yet determined.

At the cathode, the field-emission current density causes a temperature rise of the emission site due to Joule heating. This temperature rise might exceed the melting and boiling point of the contact material. The result is an eruptive evaporation of the emission site. Now, the field emission electrons can easily ionize the metal vapor due to its low ionization energy⁹. Besides an emission site at the surface, especially small¹⁰ metallic micro-particles close to the cathode also increase the electric field strength and, thereby, may initiate a similar phenomenon [KBFO00]. [Sla08]

At the anode, field emission electrons arrive with energies up to several tens of keV. With these energy levels, electrons are able to penetrate the surface. Given the nature of the electron beam, the energy is deposited in a small volume. One consequence is an increase in pressure of the small volume which may result in an explosive evaporation. Another possibility is that the increase in temperature weakens the mechanical surface strength which results in the release of a micro-particle. This micro-particle will move away from the anode due to the electric field. The ongoing bombardment of electrons from the beam will heat the micro-particle which may end in a vaporization. Due to the micro-particle's movement, the final vaporization does not have to be close to the anode¹¹. In contrast to the ionization of metal vapor in front of the cathode, electrons originating from the cathode are not able to ionize the metal vapor directly due to their high velocity. Therefore, these electrons have to be slowed down, for example, by collisions with other atoms. Another possibility is the emission of new electrons with only a few eV from the molten metal droplets due to thermal field emission. [Sla08], [Lat95]

Furthermore, the impact of a micro-particle on a contact surface can assist in a dielectric breakdown. This effect depends on the impact velocity v_i , which for a spherical micro-particle, is given by

$$v_i = \sqrt{\frac{3Q_p u_{\text{vac}}}{2\pi r_p^3 \rho_p}} \quad (2.10)$$

where Q_p is the micro-particle's charge, ρ_p its density and r_p its radius. The field-induced surface charge¹² Q_p of such a micro-particle, which has been lifted off¹³ from a contact surface can be calculated according to Equation (2.11) [Lat95].

$$Q_p = 6.6\pi\epsilon_0 E_c r_p^2 \quad (2.11)$$

Given the critical impact velocity v_c of the contact material¹⁴, there are three scenarios that can happen [Sla08]:

1. Low-impact velocities ($v_i < v_c$) result in an elastic deformation of the contact surface. The micro-particles themselves can either stick to or bounce off the surface. If this impact happens at the cathode¹⁵, this leads to an increased field emission due to local field enhancement.

⁹ ionization energy of Cu is < 10 eV [WWH01]

¹⁰ aerosol micro-particles in the sub-micron range

¹¹ same results if the micro-particles cross randomly the electron beam

¹² differs from a charge in free space

¹³ Usually, the electric field strength required to lift a micro-particle from a surface, is less than the one needed for a dielectric breakdown provided their radii are in the range of $1\ \mu\text{m}$ to $10\ \mu\text{m}$ [MS74].

¹⁴ critical impact velocity for Cu approx. $200\ \text{m s}^{-1}$ for a spherical particle [Coo58]

¹⁵ Usually, 90% of the micro-particles originate from the anode [EC83].

2. Intermediate velocities ($v_c < v_i < 5v_c$) result in a permanent deformation of the contact surface. The micro-particles themselves are consumed in the process. However, secondary micro-particles may be released while the deformation may result in a local field enhancement.
3. High impact velocities ($v_i > 5v_c$) result in a complete vaporization of the micro-particles.

In addition, gas molecules are always embedded in the metal structure of the contacts. Supported by a micro-particle bombardment or a field emission beam, these gas molecules can be released from the bulk. This mechanism may also result in the creation of a plasma cloud. [Lat95]

It is important to note that the impact velocity is linked to the voltage u_{vac} across the VI. Thus, the pre-breakdown effects in vacuum depend on the voltage as well as on the electric field strength. As a result, scaling¹⁶ of an existing VI towards higher voltages might be more extensive compared to one based on SF₆ insulation. There, the breakdown is only field dependent [Küc09].

2.2.2 Transition to breakdown

When a VI is connected to an external circuit, the pre-breakdown effects mentioned above can progress in different ways. They can evolve into a self-limiting current pulse, a non-sustained disruptive discharge, a full breakdown, or they can simply die off. In the following, the most important aspects are summarized briefly:

- *Self-limiting current pulse*: A typical example is a micro-discharge which is shown in Abbildung 2.4. Its duration varies and can be up to 100 ms with an amplitude usually up to 100 mA. Due to its

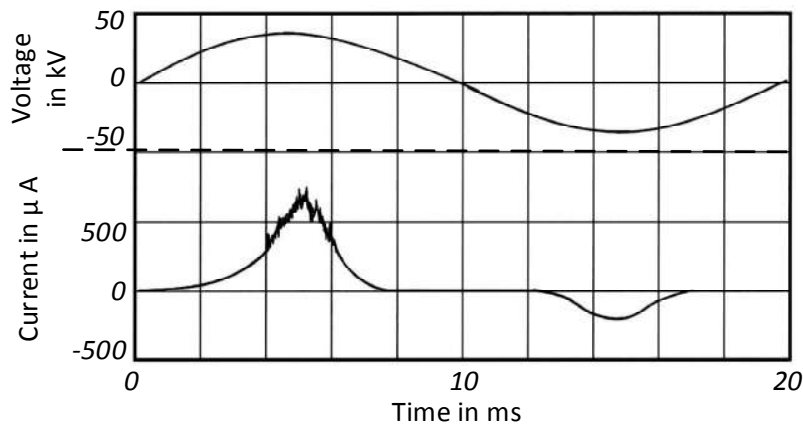


Abbildung 2.4: Example of a micro-discharge; adapted from [KH89]

transient character, its appearance is strongly influenced by the test environment. [Sla08]

- *Non-sustained disruptive discharge (NSDD)*: An increase of the electric field strength¹⁷ usually leads to an intensification of the pre-breakdown effects. The growth of the initial plasma cloud can now easily expand between the contacts. At a certain point a discharge occurs. Unlike in a gaseous medium, where this discharge is automatically self-sustained¹⁸, in a vacuum environment it can

¹⁶ from a dielectric point of view

¹⁷ for instance, by increasing the voltage or decreasing the gap distance

¹⁸ if the electric field is not highly inhomogeneous

be non-sustained. Such a NSDD consumes close to all energy stored in the electric field between the contacts which leads to a collapse of the voltage. However, the resistance of the discharge path is still sufficient that even in a electrical circuit with a small impedance no arc is formed [JS81]. [Sla08]

- *Full breakdown*: A full breakdown evolves initially similar to a NSDD. The differences lie in the supply of electrons and metal vapor as well as in the ionization mechanism. If they are efficient and fast enough, the initial discharge becomes self-sustained. Now its resistance reaches values below a typical grid impedance which allows the formation of an arc. [JS81]

However, closed theories for all listed phenomena are not yet available [Sla08], [SvK⁺15].

2.2.3 Special case of an insulator flashover

Besides a breakdown between the contacts, a flashover along the insulator in vacuum is also possible. For materials, currently used in VIs, this breakdown mechanism originates from the cathode side triple point [Gie03]. The triple point, itself, consists of vacuum, the metal of the shield and the material of the insulator¹⁹. It has, compared to the insulator individually a reduced dielectric strength. Thus, electrons are easily emitted [Küc09] from the triple point. There are many theories as to how these electrons may initiate a flashover [Mil15] [Lat95]. They all have in common the secondary electron emission and the interaction with gas molecules. Here, secondary electron emission occurs when accelerated electrons release additional ones by colliding with the insulator. This builds up to an electron avalanche²⁰ which is further enhanced by the positive space charge left in the insulator by the released electrons. Under normal circumstances, gas molecules exist inside the insulator or as adsorbed layers. By interaction with the bombarding electrons, these molecules become desorbed and ionized. The so obtained positive ions move, against the electron direction, towards the triple point and enhance the emission. The final flashover takes place in this small layer of desorbed gas similar to a gas discharge.

2.3 Electric arcs in a vacuum environment

VCBs have to switch off (breaking operation) and switch on (making operation) load currents as well as fault currents. At contact separation, an electric arc inside the VI ignites. The arc itself is a plasma which is maintained by ionizing metal vapor gained from vaporizing contact material. Thus, the arc burning between the contacts in a vacuum environment is called *metal vapor arc*. The arc power is proportional to the current due to its relatively low²¹ and roughly constant burning voltage. For this reason, VCBs are still designed to extinguish arcs at the next natural current zero and withstand the arcing phase with a minimum loss of integrity. During its lifetime, the metal vapor arc occurs in different modes, depending on the arc current. [SvK⁺15]

¹⁹ almost exclusively the ceramic Al₂O₃

²⁰ Compared to a metal, an insulator may release up to 15 new electrons [KE65].

²¹ compared to the system voltage of the distribution and transmission level

2.3.1 Arcing during opening operation

The contact surface of a VI is rough. Even in closed position, only certain areas of the contact conduct the current. During contact separation, these areas are reduced until the last one vaporizes due to the high current density. The result is a *molten metal bridge arc* with a high vapor density between the contacts. After a short time, the initial metal vapor is completely ionized and the charge carriers are drained by the external circuit. In order to maintain the arc, a new process to generate charge carriers has to be established. The formation of such a process depends strongly on the current and results in different arc modes. [Sla08]

Independent from the current amplitude is the formation of individual emission sites on the cathode (see Abbildung 2.5). Like other electric arcs, the plasma of the metal vapor arc does not directly interact

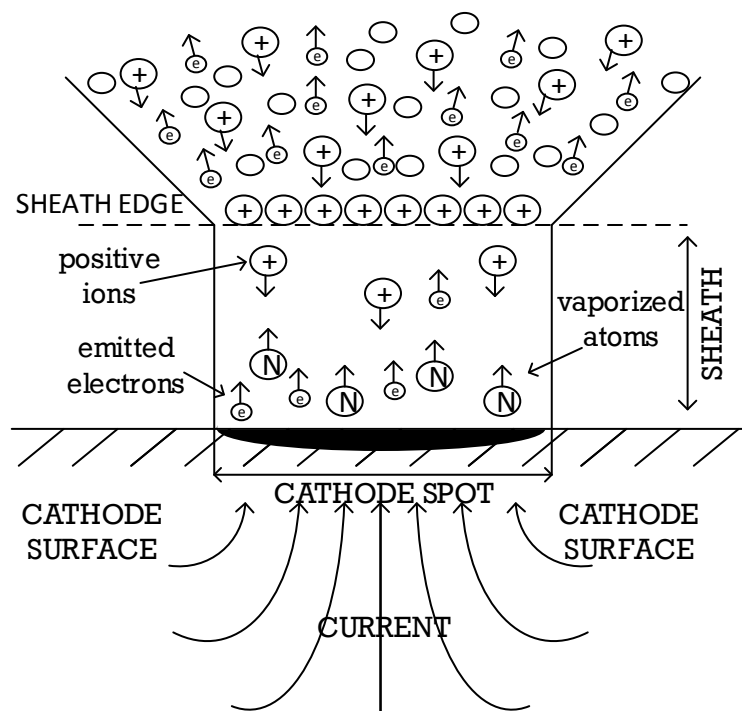


Abbildung 2.5: Idealized geometry and structure of a cathode emission site; adapted from [SvK⁺15]

with the cathode surface. Instead, it is shielded by a positive space charge region, called the *cathode sheath*, which is usually formed on top of a *cathode spot*. The cathode spot refers to an area with molten and partially vaporized contact material. It is characterized by its short life-time²², small diameter (few tens of micro-meters), high current density, random movement and random appearance across the surface. Due to its high temperature, the cathode spot is able to emit electrons by thermal field emission. Both the metal vapor and the electrons are accelerated away from the cathode spot by the vapor pressure and the electric field, respectively. After passing the cathode sheath edge, electrons have gained enough energy to ionize the metal vapor. Thus, new electrons and positive ions are created. Due to their mass difference, positive ions move slower compared to electrons and, thereby, maintain the space charge

²² Currently, no exclusive physical model exists to describe the creation and the life-time behavior of a cathode spot. In fact, two models exist which describe the creation by a stationary cathodic evaporation and a non-stationary explosive generation of material.

region. Approximately 90 % of all positive ions are accelerated towards the cathode and bombard the cathode spot. In combination with the Joule heating of the field-emission current, those two mechanisms are the primary power source of a cathode spot. Depending on the contact material, a cathode spot requires a minimum current to maintain its integrity. Besides the minimum current, it also has a maximum current value before an additional cathode spot is formed. [SvK⁺15]

Without artificial magnetic fields, a metal vapor arc can be separated into two basic modes: the *diffuse arc mode* and the *constricted arc mode*. [Lip03]

Diffuse arc mode

The diffuse metal vapor arc is a unique aspect of an arc burning in a vacuum environment. It develops at low currents, typically below 10 kA, and is a collective of various independently burning arcs. The arc itself consists of a cathode emission site and a cone shaped plasma (see Abbildung 2.6a). In the diffuse

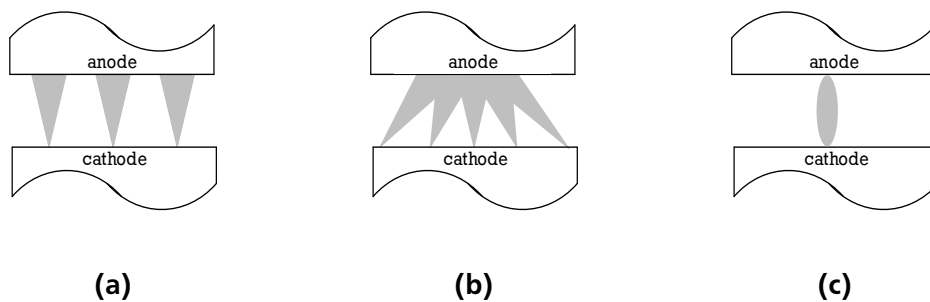


Abbildung 2.6: Different arc modes: (a) diffuse, (b) diffuse with constriction at the anode, (c) constricted; taken from [SvK⁺15]

mode, the anode functions only as a passive collector. Therefore, the arc is strongly influenced by the properties of the cathode spot. The number of parallel arcs is determined mainly by the contact material and structure²³. One special characteristic is the cathode spot's *retrograde motion* which is directed in opposite direction as proposed by the Lorentz force. Therefore, cathode spots repel each other and move towards the contact edge and cease to exist. While this phenomenon is not yet completely understood, it is, in general, useful in a VI. It distributes the thermal stress over the whole contact surface which avoids local hot spots and results in a low erosion rate. [SvK⁺15], [Lip03]

Towards current zero, the number of parallel arcs decreases. At a certain point, only one arc with one emission site is still active. As described, a cathode spot requires a minimum current to exist. Thus, it will cease to exist prior to the natural current zero. This results in a *chopping current* with amplitudes in the range of 2 A to 10 A depending on the contact material and the circuit configuration. [Hal13]

After the diffuse arc has been extinguished, plasma and metal vapor is still present between the contacts. Another unique characteristic of the metal vapor arc is the high ion speed. Thus, the plasma disappears within several micro-seconds by recombination of charged particles and condensation of metal vapor. During this time, the plasma is still conductive. In combination with an applied voltage, these particles are accelerated again. This causes *post-arc currents* which re-ionize the plasma

²³ A cathode spot on a copper surface can carry up to 100 A before a second one is formed [Lip03].

due to the thermal losses. If the re-ionization rate exceeds the recombination rate, the arc may ignite again. [SvK⁺15], [Sla08]

Constricted arc mode

A diffuse arc develops gradually into a constricted arc with an increase of the arc current. First, the high number of individual arcs leads to a partial overlap of the plasma cones in front of the anode. Their self generated magnetic fields cause the plasma to constrict (see Abbildung 2.6b), resulting in several bright spots on the anode. With a further increase in current, all spots will merge. The final anode spot produces a thermal stress that reaches the boiling point of the contact material. Thus, a second source of metal vapor is created. Due to the magnetic pinch of the arc, also at the cathode a single spot is formed. The result is a constricted arc with a well defined arc column (see Abbildung 2.6c). The constricted arc will remain in this mode until the current is decreased. Then, it re-develops into a diffuse arc. [SvK⁺15], [Sla08]

In contrast to a diffuse arc, constricted arcs usually do not move across the contact surface. The result is an extensive localized thermal stress with a high erosion rate. For instance, this causes an increased wear and a significant reduction in switching capability. The latter are the result of former anode hot spots becoming cathode hot spots after the current interruption due to a polarity change of the applied voltage. These cathode hot spots can cause a dielectric breakdown or reignite the arc due to extensive *thermal* field emission (see Section 2.2). Therefore, constricted arcs are manipulated by artificially created magnetic fields. Currently, two types of magnetic fields are used in VIs. The first one is a radial magnetic field which forces the arc into circumferential motion at the contact edge due to the Lorentz force. The thermal stress is now distributed across the whole edge region of the surface. The second one is an axial magnetic field which counteracts the self-constriction of the arc. Thus, the arc is kept in a diffuse mode even at higher currents. [Lip03]

2.3.2 Arcing during closing operation

During a making operation, the VI's contacts move from the open position to the closed position. The movement of the contacts is usually not synchronized with the voltage. Therefore, the electric field may increase while the gap distance decreases. At a certain point, this leads to a dielectric breakdown which can further develop into an electric arc. If an arc is formed, it will burn until the next current zero crossing or until the contacts touch each other. In the first case, another arc may be ignited after a certain time based on the same principle as before; or, the thermal stress of the former arc was high enough to cause an immediate re-ignition.

When these thermally stressed contacts touch each other, the arc roots may cause the contacts to weld together [Kör08]. In this case, the breaking of the welding forms new micro protrusions when the contacts are separated again. Thus, the arc formation during making operations indirectly affects the dielectric performance of the VI. The duration of this pre-ignition arc depends on the closing velocity of the VI as well as the ignition voltage and gap distance. Usually, a long arcing time and a high current amplitude cause more damage to the surface because more contact material is vaporized. However, even a short arcing time with multiple pre-ignitions at different locations at the contact surface can even be worse because multiple welding points may be formed. Due to the low arcing voltage,

the amplitude and the frequency of the pre-ignition arc are defined by the circuit configuration (see Section 2.4.2). [SvK⁺15], [Sla08]

2.4 Switching of capacitive loads

Capacitors are extensively installed in the electric power system. They ensure the voltage quality by filtering out harmonics and by compensating reactive power of the mainly inductive consumers [Sv08]. Therefore, they contribute to a loss and cost reduction, a better utilization of existing systems and in an economical design of new ones [ABB13]. For this, individual capacitors are combined to capacitor banks which are switched frequently during a day due to the fluctuations in the load. [SvK⁺15]

Besides the capacitor as a lumped element, system components show a capacitive behavior at certain operating points. The most important ones are *transmission lines*, *gas insulated lines* and *power cables* at no load operation. Typical values of their distributed capacitance are 8 nF km⁻¹ to 14 nF km⁻¹ for transmission lines [KKFN01], [Hos88] and 40 nF km⁻¹ to 60 nF km⁻¹ for gas insulated lines [Koc02]. Power cables, on the other hand, use solid dielectrics instead of gaseous ones which have a higher permittivity. This results in distributed capacitances up to several hundred nF km⁻¹ [nkt09]. However, these components have a higher *surge impedance*²⁴ compared to a discrete capacitor whereby the making operation causes less stress to the VCB.

2.4.1 Mathematical and physical basics

The capacitance C is the ability to store an electric charge $q(t)$ at a given voltage $u(t)$. With respect to the current $i(t) = \frac{dq(t)}{dt}$ this is expressed with Equation (2.12).

$$i(t) = C \cdot \frac{du(t)}{dt} \quad (2.12)$$

From Equation (2.12) it can be seen, that in case of a sinusoidal voltage, the capacitive current has a phase angle φ_{cap} of $-\frac{\pi}{2}$.

The reactive power Q_{cap} and the energy E_{cap} of a capacitor are described with Equation (2.13) and Equation (2.14), respectively [KD04].

$$E_{\text{cap}} = \frac{1}{2}CU^2 \quad (2.13)$$

$$Q_{\text{cap}} = \omega CU^2 \quad (2.14)$$

This makes the capacitor a voltage controlled energy storage. As a consequence, it stays charged to the instantaneous value of the voltage even after being disconnected. In addition, high *inrush currents* (i_m) can be drawn while being switched on. To derive this current, the equivalent circuit diagram (ECD) in Abbildung 2.7 is used. Here, a discharged capacitive load C_1 is charged by a DC voltage source u_0

²⁴ $\sqrt{(L)/(C)}$

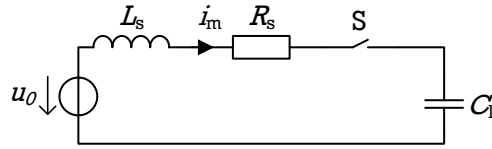


Abbildung 2.7: Energizing capacitive loads

when switch S is closed. The electrical connection in between is represented by the resistance R_s and the inductance L_s .

The current i_m in Abbildung 2.7 is described with the following differential equation

$$u_0 = R_s i_m(t) + L_s \cdot \frac{di_m(t)}{dt} + \frac{1}{C_1} \int_0^t i_m(\tau) d\tau. \quad (2.15)$$

Its relevant²⁵ solution is the damped oscillating current given in Equation (2.16),

$$i_m(t) = \frac{u_0}{\omega_e L_s} \exp(-\delta t) \cdot \sin \omega_e t \quad (2.16)$$

where $\delta = \frac{R_s}{2L_s}$ is the damping factor, $\omega_e = \sqrt{\omega_0^2 - \delta^2}$ the eigenfrequency and $\omega_0 = \sqrt{\frac{1}{L_s C_1}}$ the undamped resonance frequency. If the resistance is small compared to the inductance²⁶, it can be simplified to Equation (2.17). [Cla11]

$$i_m(t) = \frac{u_0 \sqrt{C_1}}{\sqrt{L_s}} \exp(-\delta t) \cdot \sin \omega_0 t \quad (2.17)$$

2.4.2 Making operations

Capacitors draw high *inrush currents* while being energized. As has been shown in Equation (2.17), their amplitude and frequency are strongly influenced by the network's inductance and the voltage at the switch on moment. In the three-phase electrical power grid, the individual voltages are phase-shifted by $\varphi_u = \frac{2\pi}{3}$. This means, that even if one voltage phase is at zero, the other two are stressed with $\frac{1}{\sqrt{2}}$ of the system voltage. In addition the inductance and the capacitance result from the component to be switched. Therefore, all types of circuit breakers have to handle a wide range of inrush currents. For the VCB, energizing distributed loads are usually not a problem due to their high surge impedance. Energizing capacitor banks on the other hand causes some issues [SWB⁺12]. To illustrate this, Abbildung 2.8 shows a capacitor bank with two switchable branches. This results in the two following switching configurations and their associated current-/voltage-characteristic which are shown in Abbildung 2.9a [SvK⁺15]:

- *single-bank*: In this configuration, only one capacitor will be energized while the second one is disconnected from the grid. Therefore, the current flows in loop 1. According to Equation (2.17), the

²⁵ assuming a typical power system with small ohmic losses $R_s < 2\sqrt{\frac{L_s}{C_1}}$

²⁶ This is typically given in the power grid.

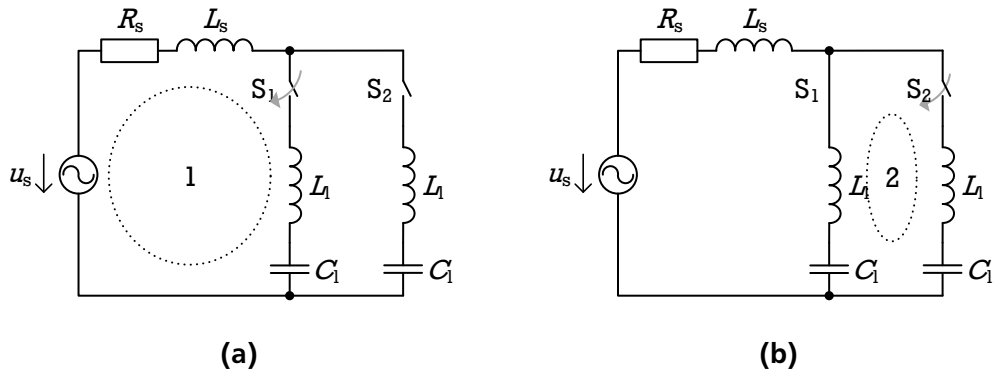


Abbildung 2.8: Single-bank (a) and back-to-back (b) capacitor bank switching; taken from [SvK⁺15]

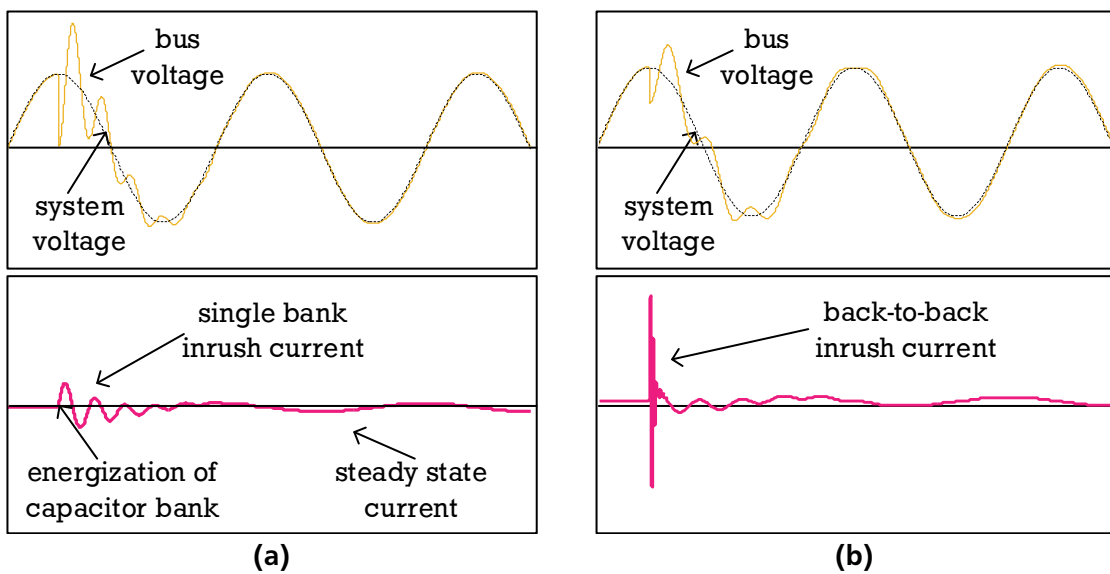


Abbildung 2.9: Example of a single-bank (a) and a back-to-back (b) capacitor energization; taken from [SWB⁺12]

inrush current will be limited by the series connection of the grid inductance L_s and the inductance L_1 of the capacitor bank branch. Due to the relative high value of L_s , this leads to moderate inrush currents. However, the bus voltage almost drops to zero due to the discharged capacitance C_1 (see Abbildung 2.9a).

- *back-to-back*: In this configuration, one capacitor is already connected to the grid. Switching on the second capacitor causes an additional current flow in loop 2. Due to the rather small value of L_1 , this current can easily reach amplitudes higher than 10 kA and frequencies of several kilo-hertz. An example of such an event is shown in Abbildung 2.9b.

In general, inrush currents do not stress a VI with closed contacts because no damaging arcs are formed. However, high inrush currents, in combination with pre-arcing (see Section 2.3.2), may lead to contact welding and, therefore, to a significant decrease in dielectric performance. [Kap11]

2.4.3 Breaking operations

Breaking capacitive currents is a normal switching duty with a rather small current amplitude (less than 500 A) compared to a short circuit. However, the voltage, after a successful current interruption, is the problem. In the following, a single phase breaking operation is explained with the ECD given in Abbildung 2.10 and the corresponding current-/voltage-characteristic shown in Abbildung 2.11. The

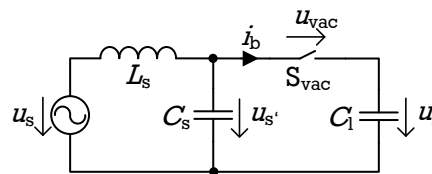


Abbildung 2.10: ECD for single phase capacitive current interruption

grid is represented by an AC voltage source u_s , an inductance L_s and a capacitance C_s whereas the load is a simple capacitor C_1 . When the switch S_{vac} , representing the VCB, opens at the time t_0 an arc ignites. Due to the arc characteristics, the current i_b is chopped at t_1 , prior to the natural current zero (see Section 2.3). At this moment, the system voltage u_s is nearly at its maximum because of the capacitive phase angle. In addition, the voltage across the capacitors is higher than the actual source voltage due to the effects of the inductance. This leads to a $\{1 - \cos\}$ - shaped recovery voltage u_{vac} across the switch with a source side $u_{s'}$ and load side u_l component. The source side transients are caused by oscillations between the elements C_s and L_s which disappear within several milli-seconds. At the load side, the capacitor stays charged because no discharge path is available.

It can be seen that, even without an over-voltage caused by a failure in the power grid, the voltage across the switch is doubled.

In a three-phase system, the current interruption, and therefore the *recovery voltage* (RV), also depends on the system earthing. In addition, a successful current interruption in one phase will affect the remaining two others. This influence can be expressed and taken into account in a single-phase system by the *first-pole-to-clear-factor* k_{pp} . In a *non-solidly-earthed neutral system*, this factor is 1.5 while it is 1.3 in a *solidly-earthed neutral system*. [SvK⁺15]

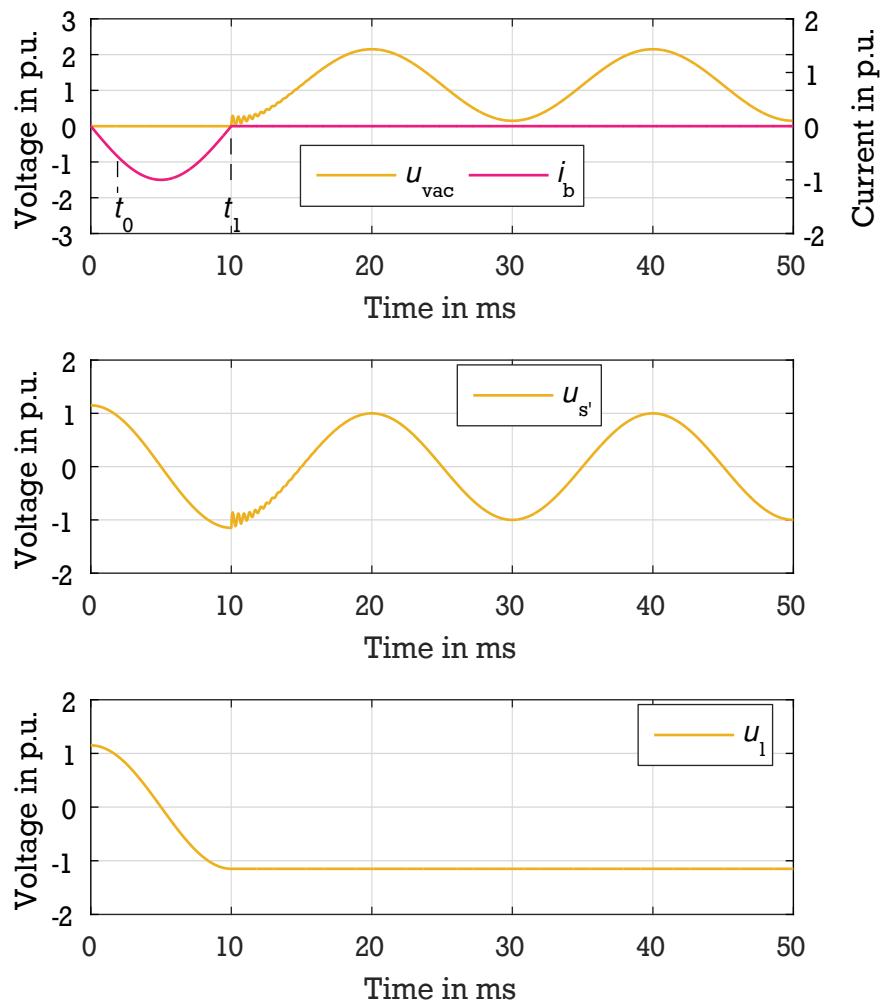


Abbildung 2.11: Current-/voltage-characteristic during capacitive load interruption; taken from [SvK⁺15]

2.4.4 Dielectric failures after a successful breaking operation

Immediately after a short circuit current interruption, plasma with a finite conductivity is still present between the opening contacts. As has been shown in Section 2.3, this leads to *post-arc currents* due to the (transient) RV which may reignite the arc. This kind of thermal breakdown is called *re-ignition*. In case of a capacitive current interruption, a thermal based breakdown is unlikely due to the small current amplitude. Here, breakdowns a few milli-seconds after current interruption are typically caused by a not yet sufficient gap distance. By definition of the standard, all failures within a quarter cycle of power frequency after current interruption are treated as pre-ignitions [Hig04].

Subsequent to a successful recombination of the plasma, the race between the increasing gap distance and the increasing RV begins. If, at any moment, the dielectric stress exceeds the dielectric strength, a *late-breakdown* occurs. In Section 2.2, it has been shown that, for a VI, two breakdown types exist. The first one is a NSDD where the voltage collapses without resulting in a renewed current flow in the main circuit. This type of breakdown is not considered directly²⁷ harmful for the VI or any connected equipment. Furthermore, their occurrence is not a sign of an insufficient VCB [Hig04]. The situation is different with a *restrike*, the second type of breakdown, where it comes to a renewed current flow in the main circuit. Due to the excellent current interruption capabilities of a VI, the occurring high frequency current is usually extinguished at the next current zero crossing. Thus, the load capacitance is recharged to the negative of the previous value plus the voltage difference across the VI at the time of breakdown. This is illustrated in Abbildung 2.12. In the worst scenario, the breakdown happens at the maximum of the RV causing a recharge from ± 1 p.u. to ∓ 3 p.u.. Extremely problematic are multiple restrikes, where this recharging is continuous in 2 p.u. steps. Finally, this may lead to a *voltage escalation* which can damage connected equipment if not limited by an adequate over-voltage protection [Sch08]. [SvK⁺15], [Lip03], [Sla08]

²⁷ However, a NSDD could cause restrikes

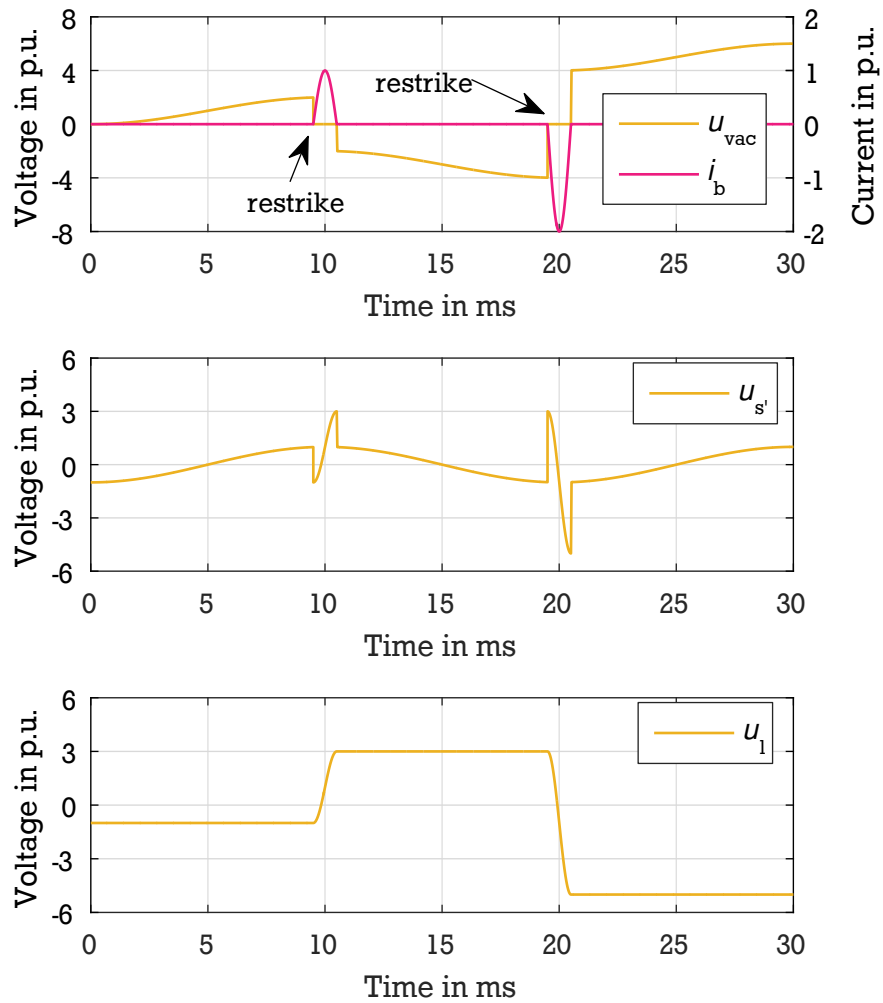


Abbildung 2.12: Multiple restrikes during capacitive load breaking; taken from [SvK⁺15]



3 Experimental investigations of late-breakdowns above the medium voltage level

This chapter discusses the challenges of future experimental investigations of late-breakdowns. Based on the recommendations given in CIGRE's technical brochure *The Impact of the Application of Vacuum Switchgear at Transmission Voltages* [CIG14], this discussion is focused on the capacitive switching duty. Therefore, this chapter starts with an analysis of suitable synthetic test circuit designs for a capacitive load switching. This is followed by a summary of the established research findings in this area. Afterwards, required test circuit parameters based on the applicable standards are taken into account. This chapter concludes with a set of derived design rules for a future test environment capable of investigating the phenomena of late-breakdowns in VCBs above the medium voltage level.

3.1 Experiences with synthetic test circuits for capacitive load switching

The test circuits used to investigate high voltage switchgear can be distinguished into three basic groups:

1. *The power grid*: Here, investigations are performed mostly within pilot projects [BGW⁺12]. In this case, the test object is used as a regular element of the grid. While these tests lead to realistic conditions, the amount of usable data is limited because switching operations are executed with respect to the needs of the power grid. Furthermore, possible risks for other components, in case of a failure, cannot be ruled out. Thus, for this kind of test, the test object has to have a high development state.
2. *Direct test circuit*: Here, the power grid is represented by special short circuit generators, transformers and lumped elements. These tests are offered in a limited number of high power test facilities around the world, for instance DNV GL KEMA Laboratories (Arnhem, The Netherlands) or XIHARI (Xi'an, China). Besides various advantages, such as a high number of switching operations, the utilization of measurement equipment and the possibility to perform a type test, the costs are rather high and the availability is limited. [SvK⁺15]
3. *Synthetic test circuit*: Here, the single big power source is replaced by at least two smaller ones, where each one is optimized either for high voltage or high current. As a consequence, these sources have to be connected to the test object with additional auxiliary systems to achieve comparable test conditions. This makes the layout of a synthetic test circuit more complex. Thus, there exist optimized designs for particular switching operations¹. However, the advantages are reduced space

¹ for instance, the *Weil-Dobke* circuit [Kap11]

requirements, lower costs, limited energy input in case of a failure, a separate control of current and voltage stresses and the possibility to include additional diagnostic tools more easily. [RC77], [KF95], [SvK⁺15]

For research and development purposes, almost exclusively synthetic tests are used which are not necessarily in accordance to the standards. Based on the fact that circuit breakers can easily conduct any capacitive load current² a pure *conduction phase* is not included in a capacitive switching test; only the few half-cycles of the breaking current, which are necessary to ignite an appropriate arc, are realized. Consequently, the following three phases have to be realized with the test circuit: *making*, *breaking* and *recovery*.

The making phase is usually realized with a *LRC*-resonance circuit due to the inrush current's high frequency and decaying amplitude [DGK⁺04], [DRG10], [KHSL10], [DTSY12], [YGL⁺14], [YWY⁺14]. Based on the missing conduction phase, this is a stand-alone test. However, the transition from the breaking to the recovery phase is continuous, and has, therefore, to be tested together. For this purpose, the test circuit principle shown in Abbildung 3.1 has been frequently used in recent years in the medium voltage level [DTSY12], [KHSL11], [YGL⁺14].

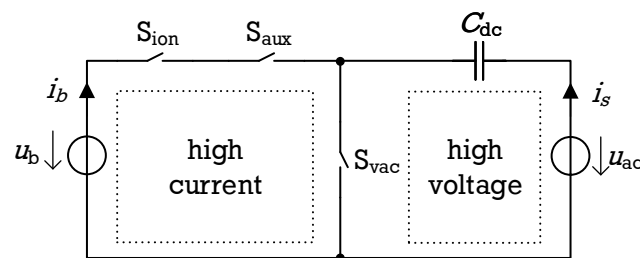


Abbildung 3.1: ECD for synthetic capacitive current interruption test

Besides the *regular* current-/voltage-characteristic, tests were also performed, where

- the $\{1 - \cos\}$ - shaped RV was replaced with a higher DC voltage [YSM⁺08],
- no breaking current was applied [DGK⁺04], [Kör08], or,
- the $\{1 - \cos\}$ - shaped RV was applied to the test object several milli-seconds after the arc has been extinguished by an additional voltage making switch [KLKG07].

Within this work, the breaking current and the $\{1 - \cos\}$ - shaped RV are realized. For this reason, the circuit shown in Abbildung 3.1 is described in more detail. In general, it is divided into a high voltage and a high current sub-circuit. Moreover, it needs a certain synchronization and control principle.

High current sub-circuit

This sub-circuit contains the voltage source u_b , the auxiliary switch S_{aux} and the (precise) current making switch S_{ion} . Besides the actual breaking current i_b , this circuit must be able to provide the (arc) voltage demands of the test object and the auxiliary breaker during contact separation. Due to the low vacuum

² due to its small amplitude compared to other operating currents

arc voltage³ [Sla08] and the moderate current amplitudes, the regular 400 V power grid can be utilized to provide current for a few periods [KHSL11]. Alternatively, a *LRC*-resonance circuit can be used [KLKG07], [YSM⁺08], [DTSY12], [YWY⁺14]. In any case, the breaking current i_b has to be switched on by the making switch to synchronize it with the high voltage sub-circuit. After the breaking phase, the high-current sub-circuit has to be separated and isolated from the test object. For this, the auxiliary switch is used. Thus, this switch has to conduct the breaking current i_b as well as to safely withstand the test voltage u_{vac} .

High voltage sub-circuit

This sub-circuit contains the voltage source u_{ac} (usually a high voltage test transformer), the capacitor C_{dc} and the test object S_{vac} . In order to provide the $\{1 - \cos\}$ - shaped RV, the voltage across the capacitor has to be equal to the amplitude of u_{ac} . To achieve this, the test object has to be operated in a certain way: In the beginning, S_{vac} is closed and a small capacitive current i_s flows. By opening S_{vac} , the current continues to flow through the burning arc until it extinguishes. After this moment, the charge carriers on the capacitor are trapped. In case of a perfect synchronization, the currents i_b and i_s have the same phase. This leads to a DC voltage across C_{dc} which matches the amplitude of u_{ac} resulting in a $\{1 - \cos\}$ - shaped RV.

Synchronization and control

The difficulty with any synthetic test circuits lies in the synchronization of the sub-circuits. In the present case, both power sources, the auxiliary switch and the current making switch, have to be controlled precisely to prevent unnecessary stress to the equipment. In addition, an exact control of the test object is needed to achieve a fixed and reproducible breaking (arcing) time. Therefore, this type of test circuit has to be controlled actively. However, the following two simplifications are possible:

Simplification 1: Test and auxiliary switch are mechanically combined

As long as the test switch is closed, the voltage u_{vac} cannot build up and the high current sub-circuit is short circuited. Thus, both sub-circuits cannot interfere with each other. However, as soon as the test object opens, the auxiliary switch has to disconnect the high current sub-circuit at the next current zero crossing at the latest. To ensure this, it can be mechanically linked to the test switch. In practice, this is realized with a three-phase circuit breaker. Here, one pole assembly is used as the test object while the remaining two others are connected in series and function as the auxiliary switch. In this way, it is also ensured that the auxiliary switch has a higher dielectric strength than the test object. [Koo11]

Simplification 2: Both power sources are connected to the identical grid

Between the breaking current i_b and the voltage source u_{ac} , a phase angle of $\varphi_c = -\frac{\pi}{2}$ is needed. This can be achieved by using an additional impedance Z_b in the breaking current path. By this means, the amplitude of the breaking current can also be adjusted. The impedance can either be an inductance L_b or a resistor R_b .

In Abbildung 3.2, the configuration with an inductance is shown. Here, both the voltage and the

³ several ten volts

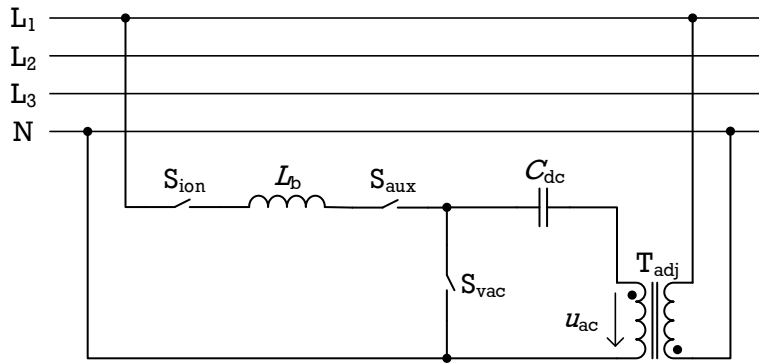


Abbildung 3.2: ECD for synthetic capacitive current interruption test

current source are connected to an identical phase which results in a phase angle of $\frac{\pi}{2}$. This is changed to a capacitive phase angle at the voltage source with the transformer T_{adj} . [Koo11]

The resistor configuration is shown in Abbildung 3.3. Here, the current source is connected between

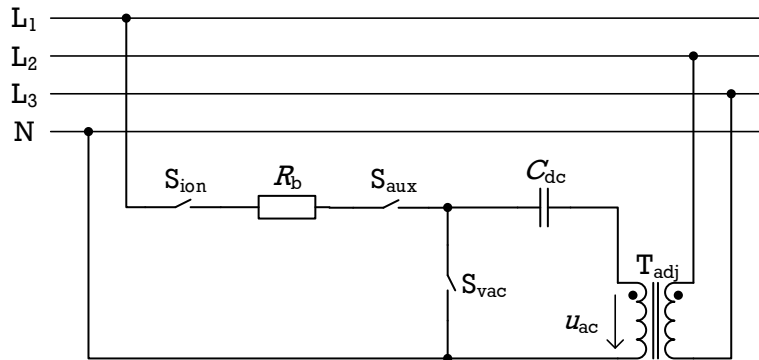


Abbildung 3.3: ECD for synthetic capacitive current interruption test

neutral N and phase L_1 . The voltage source is connected between the two remaining phases L_2 and L_3 . Now, both sources have a different reference level. To compensate this, an isolation transformer (T_{adj}) is required.

3.2 Established research findings

In the following, the main statements of established research findings are summarized. Given the scope of this work as well as the current VCB manufacturing technology, only publications based on VCBs with copper-chromium contact systems and capacitive loads are included.

- The impact of contact bouncing during making operations does not degrade the switching capability of the VCB [DZ10], [SCG⁺12].
- High inrush currents increase the breakdown probability [DTSY12] and the field-emission current amplitude [KHSL10], [YWY⁺14]. Below inrush currents of 10 kA field-emission currents are low [SKCS12].

- A low prestrike field strength (down to 1.78 kV mm^{-1}) correlates with a high field-emission current [Kör08].
- A fast closing speed increases the dielectric performance [DRG10].
- The capacitive arc current and its duration have a strong effect on the field-emission current [KHSL10], [SKCS12], [DYTM14]. In two of these publications, it has been shown that a lower arcing time increases the field-emission current [KHSL10], [SKCS12].
- The majority of late-breakdowns occur within 100 ms after the current interruption [Kör08], [Koo11]. In one of these publications, approximately 50 % of all late-breakdowns occur during the first 10 ms [Kör08].
- Field-emission currents exhibit fluctuations which might be linked to particle interactions [Koo11].
- Late-breakdowns are not necessarily preceded by high field-emission currents [Kör08], [KHSL10], [SKCS12]. So far, their origins are still inconclusive. For example, in one publication, field-emission currents are the primary source [DWG⁺06], while in another one, micro-particles are the most influencing factor [SCG⁺12].
- Mechanical shocks increase the occurrence of late-breakdowns either by micro-particle interactions [Far93], [GH93], [SEG⁺10] or due to field-emission current instabilities [JLD99].
- At higher rated voltages late-breakdown occurs more frequently [CIG14].

3.3 Test circuit parameters according to the standards

The requirements on electrical switchgear are regulated in several standards. For AC circuit breakers, these are the following:

- IEC 62271: High-voltage switchgear and controlgear
- IEEE C37-09: Standard Test Procedure for AC High-Voltage Circuit Breakers Rated on a Symmetrical Current Basis
- JEC 2300: Alternating current circuit breakers
- Chinese standard GB 1984: High-voltage alternating-current circuit-breakers

Among these standards, this work is oriented at the IEC 62271 part 100. In the following, the relevant information regarding the test circuit parameters for capacitive load switching with a 72.5 kV VCB are extracted.

Test voltage

The peak value of the single-phase test voltage \hat{U}_{test} is derived from Equation (3.1).

$$\hat{U}_{\text{vac}} = \frac{\sqrt{2}}{\sqrt{3}} \cdot 2 \cdot k_c \cdot U_s \quad (3.1)$$

In this equation, U_s is the highest value of the phase-to-phase operating voltage (r.m.s. value) and k_c the capacitive voltage factor. While the system voltage is defined by the VI's design voltage, the capacitive voltage factor depends on the neutral point treatment and the associated fault scenarios. In an solidly earthed neutral system, k_c is typically 1.4 in the presence of single- or two-phase earth faults. This value is increased to 1.7 in case of an unearthed neutral system. Thus, the highest test voltage \widehat{U}_{vac} is 201 kV⁴. This voltage has to be maintained, including the DC voltage component, for at least 300 ms after current interruption.

Breaking current

The current amplitudes are different depending on the component to be switched. Their r.m.s. values are 10 A for transmission lines, 125 A for power cables and 400 A for capacitors⁵. In addition, the current waveform should be, as nearly as possible, sinusoidal. This is achieved with a ratio between the r.m.s. value of the current to the r.m.s. value of the fundamental of less than 1.2. Furthermore, the breaking current shall not have more than one zero crossing per half-cycle of the power frequency.

Inrush current

An inrush current is only defined for back-to-back switching of capacitor banks. For this configuration, the rated amplitude is 20 kA with a frequency of 4250 Hz. The ratio between the first peak and the second peak of the same polarity has to be equal to or higher than 0.85.

3.4 Identified challenges of future investigations

Based on the established research findings and the experiences with synthetic test circuits, the following challenges of future investigations of VCBs above the medium voltage level can be identified. In general, they can be separated into two categories: handling of (low power) synthetic test circuits and detection of pre-breakdowns currents.

3.4.1 Handling of (low power) synthetic test circuits

The necessity to use test transformers for research and development tests affects the quality of the RV. With respect to a capacitive load switching test based on the test circuit design discussed in Section 3.1, this results in a decay in the DC component in addition to distortions in the AC component of the RV.

Decay of the direct voltage component

The DC component is usually generated by the test circuit principle shown in Abbildung 3.1. Here, a capacitor is charged directly by the high voltage test transformer prior to the RV. During the recovery period, it is continuously discharged by the field-emission currents and other leakage currents. An example of this voltage drop is shown in Abbildung 3.4, where the capacitor C_{dc} has 10 nF. The charge drawn from this capacitor⁶ due to field-emission currents is 110 μ C. This reduces the initial 35 kV DC voltage

⁴ for the sake of simplicity, \widehat{U}_{vac} is set to 200 kV

⁵ The presence of earth faults can be taken into account with an amplitude increased by a factor of 1.25.

⁶ The initial charge is 350 μ C.

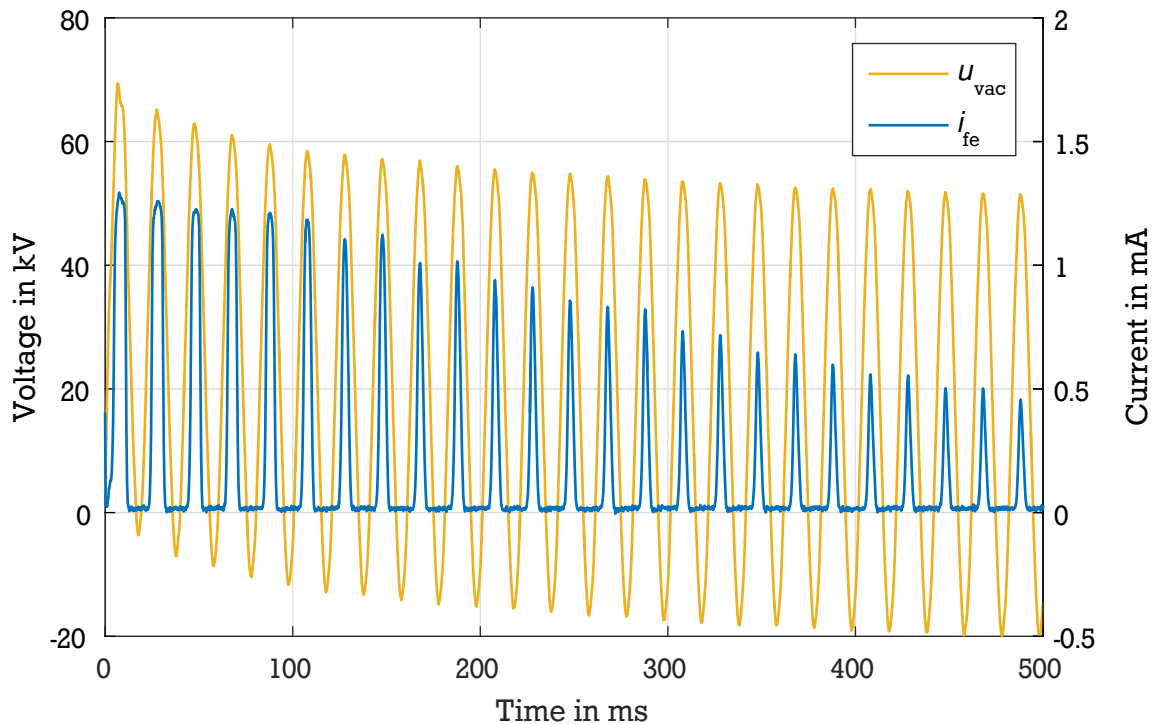


Abbildung 3.4: Direct voltage component decay due to field-emission current, adapted from data used in [Koo11]

by 32 % within the first 500 ms. Such voltage drop might be possible in the power grid with a short open-ended transmission line (low capacitance). However, it is highly unlikely during a capacitor bank switching, and it is also in direct violation of the voltage quality required by the standard.

As the power of the high voltage test transformer is limited, the load impedance towards higher test voltages is larger. As a consequence, the possible capacitance has to be smaller. Thus, the decay in the DC component will become more severe. At a certain point, the available capacitance is too small to ensure the required voltage quality. Therefore, the capacitance C_{dc} cannot be powered directly by the test transformer anymore. In fact, it has to be pre-charged with the consequence that the RV has to be connected to the test object by an additional voltage making switch.

Such a switch is, for instance, used in the publications of Körner [KLKG07], [KLKG08]. There, the RV is connected to the test object after the gap is completely open. This approach has two advantages. First, the making switch starts to close after the arc in the test object is already extinguished. Therefore, a pre-ignition in the making switch does not lead to a discharge of the pre-charged capacitor C_{dc} . Second, the electromagnetic interference (EMI), due to the voltage making, hardly triggers a dielectric breakdown in the test object because of the completely open gap.

Towards VCBs with higher rated voltages, the duration to reach a completely open and stable gap takes longer. Furthermore, the effects of micro-particles can be expected to be higher due to their voltage dependent impact velocity. As their generation and release is strongly coupled to contact erosion (arcing) and mechanical shocks (caused by the contact separation), the RV should be connected to the test object immediately after the arc is extinguished⁷. This is also recommended, considering the fact that most

⁷ So far, this has not been realized in a (low power) synthetic test circuit.

dielectric breakdowns occur within the first 100 ms of the recovery phase. Thus, a fast voltage making switch is necessary in a (low power) synthetic test circuit.

Distortions in the alternating voltage component

Another consequence of a test transformer’s low power is its high short-circuit impedance [KF95]. Thus, even a small current flow⁸ will cause a significant internal voltage drop. Hence, the voltage across the test object is reduced, and, in case of the non-linear nature of field-emission currents, it is also distorted. An example of this is shown in Abbildung 3.5 with a point-plate electrode arrangement in vacuum. Here,

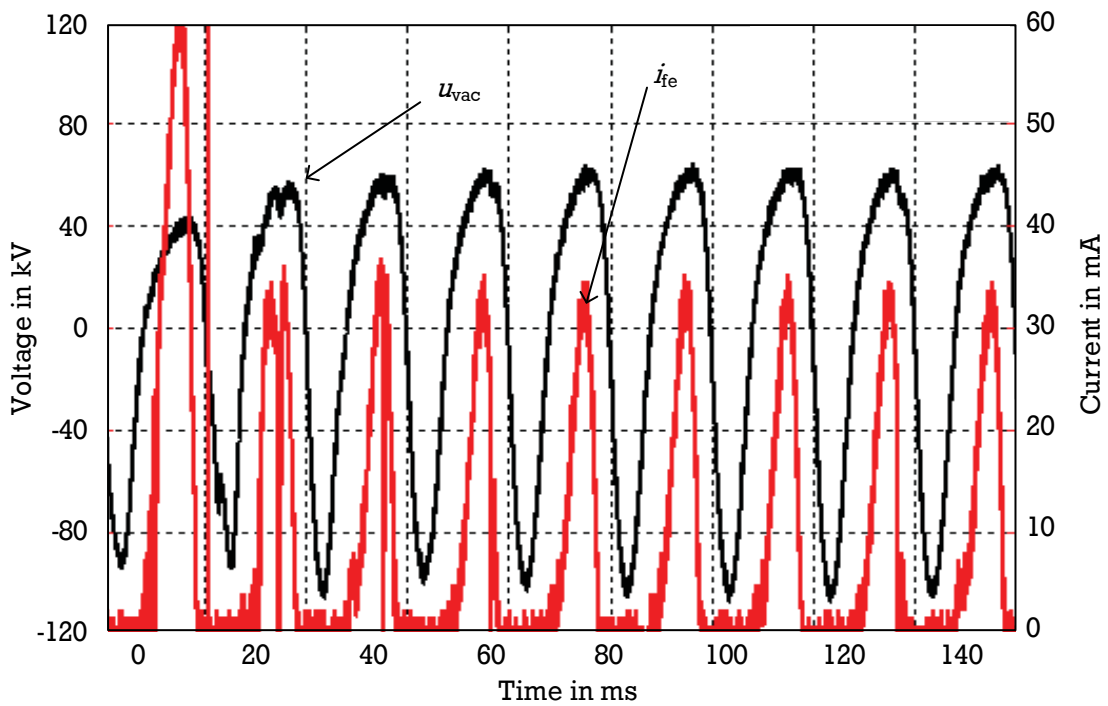


Abbildung 3.5: Voltage distortions caused by field-emission currents in a point-plate arrangement; adapted from [XKH⁺ 15]

the distortions are so severe that the voltage in the positive half-cycle⁹ hardly reaches 50 % of the no load voltage. The main issue with these voltage drops is the fact, that field-emission currents cannot exceed a certain amplitude and steepness. Thus, the available power to this pre-breakdown phenomena is limited. As a consequence, a lower breakdown probability, compared to a VCB investigated with a direct test circuit, has to be expected.

Since it is not possible to avoid this limitation, affected measurements have to be identified to avoid mistakes during their interpretation. In addition, a test circuit needs to be optimized towards a high test rate to gain a statistical coverage even with a low breakdown probability.

⁸ referred to the rated current of the test transformer

⁹ Here, field-emission currents occur.

3.4.2 Measurement of field-emission currents

The measurement of field-emission currents during the recovery phase is sometimes used in capacitive switching tests. As a measurement device, a resistor R_{lf} is utilized due to the relatively low current amplitude and frequency. To protect it against inrush and breaking currents, anti-parallel diodes are connected to the resistor [BBMR93]. The advantage of this principle lies in the automatic commutation of the current from the resistor to the diodes and back. Therefore, no control system is needed which makes this principle especially suitable for direct tests [SKCS12]. However, a disadvantage is the limited measurement resolution. Its upper limit is defined by the forward bias *voltage* [BBMR93] of the diode. If it is exceeded, the diode becomes more conductive and parts of the current bypass the measurement resistor R_{lf} . This limit can be extended to a certain degree by either reducing the value of the resistor¹⁰ or utilizing multiple diodes in series¹¹. The lower limit is defined by the leakage current of the diode which itself is linked to its possible forward current [GPS⁺51]. Thus, the necessity to conduct inrush currents has the consequence that leakage currents can reach the lower range of field-emission currents.

Furthermore, the resistor R_{lf} does not measure the pure field-emission current i_{fe} . Instead, it measures the (total) *low frequent current*¹² i_{lf} which additionally contains the power frequency capacitive displacement current i_c . However, this capacitive current can be compensated subsequently [KHK10], because its amplitude depends entirely on the voltage u_{vac} and the capacitance C_{vac} of the test object. The latter is constant as soon as the test object's contacts are open and their oscillations have stopped. An example of such a compensation is shown in Abbildung 3.6. Here, the voltage u_{vac} and the total current i_{lf} were measured and the field-emission current i_{fe} was calculated by a software compensation [KHK10].

The problem with the current i_c is that it has to be taken into account while dimensioning the resistor R_{lf} , even if the field-emission currents are smaller. Towards higher system voltages, the capacitive displacement current increases over-proportionately due to the need of additional external field grading elements. At the same time, field-emission currents are expected to be smaller due to the over-proportional increase of the gap distance [Lip03]. Therefore, achieving a sufficient low measurement uncertainty with a diode protected system is a challenge when a high number of consecutive capacitive switching operations are desired.

A characteristic of synthetic test circuits are the predefined periods of breaking and recovery. In addition, in case of a dielectric breakdown during the recovery phase, high inrush currents cannot occur¹³. Therefore, in a synthetic test circuit, the anti-parallel diodes can be replaced by a protection which does not have such severe restrictions.

3.4.3 Additional detection of micro-particles

So far, almost exclusively the field-emission current has been measured during capacitive load switching tests while the influences of micro-particles have only been investigated indirectly, for instance, with the following tests:

¹⁰ results in a smaller measurement signal

¹¹ requires additional grading elements to equalize the voltage stress across each diode during a dielectric breakdown of the VCB

¹² Compared to the typical currents caused by charged micro-particles, this current has a low frequency.

¹³ The high current sub-circuit is already disconnected and the energy is entirely supplied by the high voltage sub-circuit.

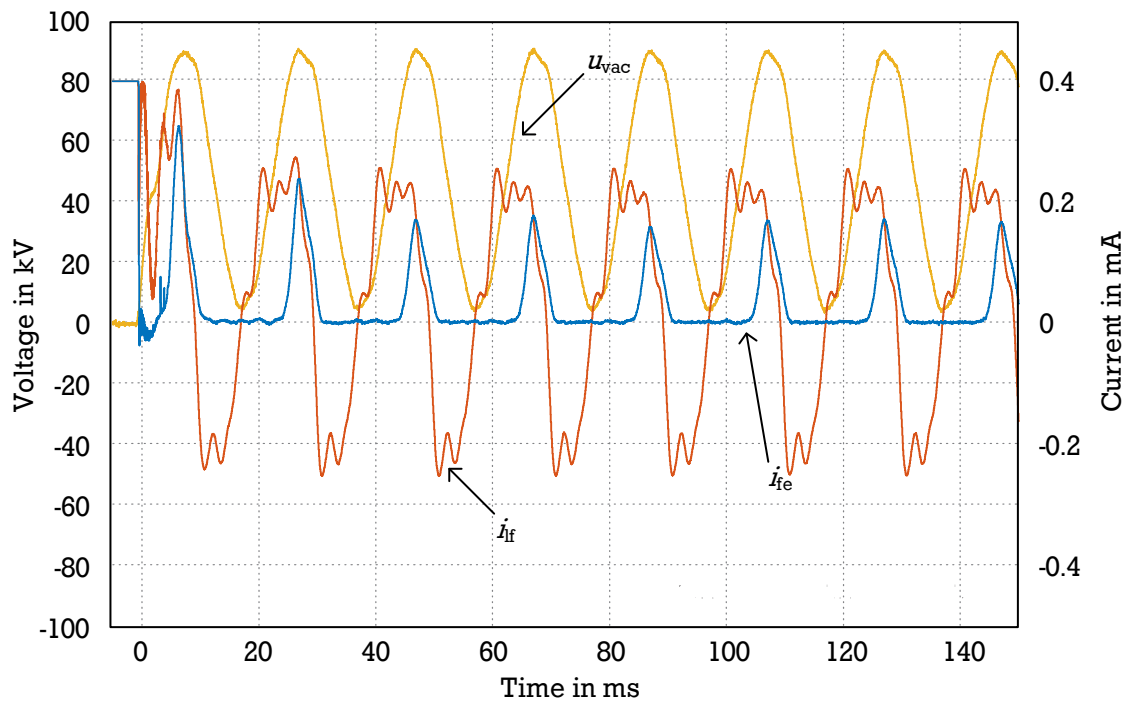


Abbildung 3.6: Comparison of the measured (total) low frequent current and the field-emission current; adapted from [Koo11]

- probability increase by rising the mechanical shocks during switching [GH93]
- occurrence increase by adding artificial micro-particles into a vacuum chamber [Sla08], [Lat95]
- detection of micro-particles electrically and visually in a model vacuum chamber [SKF00], [KMK⁺14]

However, especially a switching operation itself generates and releases micro-particles. Thus, future test environments have to be able to detect micro-particles in order to investigate late-breakdowns. For this purpose, two objectives have to be accomplished. First, a suitable measurement principle has to be identified. Second, the test circuit must have a low partial discharge (PD) and low EMI level (see Section 6.3) to be able to even detect micro-particles. Otherwise, these disturbances could be mistaken for micro-particle events.

In addition, there is evidence that late-breakdowns may be initiated by a mutual interaction between field-emission currents and micro-particles. Examples for this are the sudden start of field-emission currents [SK13] and their instabilities [JLD99]. Thus, this additional detection of micro-particles should be simultaneous with a field-emission current measurement.

4 Goal of this work

Currently, the vacuum switching technology is the standard in the medium voltage level. Although a closed theory about the dielectric properties has not yet been found (see Kapitel 2), the general demand for greenhouse gas free switchgear pushes the development of this technology towards higher voltages. The motivation of this work is subordinated to this objective, and, its goal is the development of a test environment to investigate high voltage VCB. More, specifically the following objectives are to be achieved:

1. The challenges towards dielectric testing of high voltage VCBs shall be derived. Special attention shall be devoted to the phenomena of late-breakdowns which occur in form of restrikes and NSDDs during capacitive load switching. For this purpose, the established research findings in this area as well as the experiences from test equipment used in the medium voltage level shall be taken into account. The results are then used as design criteria for the new test environment. This objective is documented in Kapitel 3.
2. A (low power) synthetic test circuit to investigate 72.5 kV VCBs shall be designed and commissioned. Its switching duty is the making and breaking of capacitive loads with the following rated parameters: 20 kA inrush current, 2000 A breaking current and 200 kV $\{1 - \cos\}$ - shaped RV. Based on the derived design criteria, the following aspects shall be improved compared to similar test circuits used in the medium voltage level.
 - The RV's DC component decay shall be reduced to gain a more realistic test scenario. This shall be accomplished by using independent voltage sources in the generation of the RV's AC and DC component. Finally, the RV shall be applied to the test object immediately after the breaking phase via a fast voltage making switch which shall be especially developed for this purpose.
 - The PD and EMI level of the test circuit shall be minimized to allow detection of micro-particles.

These objectives are documented in Kapitel 5.

3. Measurement systems to detect field-emission currents and micro-particles shall be implemented into the test circuit. In detail, the following tasks shall be accomplished:
 - The existing principle to measure field-emission currents shall be adapted towards a high number of consecutive capacitive switching operations by replacing its passive diode protection by an actively controlled switch.
 - The differences between these two protection principles shall be experimentally investigated to identify possible error sources.
 - The analysis of field-emission currents shall be extended with a harmonic analysis of the RV to identify possible interferences by the test circuit.

-
- A suitable measurement system to detect (charged) micro-particles shortly after a breaking operation shall be identified.
 - Both detection systems shall be implemented in such a way that a simultaneous measurement of field-emission currents and micro-particles is possible.
 - Tests shall be conducted to investigate the mutual interference of both systems in order to identify the best measurement circuitry.

These objectives are documented in Kapitel 6.

4. Finally, the new test environment shall be discussed. This includes the possibilities of the test circuit, but also its differences to a direct test. In addition, based on the preliminary measurement results, a suitable framework for an experimental investigation of high voltage VCBs shall be presented. This objective is documented in Kapitel 7.

5 Test circuit

In this chapter, the realized test circuit and its features are discussed. It starts with a list of requirements for the test circuit before the selected circuit topology is presented. This is followed by a brief summary of the measurement systems and the data acquisition. In the three subsequent sections, the test circuit's main components, namely the test object, the high current sub-circuit and the high voltage sub-circuit are described. This chapter ends with a discussion about the differences of the realized (synthetic) test circuit compared to a direct capacitive switching operation.

5.1 Requirements

The objective of this work is the development of a test environment to investigate the phenomena of late-breakdowns of 72.5 kV VIs during capacitive load switching. For this purpose, a test circuit with the current-/voltage-characteristic shown in Abbildung 5.1 is required. Based on the common test principle

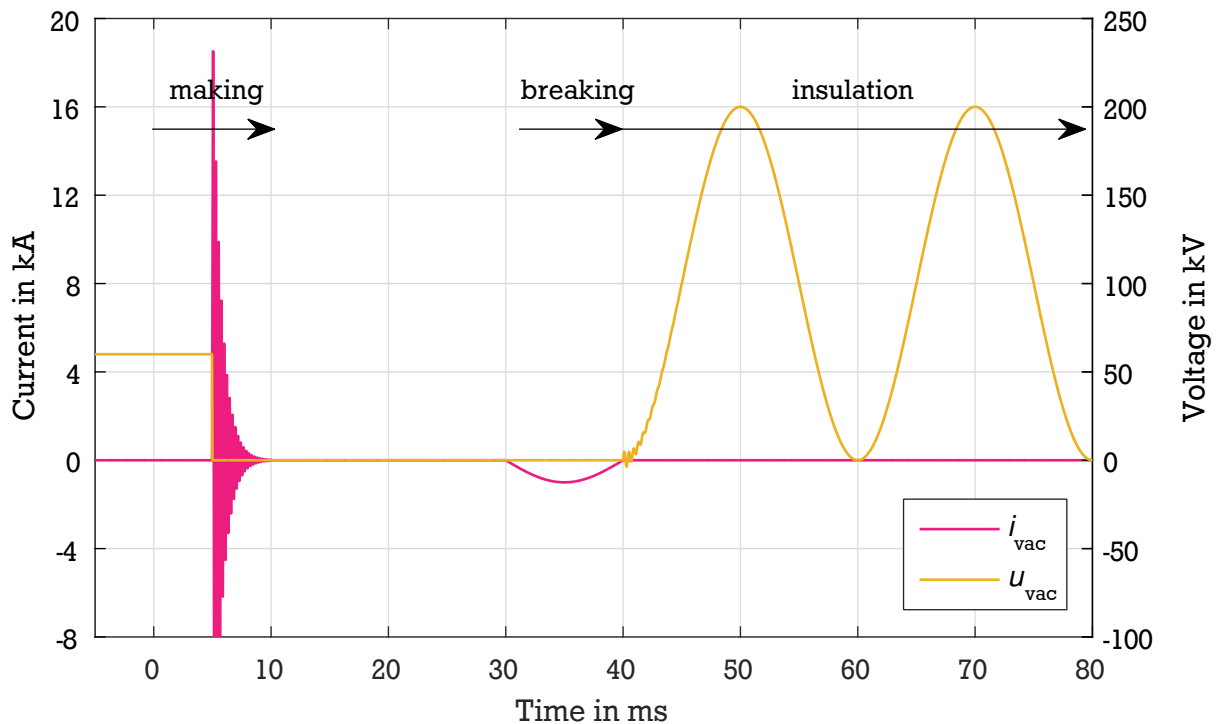


Abbildung 5.1: Single-phase capacitive-load switching

used in the medium voltage level (see Section 3.1), this *high voltage* test circuit has to fulfill the following *additional* requirements:

- low PD and EMI level of all high voltage sub-circuit components and their associated auxiliary systems

- increased value of the capacitor in the DC voltage source which is equipped with an independent¹ charging system
- implementation of a voltage making switch to apply the RV to the test object

5.2 Basic layout

The simplified ECD of the realized test circuit is shown in Abbildung 5.2 while an overview of the whole test setup is located in the Appendix. It consists of a high voltage and a high current sub-circuit which are

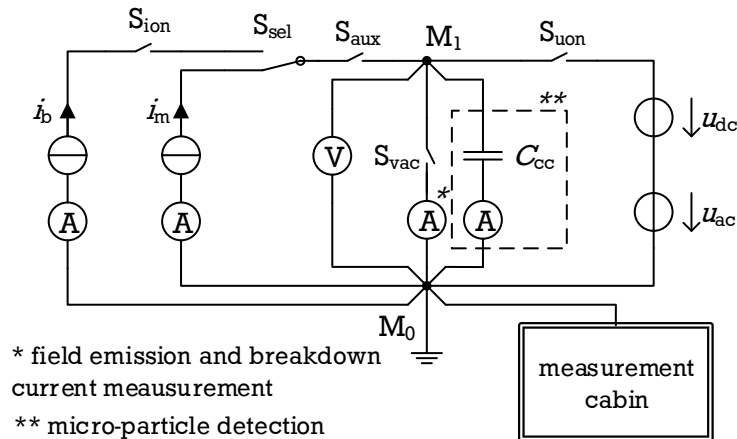


Abbildung 5.2: Basic layout of the test circuit

described in Section 5.6 and Section 5.5, respectively. Both sub-circuits are interconnected at the high voltage point M_1 and at the star shaped reference point M_0 . Between these points, the test object S_{vac} (described in Section 5.4) and the coupling capacitor C_{cc} are connected. In addition, a galvanically isolated measurement cabin is connected to M_0 . To provide a better overview of the measurement systems, they are described separately in Section 5.3.

Within this test circuit, the *coupling capacitor* C_{cc} is used for the following reasons:

- supply *fast*² energy for a breakdown during the recovery phase [JS81]
- function as a coupling capacitor in the micro-particle detection (see Section 6.3)

In all cases, a larger capacitance is an advantage. However, due to power restrictions in the high voltage sub-circuit its value is limited. As a compromise, a capacitor with the specification given in Tabelle 5.1 is used.

Operating sequences

The test circuit reproduces the switch on (making) and switch off (breaking) of a capacitive load. For this, certain operating sequences are necessary. In preparation for the making operation, the following switches are idle and locked in their respective position: S_{aux} (closed), S_{ion} (open), S_{uon} (open) and S_{sel} (lower position). In this sequence, the inrush current is triggered by closing S_{vac} . In contrast to this, the breaking operation³ requires a defined sequence with four steps which are shown in Tabelle 5.2. To avoid

¹ independent from the high voltage test transformer which is used to provide the AC part of the RV

² low inductive loop

³ S_{sel} is in the upper position.

Tabelle 5.1: Specification of the coupling capacitor C_{cc} [Omi16]

rated voltage	200 kV
capacitance	1 nF ($\pm 10\%$)
PD level	< 1 pC @ 200 kV
withstand voltage	240 kV

(possible) interference in the micro-particle detection, the involved switches and their auxiliary systems have to be idle within 5 ms after the breaking period.

Tabelle 5.2: Sequence for a capacitive breaking operation

period	S_{vac}	S_{aux}	S_{ion}	S_{uon}
idle	close	close	open	open
conduction	close	close	close	open
breaking	opening	opening	close	closing
recovery	open	open	open	close

Control system and interfaces

Minimizing the EMIs during the recovery phase is a crucial requirement. Thus, as one of the precautionary measures, all control lines are fiber optic cables to prevent distortions⁴. The control system itself is a customized micro-controller, located inside the measurement cabin. To interpret and manage the test series, the software LabVIEW from National Instruments is used. This software communicates with the control system and the data acquisition hardware (see Section 5.3). The actual data analysis is performed with the software Matlab.

5.3 Overview of the measurement systems and data acquisition

An overview of the used measurement systems is given in Tabelle 5.3. As can be seen from Abbildung 5.2,

Tabelle 5.3: Overview of the measurement systems

signal	uncertainty	model	physical principle
u_{vac}	$< 1\%$	North Star VD-150	ohmic-capacitive voltage divider
d_{vac}	± 1 mm	Penny & Giles SLS190	potentiometer
i_m	$< 1\%$	PEM CWT 150	Rogowski coil
i_b	$< 1\%$	LEM HTA1000-S	hall effect current sensor
i_{lf}	$< 1\%$	customized	resistor
$i_{hf,cc}$	-	OMICRON CLP 542	PD measuring impedance

the inrush current i_m , as well as the breaking current i_b , are measured in their respective return wires. To eliminate unwanted feedback effects, a galvanically isolated measurement principle is used in both cases. However, this is not practicable with the low frequent current⁵ i_{lf} . Instead, a resistor based current

⁴ for instance, due to ground loops and crosstalk

⁵ contains the field-emission current i_{fe} and the capacitive displacement current i_c

measurement is utilized which leads to a mutual interference with the charged micro-particle detection system. The latter consists of the coupling capacitor C_{cc} and the PD measuring impedance Z_{cc} and captures the decaying high frequency currents $i_{hf,cc}$ caused by charged micro-particles. The mutual interference between both systems is discussed in Section 6.1 while their corresponding descriptions are given in Section 6.2 and Section 6.3, respectively.

In order to measure the voltage u_{vac} across the VCB, a mixed ohmic-capacitive voltage divider (specification in Tabelle 5.4) is used and connected between the high voltage point M_1 and the reference point M_0 . Thus, it also measures the additional voltage drop of the field-emission current measurement system. However, this is in the range of several volts and can therefore be neglected.

Tabelle 5.4: Specification of the voltage divider [Nor13]

maximum direct voltage	150 kV
maximum pulse voltage	240 kV
uncertainty (< 1 MHz)	< 1 %
capacitance $C_{V_{vac}}$ (approx.)	27 pF
resistance	2 G Ω
partial discharge level	< 10 pC @ 200 kV

The data acquisition is implemented inside the shielded measurement cabin. With the exception of the high frequency current $i_{hf,cc}$ ⁶, all measurement signals are digitized using a National Instruments system. Its relevant specification is given in Tabelle 5.5. The current $i_{hf,cc}$ is measured with a stand-alone

Tabelle 5.5: Specification of the low frequent data acquisition system [Nat05]

model	National Instruments 6123 PXI
input impedance	100 M Ω 10 pF
physical bandwidth	500 kHz
input range	± 1.25 V – ± 10 V
maximum input voltage (peak)	± 36 V
maximum sampling rate	500 kS s ⁻¹
resolution	16-bit
memory	16 MS

oscilloscope due to its high frequency and possible over-voltages. In addition, it is measured at 50 Ω input impedance to avoid traveling waves. The relevant specification of the used oscilloscope is given in Tabelle 5.6.

All measurement lines are coaxial cables (type RG-58)⁷. To minimize EMIs and over-voltages, their outer shield is connected to the measurement cabin which, in turn, is connected to the reference point M_0 with a low inductive copper strip [SK07]. The measurement cabin itself is galvanically isolated via an isolation transformer.

⁶ decoupled current of a charged micro-particle

⁷ 50 Ω impedance

Tabelle 5.6: Specification of the high frequency data acquisition system [Tel15]

model	Teledyne LeCroy WaveSurfer 3024
input impedance	50 Ω
physical bandwidth	200 MHz
input range	8 mV – 8 V
maximum input voltage (peak)	± 10 V
maximum sampling rate	2 GS s ⁻¹
resolution	8-bit
memory	10 MS

5.4 Test object

In order to ensure a wide variation of possible test objects, a VI with a design voltage of 72.5 kV is used. Its specification is given in Tabelle 5.7. Compared to a typical medium voltage design (see Abbildung 2.2),

Tabelle 5.7: Specification of the test objects S_{vac} [Sie12a]

rated voltage	72.5 kV
rated normal current	2.5 kA
rated frequency	50 Hz
rated gap distance	40 mm
rated pressure	$< 1 \times 10^{-7}$ mbar
contact system	axial magnetic field

this VI has two additional internal field grading shields⁸. They have, same as to the vapor shield, a floating potential which has to be taken into account when analyzing the measured data.

The test object itself is operated with a switching platform. Within this test circuit, a customized design⁹ is used to ensure a low PD level. Its high voltage part is shown in Abbildung 5.3. It consists of the test object, which is mounted horizontally inside an acrylic glass (PMMA) enclosure¹⁰. The space between both components is filled with the liquid insulation medium FC-43 because of its high dielectric strength (18.1 kV mm⁻¹), low dielectric constant (1.90) and non-flammability [3M99]. The necessary *external* field control is achieved using metallic toroidal structures on both sides.

In Section 3.2 it has been stated that the operating mechanism's mechanical chain influences the probability of late-breakdowns. To investigate this fact also at higher voltage levels, an adjustable mechanical chain in terms of opening speed, closing speed and contact force is needed. Therefore, a hydraulic actuator is utilized instead of a spring mechanism¹¹. The movement is transferred to the test object via an operation rod and a spring. In this case, the spring is used to damp the mechanical shocks during contact separation and to ensure a contact force in closed position. It is located between the actuator and the operation rod. The gap distance is measured at the movable contact of the test object against the housing of the switching platform with a potentiometer (see Section 5.3).

⁸ For confidentiality reasons, a cross section of the test object is not in this work.

⁹ developed in cooperation with Siemens AG

¹⁰ poly(methyl methacrylate)

¹¹ A magnetic actuator was excluded in an early stage of this project due to EMI concerns.

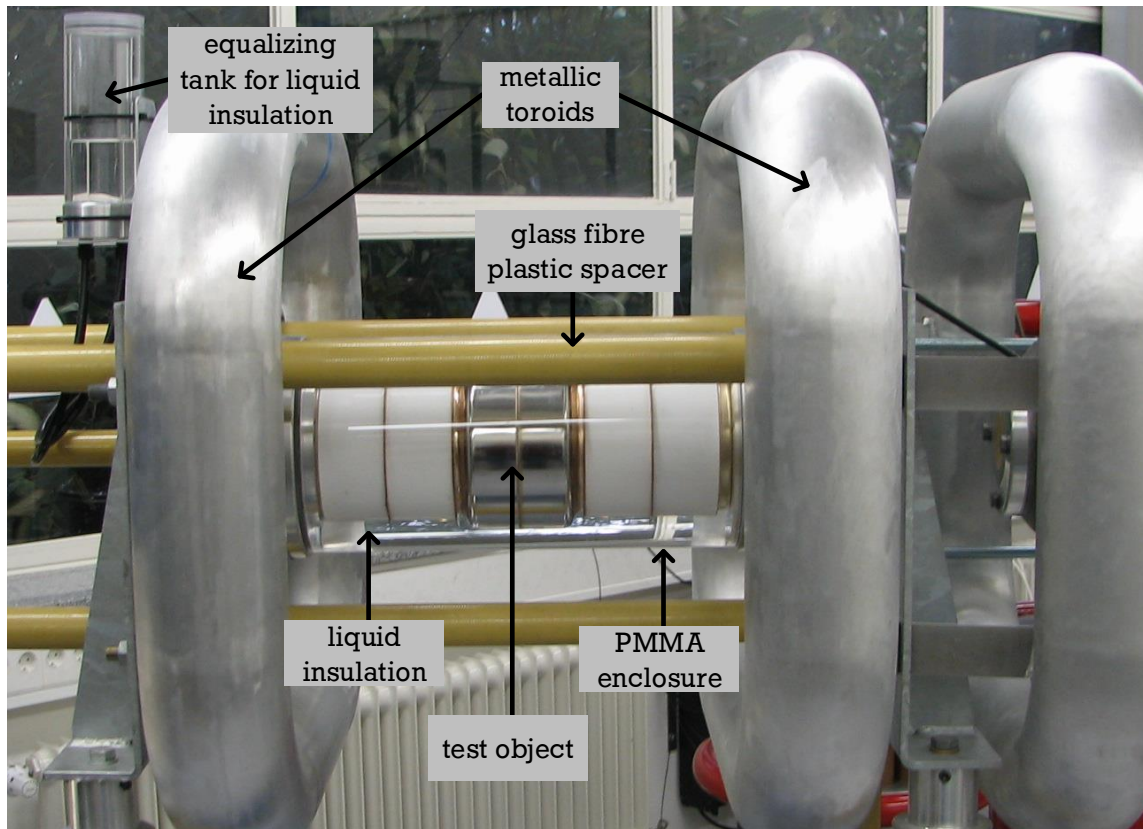


Abbildung 5.3: High voltage part of the test platform

In Tabelle 5.8, the mechanical and electrical specification of the test platform in combination with the test object is given.

Tabelle 5.8: Specification of the test platform

rated power frequency withstand voltage	220 kV
closing speed (no load condition)	$0.5 \text{ m s}^{-1} - 1 \text{ m s}^{-1}$
opening speed	$0.5 \text{ m s}^{-1} - 2.5 \text{ m s}^{-1}$
contact force	2 kN – 3.2 kN
gap distance	4 mm – 40 mm

5.5 High current sub-circuit

Abbildung 5.4 shows the simplified ECD of the high current sub-circuit¹². It includes the breaking and inrush current source, the current selection switch S_{sel} , the auxiliary breaker¹³ S_{aux} and the current making switch S_{ion} .

The auxiliary breaker S_{aux} has to separate the high voltage and high current sub-circuit from each other. Therefore, it must

- withstand the 200 kV test voltage,

¹² Not included are the auxiliary, safety and (dis-)charging systems.

¹³ provided by Siemens AG

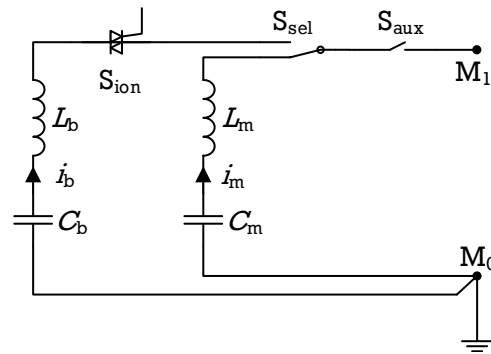


Abbildung 5.4: Simplified ECD of the high current sub-circuit

- conduct the 20 kA inrush current, and,
- switch off the (up to) 2000 A breaking current.

In addition, due to the micro-particle detection, it must have a low PD level. Based on these prerequisites, a single phase SF₆ circuit breaker is used. Its specification is shown in Tabelle 5.9. As a result of the high

Tabelle 5.9: Specification of the auxiliary breaker [Sie11]

rated voltage	145 kV
rated normal current	4 kA
rated frequency	50 Hz and 60 Hz
rated power frequency withstand voltage	275 kV
rated peak withstand current	108 kA

SF₆ arc voltage¹⁴, significant current suppression occurs in the breaking current path. To minimize this effect, the auxiliary breaker is opened within 1 ms before the natural current zero at the end of the breaking phase.

The current selection switch S_{sel} is used for automation of the making and breaking test sequence. It is designed as a disconnecter and switches at no-load.

5.5.1 Inrush current source

The inrush current source has to provide a decaying sinusoidal current with an initial amplitude of 20 kA at a frequency of 4250 Hz and an initial voltage of 59.2 kV¹⁵. As has been shown in Section 3.1, a *LRC*-resonance circuit is most suitable for this task. However, with the available capacitors¹⁶, all the requirements cannot be fulfilled exactly. Based on a practical aspect¹⁷ and taking into account the impact on the breakdown probability¹⁸, the initial voltage amplitude has been given preference over the current amplitude¹⁹. Thus, the current amplitude has been reduced. The final configuration is shown in Tabelle 5.10. Due to the low required inductance and the spatial expansion of the test circuit, the inductance

¹⁴ in the kilo-volt range [Flu82]

¹⁵ single-phase peak voltage in 59.2 kV in a 72.5 kV system

¹⁶ six capacitors of 7.5 μF and a rated voltage of 30 kV

¹⁷ a frequency increase causes additional grounding issues

¹⁸ A lower voltage delays the arc ignition and thereby the chance for multiple pre-ignitions.

¹⁹ In order to investigate late-breakdown a high breakdown probability is useful.

Tabelle 5.10: Specification of the making current source

capacitance C_m	11.25 μF ($\pm 1\%$)
discrete inductance L_m	115 μH ($\pm 10\%$)
parasitic inductance $L_{\sigma m}$	10 μH ($\pm 10\%$)
maximum charging voltage	60 kV
maximum peak current	18 kA
peak current per 1 kV	300 A

has two significant components; the discrete single layer air coil L_m and the extended inductance of the loop²⁰ $L_{\sigma m}$.

In Abbildung 5.5, an example of the maximum inrush current with the associated gap distance and multiple pre-ignitions is shown²¹. As can be determined from the first two peaks, the resulting frequency is 4065 Hz with a maximum current peak of 16.7 kA. The deviation from the values given in Tabelle 5.10 are caused by the damping effects of the burning arc. The decreased closing speed of the gap ($\leq 0.2 \text{ ms}^{-1}$) is the result of an opposing mechanical force²² while its oscillations are caused by eigen-frequency of the test object's mechanical chain.

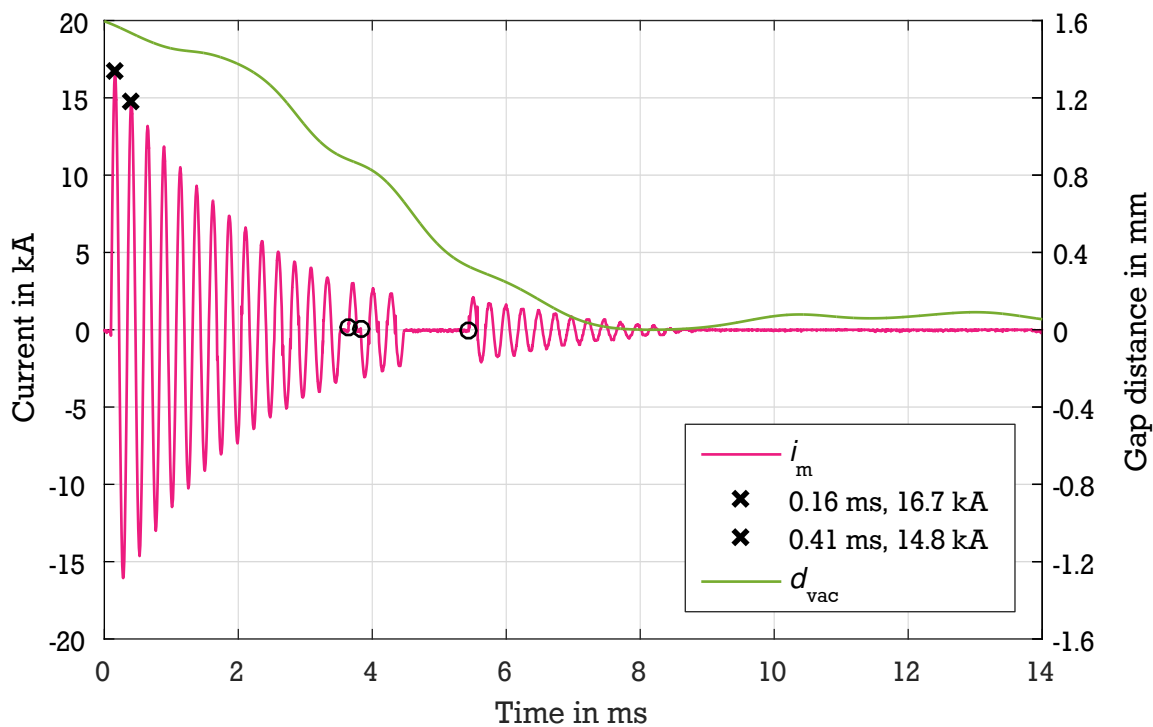


Abbildung 5.5: Example of the making test sequence with multiple pre-ignitions; indicated by black circles

To limit the inductive voltage drop²³ across the return wire (from M_0 to C_m) to a value below 1 kV, the earthed reference point M_0 of the test circuit is located as close as possible to the low potential terminal of the capacitance C_m . This influences the micro-particle detection and is further discussed in Section 6.1.

²⁰ rough dimensions: 5 m length and 2 m height

²¹ The moment of mechanical contact touch at 7.9 ms.

²² Lorenz force acting on the contact system provoked by the inrush current

²³ Due to economical reasons, all auxiliary systems are limited to a potential against earth of 1 kV.

5.5.2 Breaking current source

This source supplies the 50 Hz current for the breaking phase. Its amplitude is in the range of 10 A to 500 A. To validate the positive conditioning effect of the breaking arc also at high voltage VCBs and to achieve a sufficient current level at the breaking period, the design amplitude is 2000 A. In order to synchronize the breaking current to the RV, it has to be switched on at a precise moment. For this purpose, a semi-conductor based making switch S_{uon} is used²⁴. In contrast to the inrush current source, the driving (or initial) voltage is not directly defined. However, given the state of the switches during the arcing period (see Tabelle 5.2), it has to compensate the arc voltage demand of the auxiliary breaker and the test object as well as the voltage drop across the making switch. Based on this, the breaking current source is realized as a *LRC*-resonance circuit instead of utilizing the 400 V power grid. Its specification is given in Tabelle 5.11.

Tabelle 5.11: Specification of the breaking current source

capacitance C_b	585 μ F (± 1 %)
inductance L_b	17.3 mH (± 1 %)
maximum charging voltage	15 kV
maximum peak current	2.7 kA
peak current per 100 V	18 A

5.6 High voltage sub-circuit

Abbildung 5.6 shows the simplified ECD of the high voltage sub-circuit. It consists of the AC source

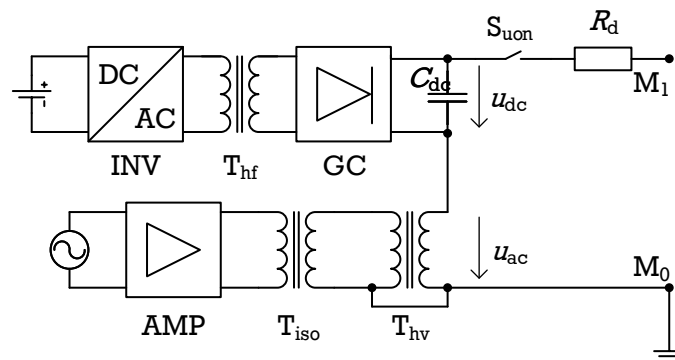


Abbildung 5.6: Simplified ECD of the high voltage sub-circuit

u_{ac} , the DC source u_{dc} , the voltage making switch S_{uon} and the 50 k Ω damping resistor²⁵ R_d . Due to the required low PD and EMI level, both sources and the making switch are combined to form one component. An overview picture of this is shown Abbildung 5.7.

²⁴ By the end of this work, only a half-module of this switch has been implemented. This limits the breaking current to 1250 A.

²⁵ minimum value to protect the equipment against over-voltages in case of a dielectric breakdown of the test object

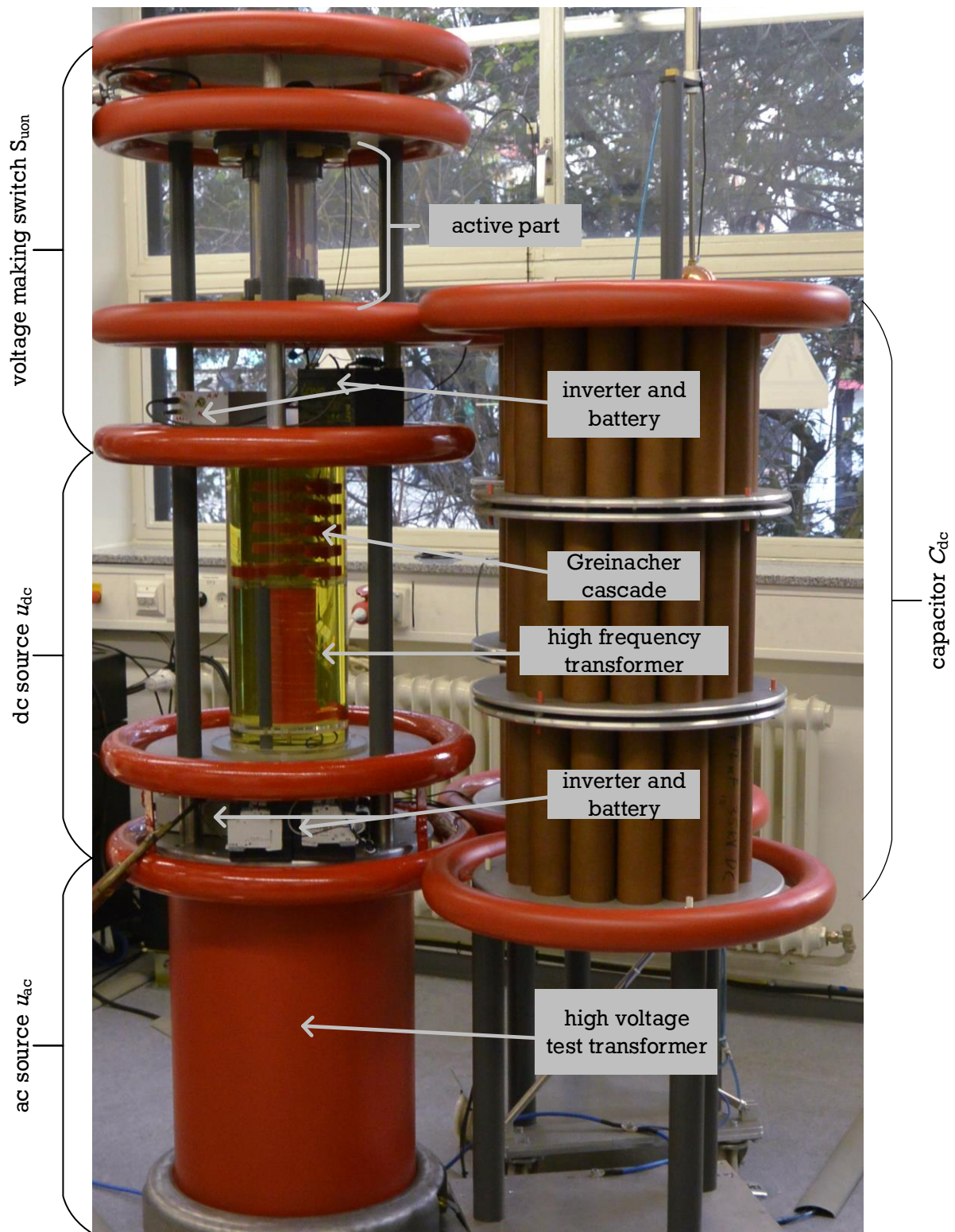


Abbildung 5.7: RV source and the making switch

5.6.1 Alternating voltage source

The AC voltage source has to supply

- the 100 kV peak test voltage with a frequency of 50 Hz,
- the up to 10 mA maximum expected field-emission currents²⁶, and
- the 1.7 kVA reactive power demand of the coupling capacitor (1 nF), the test object and the voltage divider.

For this task, the high voltage test transformer²⁷ T_{hv} is used. Its specification is given in Tabelle 5.12. In

Tabelle 5.12: Specification of the high voltage test transformer T_{hv}

model	MWB TEO 100/10
rated voltage (r.m.s. value)	100 kV
rated current (r.m.s. value)	50 mA
rated continues power	5 kVA
rated power (max. 60 min)	10 kVA
short circuit impedance	3.8 %

order to minimize distortions arising from the low voltage power grid, the transformer is supplied by an amplifier²⁸ (AMP) with a rated power of 11 kVA. For safety and economical²⁹ reasons, the amplifier and the high voltage transformer are galvanically separated by an isolation transformer T_{iso} (rated power 13.8 kVA; isolation level 5 kV).

5.6.2 Direct voltage source

The DC source has to supply a voltage of 100 kV which has to comply with the following conditions:

- low PD and EMI level
- limit the DC voltage drop of an individual period of the RV to an acceptable level
- limit the AC voltage drop across the DC source³⁰ to an acceptable level

For this purpose, the (foil) capacitor C_{dc} of 616 nF and rated voltage of 105 kV is used. This capacitance ensures a DC voltage drop³¹ of less than 0.16 % within one period of the RV and limits the AC voltage drop to approximately 0.2 %. As a consequence, this capacitor has to be charged prior to the recovery phase with its own charging system. In order to further improve the RV, it is also constantly re-charged during the recovery phase. This has been proven feasible in the work of Dullni [DWG⁺06].

²⁶ based on in-house experiences with medium voltage VIs

²⁷ selected due to practical and economical reasons

²⁸ consisting of three, parallel operated, class AB single phase commercial hi-fi power amplifiers (model: Thomann the t.amp Proline 3000)

²⁹ to protect the expensive amplifier and high voltage test transformer

³⁰ due to the capacitive voltage divider formed by C_{dc} and $(C_{cc} + C_{Vvac} + C_{vac})$

³¹ due to field-emission currents of 10 mA with a duration of 10 ms

The charging system consists of an inverter (INV), a high frequency transformer³² (T_{hf}) and a five-stage Greinacher cascade (GC). Due to the missing earth potential, the inverter is powered by a 24 V lead battery. Its topology is a full bridge with a fixed switching frequency of 55 kHz. Thus, two aspects are accomplished. First, the significant part of the inverter's EMI³³ has a reproducible spectrum and can therefore be taken into account during the micro-particle detection. Second, the re-charge duration is significantly shorter compared to the frequency of the load (see Section 6.2.1) which leads to a smaller ripple in the DC voltage [Küc09]. While the inverter and the battery are located in a virtually field free space between two shielding toroids, the transformer and the Greinacher cascade are installed in an oil filled acrylic glass enclosure to prevent PDs. The maximum output voltage is 110 kV at a current of 5 mA.

5.6.3 Voltage making switch

The fast voltage making switch S_{uon} connects the RV at a precise moment to the test object. It is the key element of this test circuit and has to fulfill the following requirements:

- a withstand voltage of 220 kV in open position (test voltage plus 10 % safety margin)
- a current carrying capability of 5 A (maximum current during a dielectric breakdown of the test object)
- a precise closing time of 10 ms with an allowed jitter of 200 μ s
- no bouncing after the contacts touched each other to avoid a disconnection of the RV from the test object
- no pre-ignition during closing operation to avoid a discharge of the capacitor C_{dc} ³⁴
- no PD and EMI level in close position

The requirements, *no bouncing* and *no pre-ignition*, make it difficult to use a regular load switch. In addition, due to the low current amplitude (< 50 mA) during the recovery phase, combined with the high withstand voltage, power semiconductor devices cannot be used either. Therefore, a customized mechanical voltage making switch was developed. A sketch of this switch is shown in Abbildung 5.8. It consists of a highly dynamic actuator with a light (175 g) movable contact system. They are installed in a pressure vessel which is filled with SF₆ at 4.5 bar (absolute value). The pressure vessel is made of a PVC³⁵-tube. At both ends, PVC-flanges are used to seal the pressure vessel with metal disks. The construction is braced with glass fibre plastic spacers to provide the necessary mechanical strength. The external field grading is accomplished with metallic toroids.

The switch's battery powered and inverter controlled actuator is operated as indicated in Abbildung 5.9. During the contact closing, the gap distance d_{uon} is kept proportional to the voltage³⁶ u_{uon} .

³² based on a design of Dr. T. Wietoska (High Voltage Laboratories, TU Darmstadt)

³³ The fundamental switching frequency and its harmonics are below the relevant frequency band used in the micro-particle detection.

³⁴ The test object is short circuited by the arc.

³⁵ Polyvinylchlorid

³⁶ similar to the voltage u_{vac} , but due to a capacitive-ohmic phase angle not identical

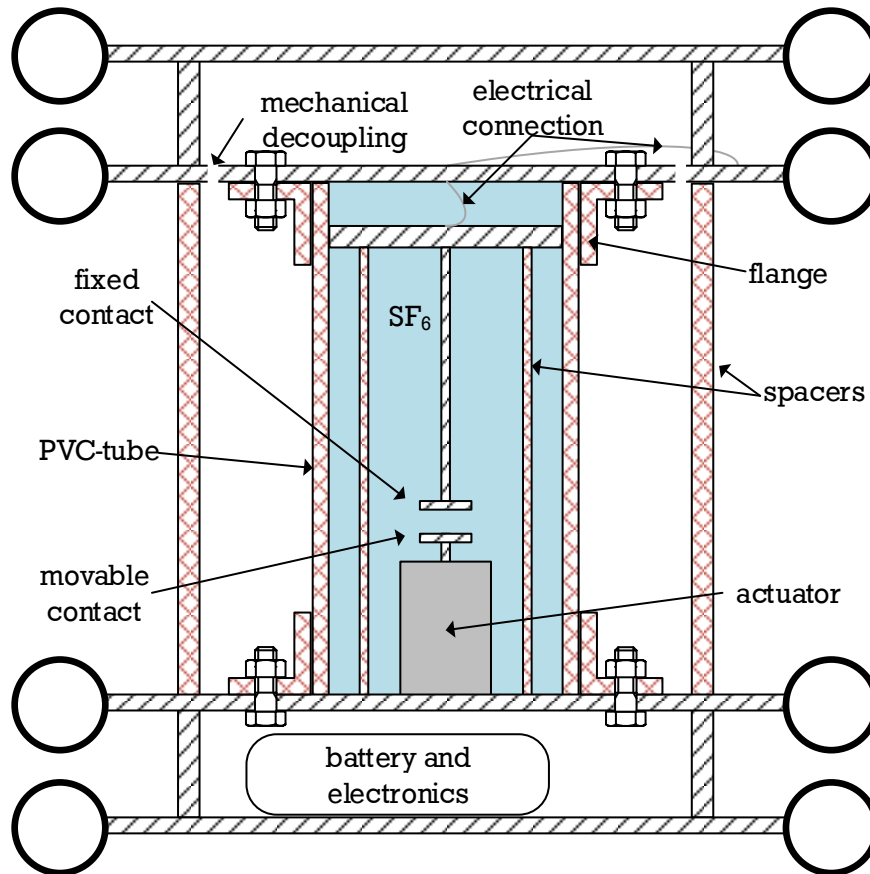


Abbildung 5.8: Sketch of the voltage making switch

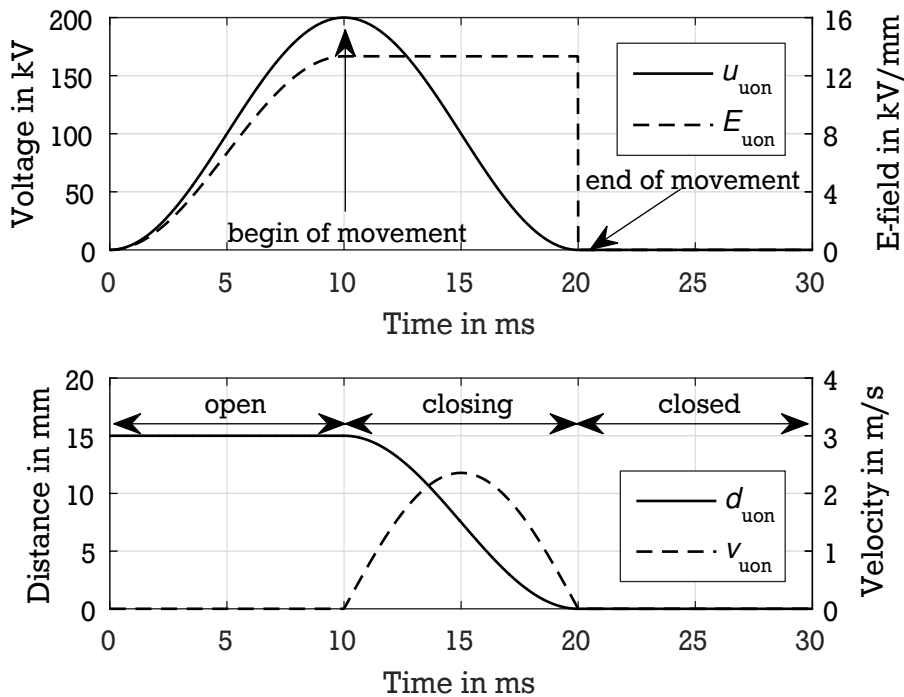


Abbildung 5.9: Basic functionality of the voltage making switch

This results in a nearly constant electric field stress E_{uon} between the *Borda* shaped contacts which is illustrated in Abbildung 5.10. With this nearly identical stress within a SF_6 environment, dielectric

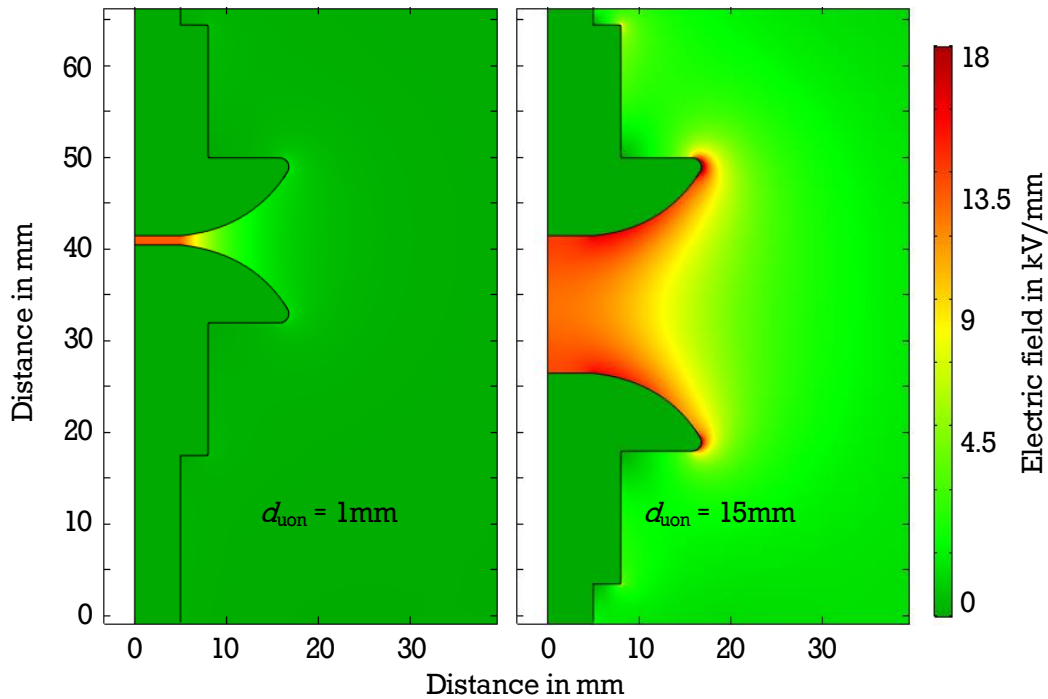


Abbildung 5.10: Electric field distribution of the voltage making switch in different positions

breakdowns, which would lead to pre-ignitions, practically do not occur. In addition, it also ensures a very low impact velocity v_{uon} when the contacts touch. In this way, contact bouncing is almost completely prevented. After the switch is closed, the inverter is deactivated and the contacts are held on position by a small DC current. This current is supplied directly from the battery to prevent EMIs during the recovery phase.

5.7 Deviations to a direct test

Certain properties of the realized test environment are different compared to a direct test. These differences are associated with the breaking test sequence³⁷ and are described in the following.

5.7.1 Initial phase of the recovery voltage

An example of the realized breaking test sequence³⁸ is shown in Abbildung 5.11. It can be seen that the current-/voltage-characteristic is in accordance with the desired one shown in Abbildung 5.1. However,

³⁷ Within this test circuit, the making test sequence is used entirely to de-condition the surface to increase the probability of a dielectric breakdown.

³⁸ By the end of this work, only a capacitive factor of 1.4 (instead of 1.7) had been realized, due to issues with the DC voltage source.

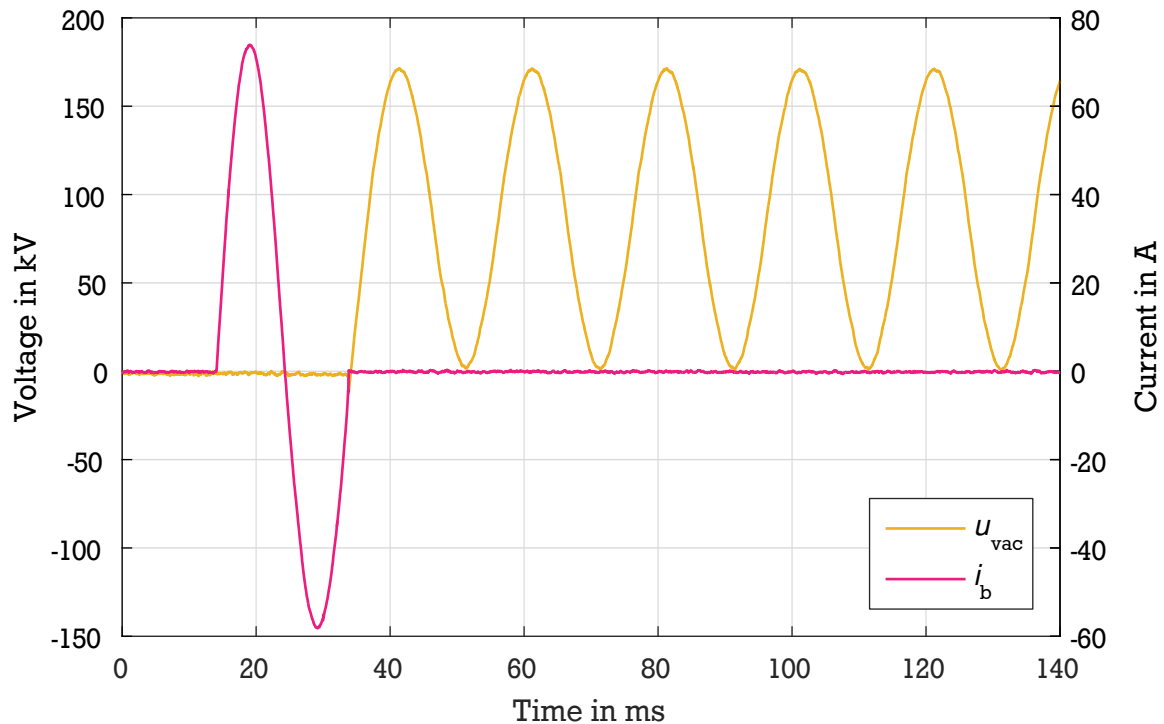


Abbildung 5.11: Realized breaking test sequence

compared to a direct test, the initial phase of the RV is different. Firstly, the transient part of the $\{1-\cos\}$ -shaped RV is not realized³⁹. Secondly, the transition from the breaking phase to the recovery phase is not properly reproduced. Due to the effect of current chopping, the arc ceases to exist prior to the natural current zero crossing. Concurrently, the voltage making switch is programmed to close exactly at the natural current zero crossing. Thus, a short period with a *undefined* voltage stress occurs at the test object. During this period, only an undefined fraction of the AC part of the RV drops across the test object⁴⁰. Due to the statistical nature of the chopping currents and the complete de-coupling of the breaking and recovery phase, this period cannot be avoided. Its duration is usually less than $200\mu\text{s}$ for breaking currents above 100 A. However, smaller breaking currents exhibit earlier current chopping [Hal13] which increase the period's duration up to milli-seconds.

This *unwanted* feature of the test circuit has a strong influence on the development of post arc currents. However, capacitive loads do not cause any significant post arc currents due to their low amplitude. In addition, the high plasma re-combination rate in VIs⁴¹ and the different origins of *cold* dielectric breakdowns suggest that this test circuit feature does not influence the occurrence of late-breakdowns.

5.7.2 Characteristics of late-breakdowns

Late-breakdowns will occur in a direct test as well as in a synthetic test. However, there is a strong difference regarding the involved components which, among other things, provide the energy for the dielectric breakdown [Leu00]. An overview of the involved energy sources for both test scenarios is

³⁹ It can be realized by additional components, but is not the focus of this work due to the research of late-breakdowns.

⁴⁰ The DC part is blocked due to the capacitance of the still open making switch while the AC part is determined by the capacitance ratio of the voltage making switch and the load (test object, coupling capacitor and voltage divider).

⁴¹ usually within several hundreds of micro-seconds [Sla08]

shown in Tabelle 5.13. From this table it can be seen that the entire breakdown energy in a synthetic test

Tabelle 5.13: Difference between the energy supply of a late-breakdown in a synthetic and direct test

breakdown type	direct (see Abbildung 2.10)				synthetic (see Abbildung 5.2)			
	C_{vac}	C_l	C_s	u_s	C_{vac}	C_{cc}	u_{ac}	u_{dc}
restrike	yes	yes	yes	yes	yes	yes	no	no
NSDD	yes	yes	yes	no	yes	yes	no	no

is provided by the capacitance of the test object C_{vac} and the coupling capacitor C_{cc} . The voltage sources u_{ac} and u_{dc} are effectively disconnected from the test object during a breakdown due to the high internal impedance of the test transformer. As a consequence, the value of the coupling capacitor C_{cc} significantly influences the breakdown characteristic [JS81]. Compared to a direct test, it is not possible either to distinguish between a restrike and a NSDD, because in both cases the same elements are involved. Therefore, all breakdowns will be summarized as late-breakdowns.

All this are restrictions of synthetic testing and are not limited to the test circuit design implemented in this work.

6 Simultaneous detection of field-emission currents and charged micro-particles

This chapter starts with the presentation of the basic principle used to detect field-emission currents and charged micro-particles simultaneously. It is followed by a detailed description of each measurement system. In case of the field-emission current measurement system, its data analysis is also presented in detail. This chapter ends with a discussion of the preliminary results and identified restrictions of the simultaneous measurement principle.

6.1 Basic principle

A charged micro-particle moving between the contacts of a VI typically causes a short high frequency current pulse. Compared to this, field-emission currents have a much longer duration and lower frequency components. Therefore, each phenomenon requires its individual measurement principle.

In order to detect field-emission currents and charged micro-particles simultaneously, two different measurement systems have to be implemented in the test circuit. However, this leads to a mutual interference which depends on their interconnection. Based on the general layout of a synthetic test circuit, two interconnection alternatives exist. In any case, either the charged micro-particle detection or the field-emission current measurement is favored. In the following, the pros and cons of both alternatives are described.

Circuitry optimized to measure field-emission currents

The ECD of the field-emission current optimized measurement (FEOC) is shown in Abbildung 6.1. Here,

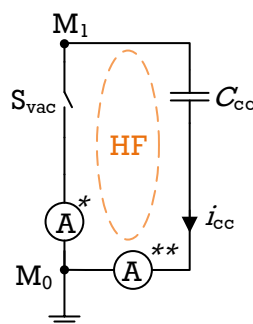


Abbildung 6.1: Field-emission current optimized measurement circuitry

both measurement systems are connected to the star shaped reference point M_0 . This has the advantage that all measurements are conducted against the common ground potential. In addition, the capacitive current i_{cc} , caused by the capacitance of coupling capacitor C_{cc} and the AC component of the RV, bypasses the field-emission current measurement system. Within this test environment, the amplitude of this

capacitive current is up to 31.4 mA at rated operating conditions. Therefore, it is much larger than the expected field-emission currents which would result in a significant decrease of the signal-to-noise ratio in the field-emission current measurement. However, during a dielectric breakdown of the test object, the field-emission current measurement system is subjected to the discharge of the coupling capacitor C_{cc} .

Circuitry optimized to detect charged micro-particles

This ECD of the micro-particle optimized measurement (MPOC) is shown in Abbildung 6.2. Here, the

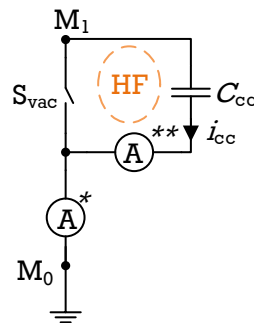


Abbildung 6.2: Charged micro-particle optimized measurement circuitry

charged micro-particle detection system is connected in parallel to the test object. Compared to the FEOC, this results in a much smaller surge impedance (indicated as HF loop) which makes the system less vulnerable to interferences. The smaller surge impedance itself has two reasons. First, the impedance of the field-emission current measurement system is bypassed. Second, its spatial expansion is smaller because no connection to the common reference point M_0 is necessary¹. However, a disadvantage of this configuration is the missing ground potential of the charged micro-particle detection. Thus, an additional galvanic isolation or a data processing on potential² is required.

6.2 Field-emission current measurement

After a capacitive switching operation with a VCB, field-emission currents can arise with amplitudes typically in the range of several tens of micro-amperes to several milli-amperes [Sla08], [KHK10], [SKCS12]. In addition to this current, a capacitive displacement current i_c also occurs. In the past, it has been demonstrated that their sum, here referred to as the low frequent current i_{lf} , is effectively measured with a resistor [Lat95], [Lip03], [Sla08], [Küc09]. As usual, such a resistor is realized by a parallel connection of several resistors to distribute the thermal stress in case of high measurement currents. However, in order to protect this resistor as well as the connected data acquisition devices against inrush currents (i_m), breaking currents (i_b) and discharge currents³ (i_{bd}), additional protection is required.

While the making current and breaking current periods are exactly known and defined within a synthetic test circuit, the occurrence of discharge currents cannot be predicted. As a consequence, two different

¹ The common reference point M_0 is positioned close to the low voltage terminal of the making current source due to its earthing.

² The potential rise during a dielectric breakdown is the primary concern.

³ in case of a dielectric breakdown

protection systems, an *operating current protection* (OCP, described in Section 6.2.2) and a *discharge current protection* (DCP, described in Section 6.2.1), are needed. Within this work, the protection systems are based on the ECD that is shown in Abbildung 6.3. In the following, their functionality as well as the

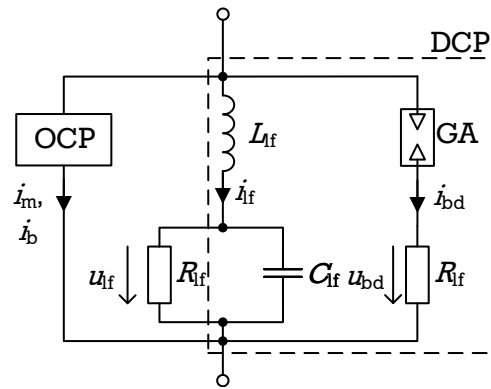


Abbildung 6.3: Field-emission current measurement system with protection (explanation is given in the subsequent text)

impact of power diodes as OCP are discussed. As no standards regarding the analysis of field-emission currents exist, the data analysis procedure used within this work is also presented.

6.2.1 Discharge current protection

The DCP is realized based on the system used in the work of Jüttner [JS81]. It consists of the 100 mH ferrite core inductance L_{if} , the gas discharge arrester⁴ GA and the 1.5 nF capacitance C_{if} of the measurement line.

During the recovery phase, the gas discharge arrester has a high impedance and the current i_{if} flows through the resistor R_{if} and the inductance L_{if} . Due to its low amplitude and frequency, the voltage drop across the inductance is small. However, in the event of a breakdown, the transient nature of the discharge current i_{bd} will induce a large voltage across the inductance which triggers the gas discharge arrester. Therefore, the measuring path is bypassed while at the same time, the capacitance C_{if} reduces the voltage u_{if} and its steepness across resistor R_{if} . This limits the energy input into the resistor and, in addition, functions as a first stage over-voltage protection for connected data acquisition devices.

The discharge current i_{bd} is measured with the low inductive resistor R_{bd} of 0.8Ω ⁵. In Abbildung 6.4, the measured discharge current during a breakdown at 105 kV is shown⁶ After the initial transients, a pulsed shaped current with an amplitude of 1 A is visible which equals to a charge⁷ Q_{bd} of $122 \mu C$. This matches roughly the $105 \mu C$ which is stored in the coupling capacitor during the breakdown.

⁴ model: TDK EC90, DC spark-over-voltage: 90 V, typical impulse ($1 \text{ kV} \mu s^{-1}$) spark-over-voltage: $< 550 \text{ V}$ [TDK15]

⁵ Its objective is to provide the theoretical possibility to distinguish between a restrike and a NSDD by analysing the breakdown current. This distinguishing is, given only the voltage signal, in this synthetic test circuit not possible (see Tabelle 5.13).

⁶ Within this work, this late-breakdown had the highest breakdown voltage. Due to clipping, the voltage has been extrapolated.

⁷ roughly estimated by integration of the filtered (red) curve in Abbildung 6.4

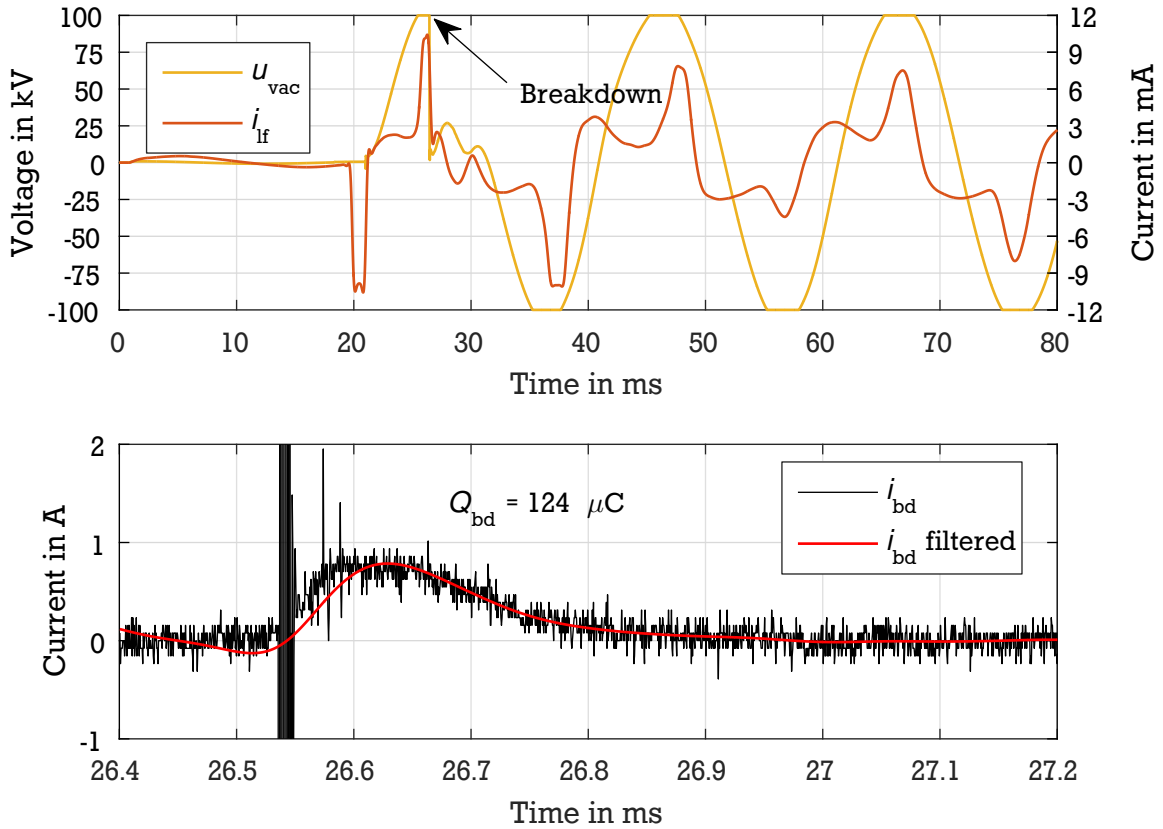


Abbildung 6.4: Measured discharge current in FEOC configuration during a dielectric breakdown

An advantage of this DCP principle are the low leakage currents⁸ which are smaller than 10 nA. Thus, compared to the low frequent current i_{lf} , they can be neglected. However, the physical bandwidth of the measurement system depends on the value of the resistor R_{lf} . In order to estimate the required spectrum of the expected field-emission currents, Equation (2.7) is analyzed⁹ with respect to the field enhancement factor β . The result is shown in Abbildung 6.5, where the highest frequency component¹⁰ necessary to measure 99.9 % of the original signal energy is plotted against the field enhancement factor. As can be seen, a higher field enhancement factor causes a lower non-linearity of the field-emission current which results in lesser relevant frequency components. For typical expected values, a highest frequency component of 1 kHz is sufficient¹¹. In Equation (6.1), the transfer function of the measurement system is given.

$$H_{lf}(f) = \frac{1}{1 + j2\pi f R_{lf} C_{lf} - 4\pi^2 f^2 L_{lf} C_{lf}} \quad (6.1)$$

With a frequency of 1 kHz and the values of the DCP components, the maximum usable resistance to measure 99.9 % of the original signal energy is 4.7 k Ω . Within this work, the value of R_{lf} is 500 Ω .

⁸ They are defined by the isolation resistance of the gas discharge arrester (> 1 G Ω below 50V [TDK15]) and caused by the voltage drop in the measuring path.

⁹ $u_{vac} = 200$ kV; $d_{vac} = 40$ mm

¹⁰ Due to the non-linearity of the field-emission current, its frequency components are integral multiples of the basic voltage oscillation.

¹¹ This is also in accordance with various field-emission current measurements of medium voltage VCBs [KHK10], [SKCS12], [YWY⁺14].

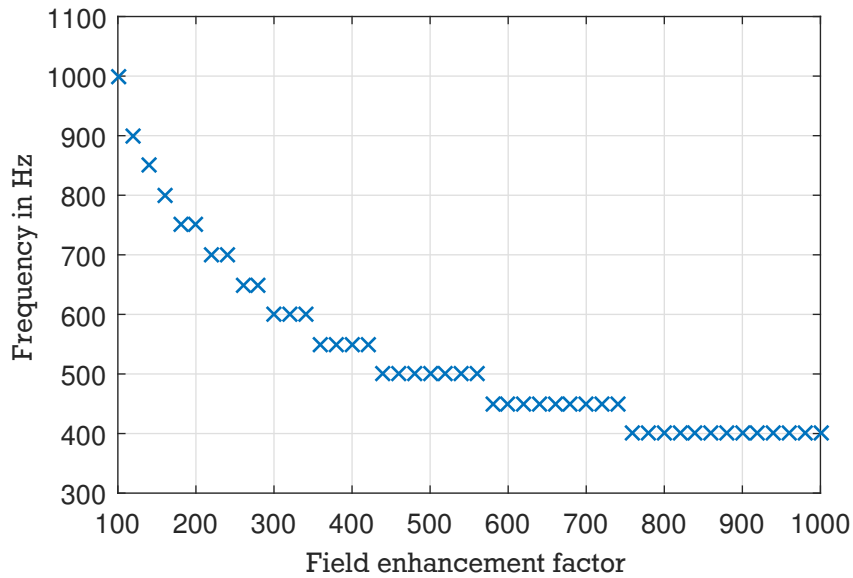


Abbildung 6.5: Frequency components (99.9 % of the signal energy) of the field-emission current in accordance with the theory

6.2.2 Operating current protection

As can be seen in *Abbildung 6.3*, the OCP is operated similar to the DCP in parallel to the resistor R_{lf} . Consequently, the breaking and inrush currents (operating currents) must be bypassed with a low impedance ($Z_{ocp,on}$). However, during the recovery phase, its impedance $Z_{ocp,off}$ must be sufficiently high to prevent undesired leakage currents. In contrast to discharge currents, operating currents exhibit a higher amplitude and a longer time duration. Hence, they cause non-negligible power losses due to the impedance $Z_{ocp,on}$, leading to a temperature rise of the OCP. As a consequence, the OCP's high impedance $Z_{ocp,off}$ has to be especially robust against changes in temperature to avoid additional required cooling phases.

In recent years, an OCP based on anti-parallel power diodes has been widely used. Its ECD¹² is shown in *Abbildung 6.6a*. The reason for the power diode application lies in its non-linear current-/voltage-

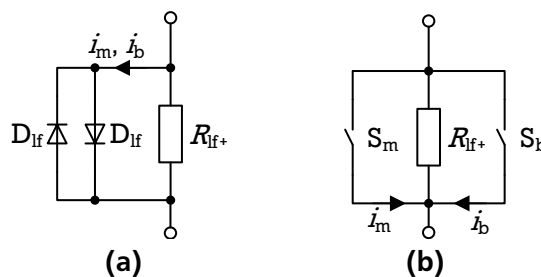


Abbildung 6.6: Different OCP principles, (a) passive (diode) protection and (b) active (contactor) protection

¹² For the sake of improved clarity, the resistor R_{lf} and the DCP are summarized to R_{lf+} .

characteristic. This characteristic is described by the following *Shockley diode equation*,

$$i_d = i_{\text{sat}} \left(\exp\left(\frac{u_d}{nu_T}\right) - 1 \right) \quad (6.2)$$

where i_d is the diode's current, u_d its voltage, i_{sat} the (temperature-dependent) reverse bias saturation current, u_T the thermal voltage and n the ideality factor¹³ [GPS⁺51]. According to Equation (6.2), the diode current i_d is very small below a certain voltage level corresponding to a high impedance. Above this voltage level, the properties are reversed. In addition, this transition is voltage controlled. Thus, diodes in an anti-parallel¹⁴ configuration are very suitable as an OCP because the current automatically commutates from the resistor to the diodes and back without an additional control system. However, a diode based OCP has disadvantages regarding its measurement uncertainty because of non-linear, temperature-dependent¹⁵ leakage currents. If only a small number of test are conducted, the temperature rise in the diode is limited and the leakage currents can be compensated (e.g. with a temperature model of the diode).

Given the desired number of high consecutive capacitive switching operations of this test environment, the OCP is realized with switches¹⁶ (see Abbildung 6.6b). However, as a drawback, this system has to be actively controlled due to the loss of the automatic current commutation. Based on the different requirements regarding the making and breaking phase, two individual switches are used. Here, the inrush current protection switch S_m is optimized to conduct high currents with a very low voltage drop. Its opening and closing velocity are of secondary importance because the making phase is a separate event. Therefore, it is designed as a disconnecter which is operated together with the current selection switch S_{sel} in advance to a test. In return, the breaking current protection switch S_b is a commercial low voltage contactor¹⁷ with a control system optimized for a precise opening $1 \text{ ms} \pm 100 \mu\text{s}$ after the current interruption.

6.2.3 Impact of a power diode based protection

In the following, a possible impact of a power diode based OCP to the field-emission current measurement is demonstrated. For this purpose, two identical measurement systems with the exception of the OCP are operated in series as indicated in Abbildung 6.7. With the data acquisition device's differential inputs, both low frequent currents, i_{lf} (switch OCP) as well as $i_{\text{lf,d}}$ (diode¹⁸ OCP), are measured simultaneously¹⁹. In this test scenario, the gap distance was set to 4 mm and the RV had only an AC component with an amplitude of 120 kV to provoke field-emission currents in both polarities.

The result is given in Abbildung 6.8. Here, the upper plot shows the low frequent currents and the lower one shows the associated field-emission currents. The latter are calculated by compensating the

¹³ typically varies from 1 to 2

¹⁴ to handle positive and negative currents

¹⁵ The resistance of R_{lf} increases with temperature while the diode's resistance decreases.

¹⁶ This principle has been used prior to the diode protection [MNK⁺75].

¹⁷ EATON XTCE series: $Z_{\text{ocp,on}} < 1 \text{ m}\Omega$

¹⁸ Each diode consists of a series connection of three individual diodes (model: Semikron Skn130/04) following the work of Koochack Zadeh [Koo11].

¹⁹ The measurement reference of the diode based system is different from the ground potential.

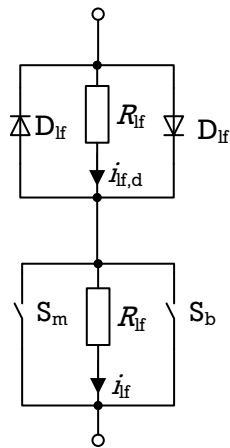


Abbildung 6.7: ECD of the comparison measurement between the two OCP principles

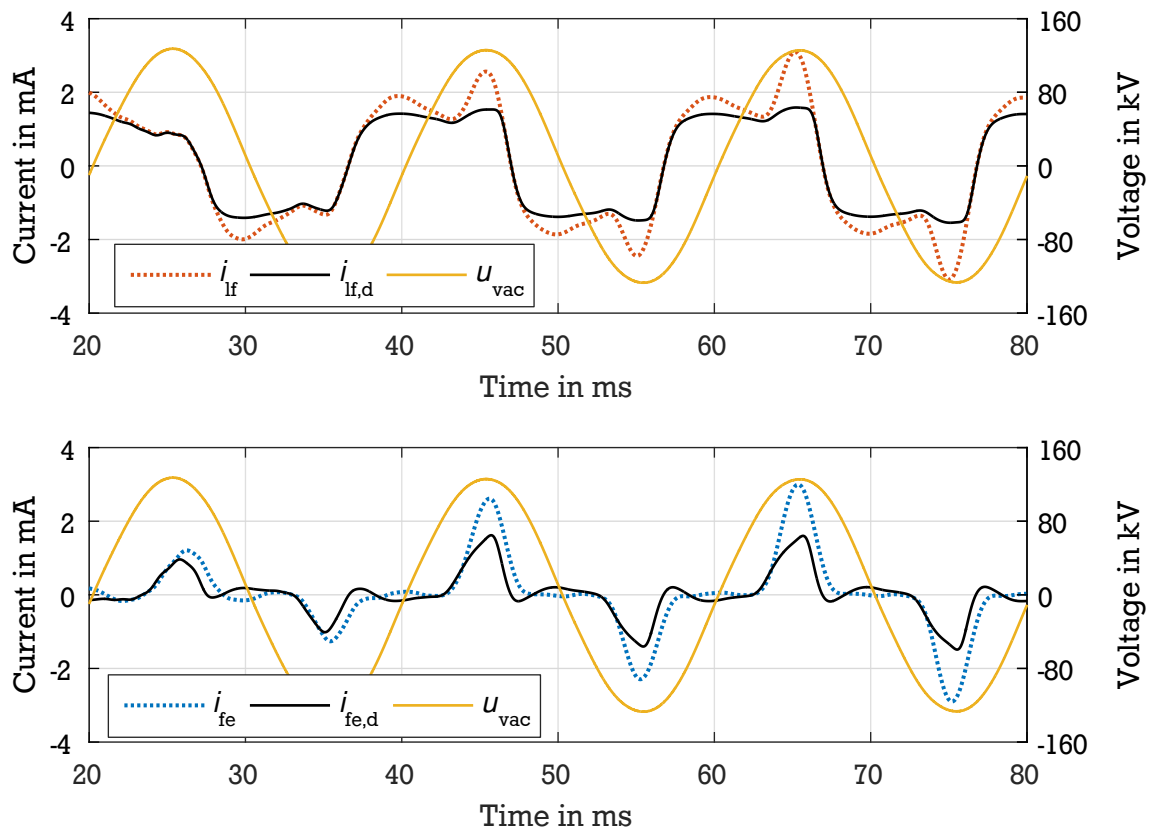


Abbildung 6.8: Section of the comparison measurement between a passive (diode) and active (switch) OCP

capacitive current (software algorithm described in Section 6.2.4). It can be seen directly that the peaks in the low frequent current $i_{f,d}$ are truncated. This has, besides the reduced amplitude, an additional impact on the field-emission current $i_{f,e,d}$. In the event that the capacitive current component is also truncated (which is more likely in high voltage VCBs), the final field-emission current $i_{f,e,d}$ slightly distorted. In detail, its falling edge is shifted to the left while its current peak is slightly to the right.

While these impacts are quite visible with reference to the *original* current shape, they are hard to identify if a power diode based OCP is used exclusively. In particular, fluctuations in the low frequent current i_{f} are likely to be missed. In addition, this situation is further aggravated because, in both cases, a FN analysis can be performed with reasonable results. This has been demonstrated in Tabelle 6.1 where, for this measurement, the field enhancement factors (mean and standard derivation) of both half-cycles have been calculated²⁰.

Tabelle 6.1: Field enhancement factors for the complete OCP comparison measurement

half-cycle	diode based OCP	switch based OCP
positive	508 ± 61	221 ± 25
negative	411 ± 46	217 ± 12

6.2.4 Data analysis

The data analysis of a field-emission current measurement consists of several steps where usually the last one is a FN analysis to estimate the field enhancement factor²¹ β_{est} . Within this work, the data analysis is extended by a voltage evaluation to identify limitations caused by the test circuit. Because the field-emission current data analysis is not standardized, all key aspects of the individual steps are described in the following.

Period and edge detection

In this step, the whole duration of the $\{1 - \cos\}$ - shaped RV is separated into time periods²² (based on the power frequency) where each contains a rising and a falling edge. The FN analysis itself will be applied only to a certain area of each edge²³ which is shown in Abbildung 6.9. To be independent from the changing field-emission currents, these areas are determined by the voltage level and are evaluated in the range of 0.75 p.u. to 1 p.u..

Breakdown detection

In this step, breakdowns are detected to exclude affected time periods from the capacitive current compensation (see next paragraph) and the FN analysis. This has two reasons. First, the contact surface is changed after a breakdown. Therefore, the (microscopic) field enhancement factor β_m , before and after a breakdown, is different and should be treated separately. Second, the transient currents associated

²⁰ described in Section 6.2.4

²¹ Within this work, an estimation of the emission area $A_{e,est}$ is not performed because of its high uncertainty.

²² In case of pure AC two periods of time are used, one for the positive half-cycle and one for the negative.

²³ This is necessary due to disturbances and noise in the current signal.

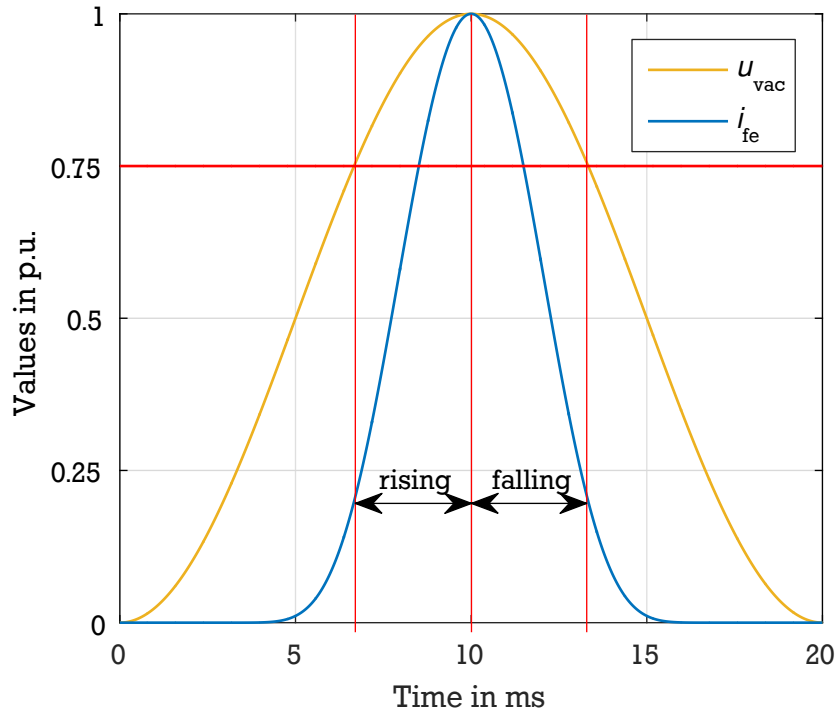


Abbildung 6.9: Edge selection for the Fowler-Nordheim analysis

with a breakdown are not correctly measured due to the measurement system's low-pass behavior and protection circuitry.

Capacitive current compensation

In this step, the field-emission current i_{fe} is calculated from the measured low frequent current i_{lf} and voltage u_{vac} with Equation (6.3).

$$i_{fe} = i_{lf} - i_c - i_{iso} = i_{lf} - \widehat{C}_{vac} \cdot \frac{du_{vac}(t)}{dt} - i_{iso} \quad (6.3)$$

Here, \widehat{C}_{vac} is the *acting* capacitance of the test object and i_{iso} an additional resistive current through its insulation. The derivative $\frac{du_{vac}}{dt}$ is executed numerically and filtered with a Butterworth low-pass filter (filter order = 3, cut-off frequency = 500 Hz). Currently, the uncertainty of the measurement system allows the reliable processing of field-emission currents with amplitudes higher than $100 \mu A^{24}$. Since the current i_{iso} is much smaller, it is neglected.

To estimate the capacitance \widehat{C}_{vac} , i_{fe} is calculated with the expected value range of 10 pF to 200 pF. As has been shown in other publications [KHSL11], the optimal compensation is reached at the value of \widehat{C}_{vac} , where the signal of i_{fe} contains the lowest energy. In order to decrease the uncertainty, an individual $\widehat{C}_{vac,i}$ of each period is determined. Afterwards, these values are used to calculate the final capacitance of the whole signal by averaging. However, only periods without a breakdown and with a stable²⁵ gap distance are taken into account.

²⁴ The uncertainty can be reduced by increasing the value of R_{lf} . At this phase, a low value was needed to capture the high capacitive displacement currents (at low gap distances) for commissioning purposes

²⁵ no oscillations and completely open

Phase shift compensation

In this step, a possible phase shift²⁶ between the current and voltage signal is compensated. The uncertainty of this compensation²⁷ is $2\mu\text{s}$, and the following criteria, depending on the field-emission current level, are used:

- $i_{fe} > i_c$: $t(\max(i_{fe})) \equiv t(\max(u_{vac}))$
- $i_{fe} < i_c$: $t(\max(i_c)) + 5\text{ ms} \equiv t(\max(u_{vac}))$

Moreover, it uses the same averaging principle as in the previous capacitive current compensation. However, since the phase shift also affects the capacitive current compensation, both steps are run iteratively until an uncertainty $\pm 2\mu\text{s}$ is reached.

Frequency analysis

In this step, first a frequency analysis of the voltage signal is performed. Its goal is to identify influences in the pre-breakdown development by the test circuit. As has been shown in Section 3.4.1, such an influence is a drop in the test voltage u_{vac} caused by the test transformer due to a high current steepness. For this purpose, a *Fourier series* calculation of each individual RV period is performed and the total harmonic distortion (THD) determined. It is calculated according to Equation (6.4),

$$\text{THD} = \frac{\sqrt{\sum_{i=2}^{10} u_{vac,i}^2}}{u_{vac,1}} \quad (6.4)$$

where $u_{vac,i}$ represents the voltage of the i th-harmonic [Toz04]. Within this work, a THD larger than 1 % is considered as an interference and the affected period is excluded from further analysis. An example of this is given in Abbildung 6.10, where for instance, the field-emission current in the first period is strongly limited by the test circuit.

In case of no interference, an additional Fourier series of the current signal is conducted. However, instead of calculating the THD, all frequency components necessary to recreate 99.9 % of the signal's energy are determined. The highest frequency component is used then to verify that the cut-off frequency of the measurement system as well as the software filter settings are appropriate.

Fowler-Nordheim analysis

In this step, the field enhancement factors for each period and edge are estimated. For this purpose, FN plots are used. The slope m_{FNp} of each plot is calculated using a linear best fit line. The fit quality is evaluated automatically using the *residual sum of squares* method²⁸. Based on the fact that

- the majority of dielectric breakdowns are observed during the first periods of the RV where the gap may not yet be stable, and

²⁶ It is caused by different response times of the measurement systems. A value of $4.7\text{ k}\Omega$ of the resistor R_{if} causes a phase shift of $7\mu\text{s}$ at 50 Hz .

²⁷ based on the sampling frequency of 500 kHz

²⁸ Within this work, the minimum is 0.995 .

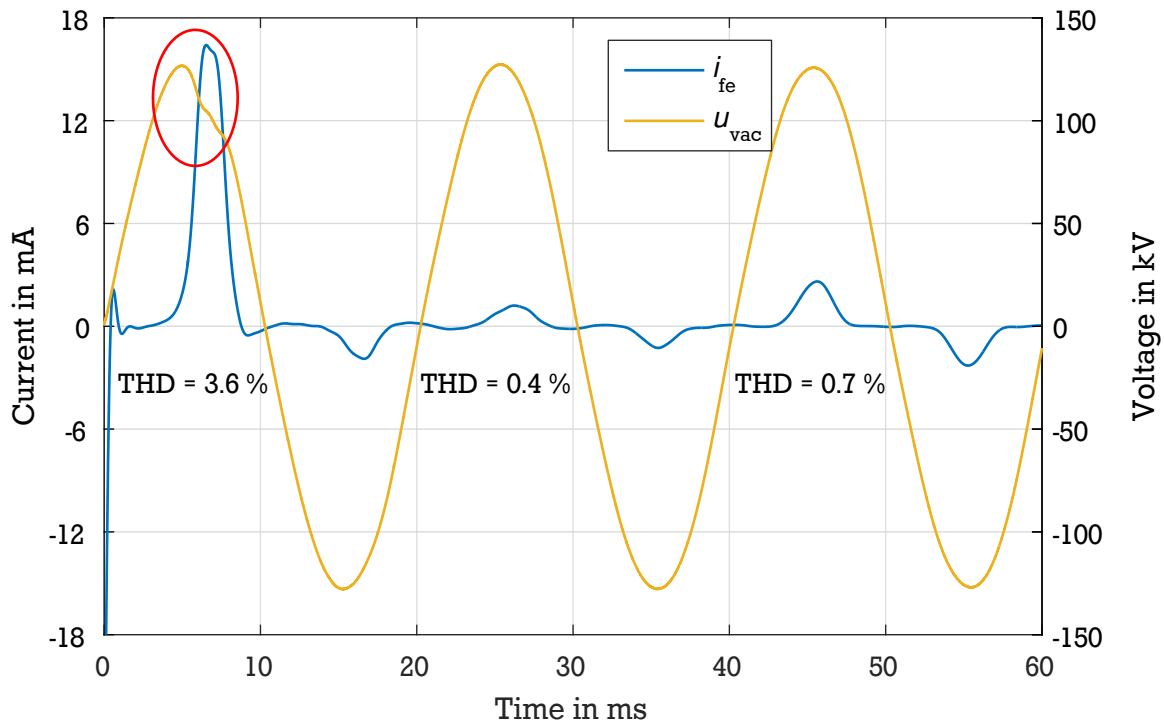


Abbildung 6.10: Example of test circuits interference screening with the voltage signal's THD

- towards VCBs with higher design voltages, the duration to reach a completely open and stable gap distance takes longer,

the true electric field strength²⁹ E_{vac} is used in a FN plot.

6.3 Charged micro-particle detection

In Section 2.2.1, it has been stated that micro-particles

- differ from each other primarily regarding their radius, charge and density³⁰,
- are constantly vaporized, re-created and attached/detached from a surface by electrical, mechanical or thermal stress, and,
- are currently impossible to characterize exactly without opening the VI.

However, the current caused by a moving micro-particle with an electric charge Q_p can be detected. It usually appears as a high frequency pulse due to interactions with parasitic elements. Thus, charged micro-particles can be detected in a non-destructive way by measuring their apparent high frequency current pulse.

Before this is described in Section 6.3.2, the charge Q_p and transit time³¹ t_p of typical micro-particles are roughly estimated. Under the assumption of a spherical shape and an origin on one of the contact surfaces, the charge Q_p can be estimated according to Equation (2.11). The results for typical particle radii r_p and different surface field strengths E_c are shown in Abbildung 6.11. Assuming that the micro-

²⁹ determined by a voltage and gap distance measurement

³⁰ due to different materials

³¹ the time a charged micro-particle requires to travel from one contact's surface to the opposite one

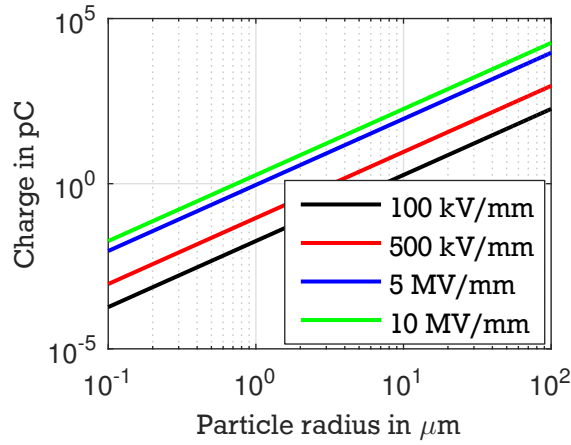


Abbildung 6.11: Charge estimation of a spherical micro-particle detached from a surface with respect to the contact surface microscopic field strength E_c

particle's charge Q_p and mass m_p do not change during transit³² and that the electric field strength E_{vac} is constant, the transit time t_p can be calculated by solving Equation (6.5).

$$m_p \ddot{x} = Q_p E_{vac} \quad (6.5)$$

The micro-particle's mass m_p can be further substituted by its volume and density. For a spherical shape, this is expressed with Equation (6.6).

$$m_p = \frac{4}{3} \pi r_p^3 \rho_p \quad (6.6)$$

Finally, the transit time t_p is given by Equation (6.7).

$$t_p = \sqrt{\frac{0.404 d_{vac}^3 r_p \rho_p}{u_{vac}^2 \epsilon_0 \beta}} \quad (6.7)$$

The graphical results of this equation are shown in Abbildung 6.12. As can be seen, the transit time is much smaller than a period of the power frequency. In combination with the charge estimation, this suggests a certain similarity to partial discharges.

6.3.1 Similarities to partial discharges

PDs occur in solid, fluid or gaseous insulation systems under a high voltage stress. They are caused by dielectric imperfections and lead to locally restricted dielectric breakdowns. As a result, high frequency transient current pulses with an individual duration in the range of nano-seconds to micro-seconds appear. The accumulated electric charge of an insulation system with PD activity is usually in the range of pico-coulombs to nano-coulombs per period of the power frequency. [HL14]

Thus, charged micro-particles and PDs share the following similarities:

³² for instance, by an interaction with field-emission currents

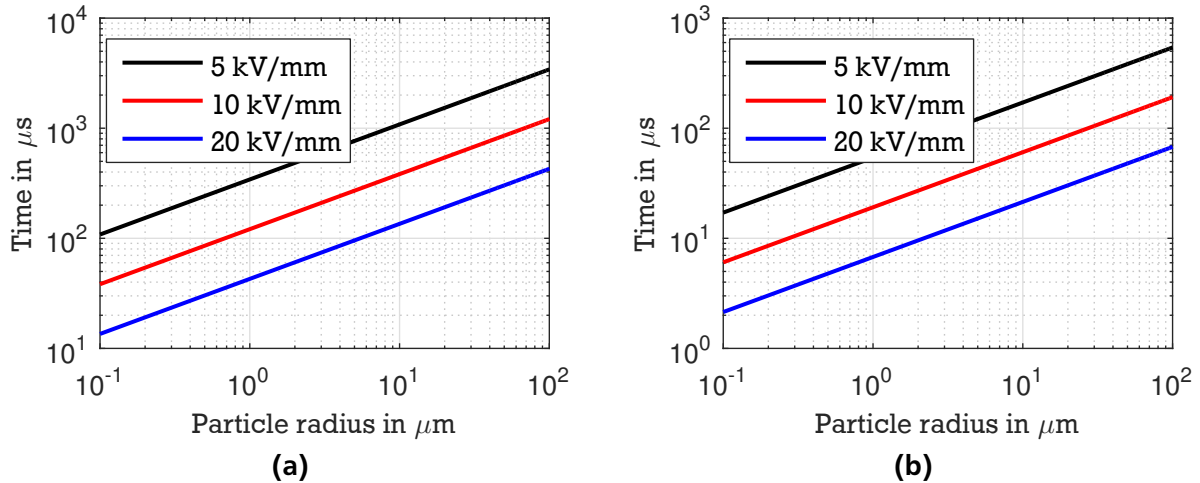


Abbildung 6.12: Transit time estimation (gap distance $d_{\text{vac}} = 40$ mm) for a spherical particle for different homogeneous field strengths and field enhancement factors ($\beta = 10$ in (a) and $\beta = 400$ in (b))

- transient current impulses with a high frequency
- accumulated charge in the same order of magnitude

In contrast to charged micro-particles, the physics of PDs are well known. In addition, many sophisticated measurement devices as well as software based analyzing and evaluation tools have been developed in the last decades [Küc09], [HL14]. Therefore, it is recommended to start the detection of charged micro-particles based on established PD measurement techniques.

As a consequence of this similarity, a test environment suited to detect charged micro-particles must have a low PD level. Otherwise, both phenomena can hardly be distinguished from each other. In addition, also a low EMI level is necessary because they cause disturbances in a high frequency current measurement. As has been stated in Section 5.1, both requirements have been taken into account in the test circuit design. A method to verify a sufficient low PD and EMI level is given in Section 6.3.3.

6.3.2 Description of the measurement principle

As has been pointed out, PDs cause high frequency current pulses. These currents are powered by the electric field in the affected insulation and result in a local energy imbalance. In general, this imbalance will be compensated by the connected power source. However, its internal inductance in combination with the current's high frequency *delay* this compensation. Thus, this delay can be used to *decouple* and measure the current pulses with an additional coupling capacitor.

In case of charged micro-particles, energy is needed for their acceleration. It is provided by the electric field E_{vac} between the VI's contacts as well as by the adjacent stray fields. Similar to a PD, this acceleration results in a local energy imbalance. However, its delayed compensation strongly depends on the micro-particle's transit time t_p and charge Q_p ³³. Based on the PD measurement principle, the ECD resulting in Abbildung 6.13 can be used to describe the charged micro-particle detection. Here, C_{par} ³⁴ and C_{par} ³⁵ are

³³ a long transit time or a low charge result in a small current

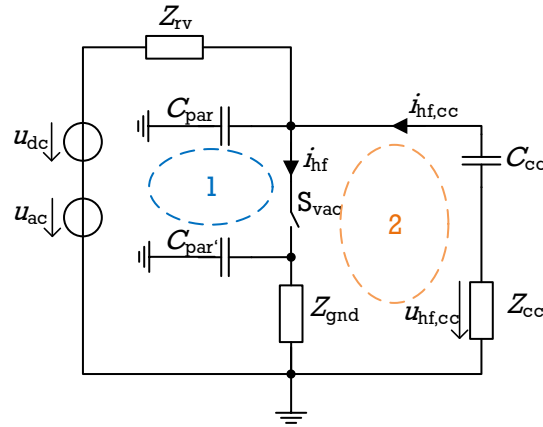


Abbildung 6.13: Simplified ECD for a charged micro-particle detection

the parasitic capacitances of the stray fields (combined approximately 50 pF, Z_{rv} the series impedance of the high voltage sub-circuit, Z_{gnd} the impedance of the return wire and Z_{cc} a PD measuring impedance. The impedance of Z_{gnd} and Z_{rv} are mainly determined by the inductance of the current path. For this test circuit, the inductance of the 10 m return wire is approximately $10\mu\text{H}$. The inductance of the high voltage sub-circuit is much larger than 100 H due to the test transformer.

Without the additional capacitor, the high frequency currents i_{hf} would oscillate and decay mainly in the parasitic loop 1. However, by adding a coupling capacitor C_{cc} close to the VCB, an alternative parallel current path is created (indicated by loop 2). In contrast to the parasitic loop, this path consists of discrete elements. Thus, it is possible to measure the decoupled apparent current $i_{hf,cc}$ with the impedance Z_{cc} . However, this decoupled apparent current $i_{hf,cc}$ is only a certain fraction of current i_{hf} . In order to increase this fraction as close as possible to 1, the following requirements have to be fulfilled:

- the capacitance of C_{cc} must be large compared to the capacitance of the test object³⁶ C_{vac}
- the surge impedance of loop 2 must be much smaller than the one of parasitic loop 1

In spite of all efforts, the second requirement is, especially, hard to accomplish. This is based on the spatial expansion of loop 2 and the moderate equivalent series resistance of the oil filled capacitor C_{cc} . The latter is necessary to accomplish the first requirement in a suitable way. As a consequence, the measurement of the apparent charge of micro-particles implies a high quantitative uncertainty and is, at this point, rather a detection. Thus, the calibration of the system is much easier compared to a real PD measurement, where the exact apparent charge shall be determined.

Within this test environment, the apparent currents $i_{hf,cc}$ are measured with the commercially available PD measuring impedance³⁷ Z_{cc} . This has two advantages. First, it is optimized for current pulses in the expected frequency range. Therefore, the unwanted power frequent currents are already filtered out. This can be seen from its transfer function³⁸ given in Abbildung 6.14. Second, it has several implemented protection systems against over-currents and over-voltages.

³⁴ high voltage terminal of the test platform against earth

³⁵ low voltage terminal of the test platform against earth

³⁶ resulting capacitance between the VI's contacts and the associated parasitic ones; usually less than 55 pF

³⁷ OMICRON CLP 542

³⁸ measurement uncertainty < 10 %

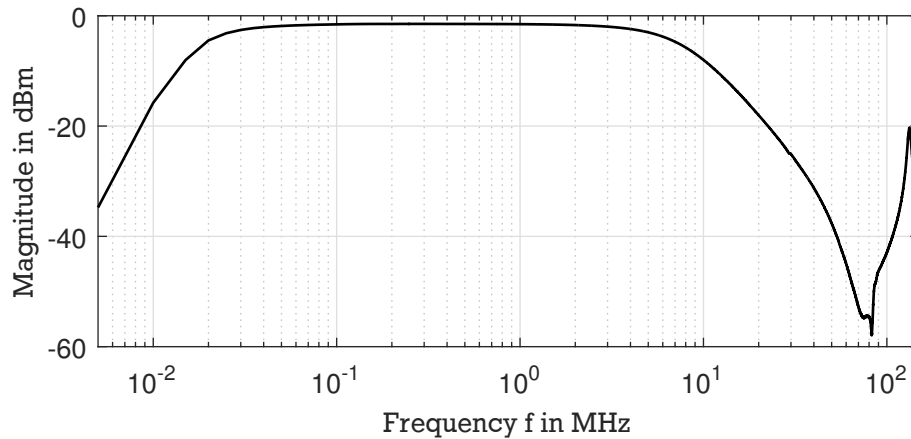


Abbildung 6.14: Measured transfer function of the used measuring impedance Z_{cc}

Interference due to the breaking arc ignition and extinction

PD measurement systems are designed to investigate dielectrics in the absence of a power frequent arc. The later is the result of a breakdown which usually ends all PD measurements. In order to detect the apparent charge of micro-particles, it is now necessary for the system to operate shortly after a real switching operation. Within this test environment, this includes breaking currents³⁹ up to 2000 A and their corresponding arcing during the contact separation. Based on the negligible voltage drop across a VI with closed contacts, the system can only be damaged or influenced during the arcing itself.

In the following, the possible influences of a diffuse arc are briefly discussed. For this purpose, the simplified current-/voltage-characteristic of an arc in Abbildung 6.15 is used. It can be seen, that usually

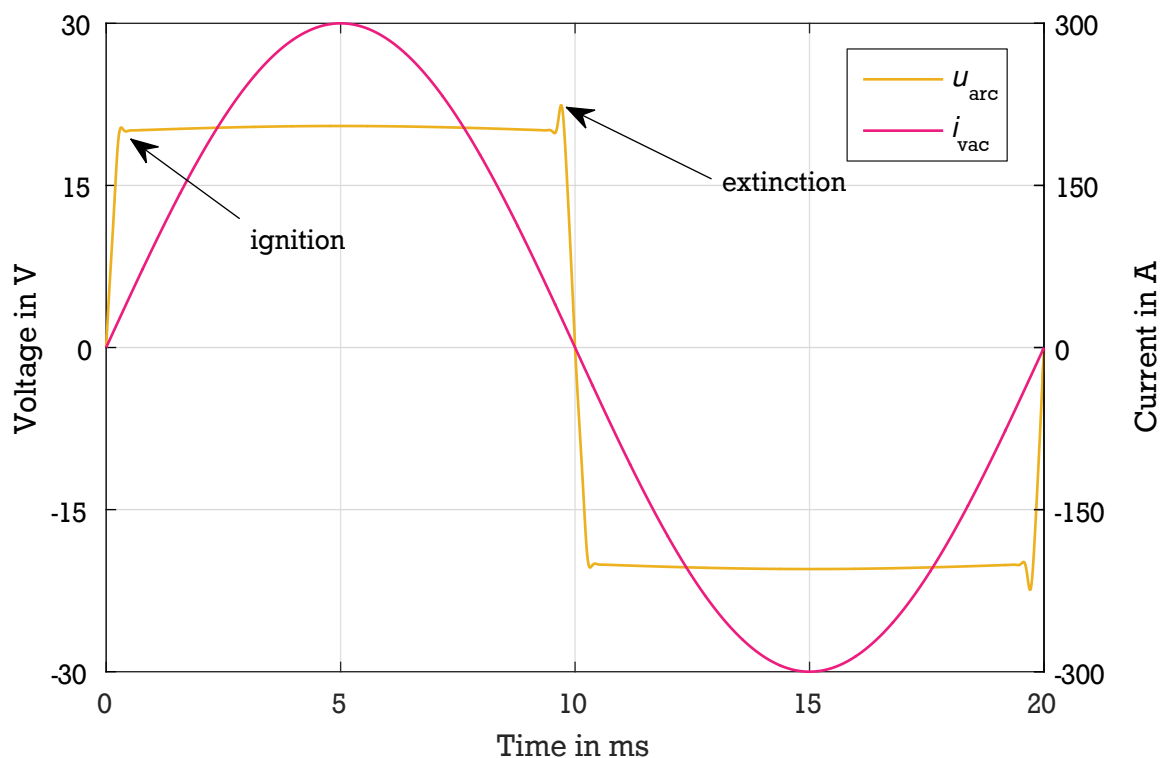


Abbildung 6.15: Typical variation of the arc voltage with respect to the arc current; taken from [Kap11]

³⁹ The making phase is a single event where the PD measurement device can be disconnected.

the highest voltage steepness⁴⁰ occurs during arc ignition and arc extinction while the period in between shows almost no change in voltage⁴¹. From these events, the arc extinction is the most critical. First, it is followed directly by the period when charged micro-particles shall be detected. Second, its voltage steepness is usually higher compared to that of an arc ignition. In general, the apparent charge of regular PDs or typical micro-particles is much smaller compared to those involved in the arc extinction. Therefore, it must be assumed, that the protection⁴² of the PD measurement system will be triggered due to the arc extinction. As a consequence, the system might be *blind* for a certain period of time.

6.3.3 Procedure to verify the absence of disturbances

There are two types of disturbances, PDs and EMIs, which can interfere with the charged micro-particle detection. Within this test environment, the absence of PDs can easily be verified due to the utilization of a PD measurement. For this purpose, the test circuit has to be set according to the operating sequence *recovery*, and rated RV has to be applied. However, verification of absence of EMIs is more complicated due to the auxiliary systems needed in a synthetic test circuit. In order to ensure a sufficient low EMI test environment, the following steps have been conducted:

- all four main switches involved in the capacitive switch off test sequence (see Tabelle 5.2), including the switch of the field-emission current measurement system's OCP, have been operated individually under no load
- the DC voltage source and the AC voltage source have been activated one after the other while the switches of the test circuit were set according to the operating sequence *recovery* (see Tabelle 5.2)
- a complete capacitive switch off test sequence has been performed with the exception that the RV was set to 0 V
- the RV has been applied with the voltage making switch to an already open test object while the high current sub-circuit was disconnected

During this time, the PD measurement system was connected in the FEOC configuration, and the output of the measurement impedance Z_{cc} was investigated. After identifying and solving an EMI⁴³, the verification steps were repeated. This procedure was repeated until no further EMI issues occurred.

Finally, the charged micro-particle detection was tested *manually*. As has been shown in Section 3.2, there is strong evidence that charged micro-particles are correlated with mechanical shocks. Thus, shocks were introduced to the VCB by hitting its movable terminal with a wooden stick. During this time, the test circuit was set to the operating sequence *recovery* and a RV was applied. As a result, multiple high frequency pulses have been captured while hitting the VI. An example is given in Abbildung 6.16 where three pulses have been captured⁴⁴. The time between two pulses and their number varies with each mechanical shock. Here, it is 8.6 ms and 9.6 ms. However, their shape and duration are similar.

⁴⁰ which causes compensation currents between the VCB and the coupling capacitor C_{cc}

⁴¹ high frequency components of the arc voltage are neglected

⁴² for example Zener diodes in parallel to the output

⁴³ for instance, the trigger system of the current making switch, position relays in the auxiliary breaker, ...

⁴⁴ The first pulse triggers the oscilloscope.

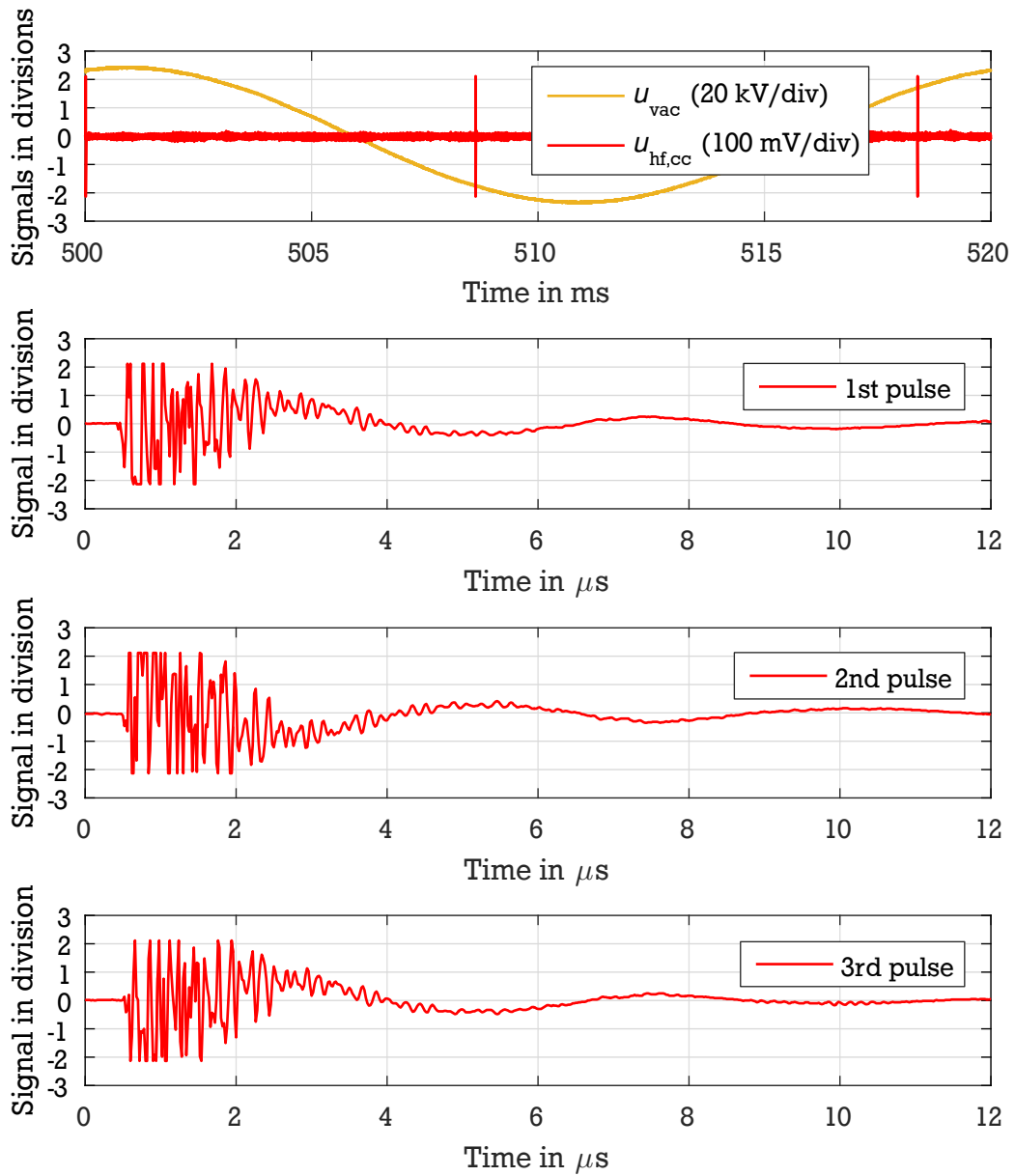


Abbildung 6.16: Captured high frequency pulses caused by a mechanical shock insertion

6.4 Preliminary results

In the following, the preliminary results of the simultaneous detection of field-emission currents and charged micro-particles are presented. They have been primarily designed for evaluation purposes of the measurement systems⁴⁵. As a consequence, the majority of these tests were conducted at an extremely reduced gap distance (down to 4 mm). This decision was based on the fact that under rated conditions⁴⁶, no late-breakdowns or field-emission currents above $20\ \mu\text{A}$ occurred. In addition, some tests were performed only with the AC part of the RV based on the following reasons:

- PD systems are optimized for AC systems
- in case of field-emission currents, two different dominant emission sites are possible due to the change of polarity

Furthermore, an arcing time t_{arc} of 5 ms or more has been used. This reduces the electric field stress within the first period of the RV which otherwise easily causes re-ignitions. This situation is demonstrated in Abbildung 6.17, where the electric field strength E_{vac} is given for two different arcing times.

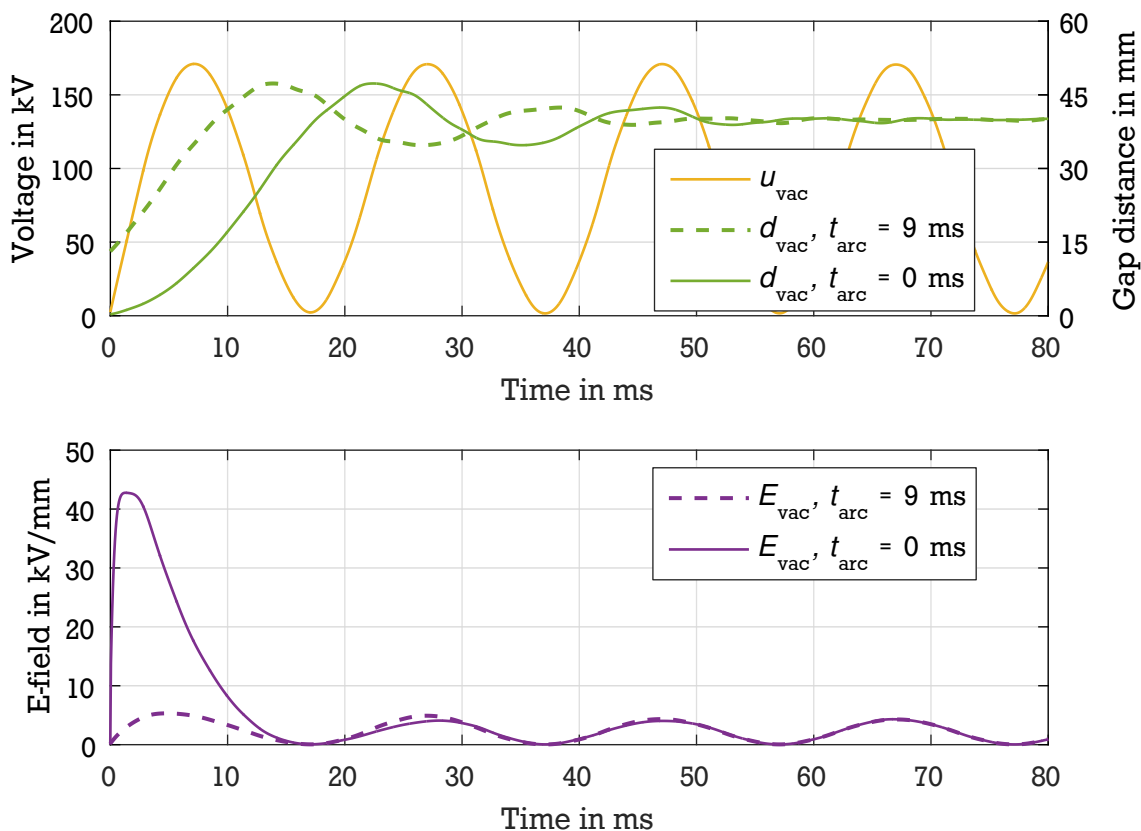


Abbildung 6.17: Homogeneous electric field strength E_{vac} inside the VI during contact separation with different arcing times

⁴⁵ They do not represent a scientific investigation of the test object.

⁴⁶ 40 mm, 200 kV

Simultaneous detection in MPOC configuration

The first tests of the simultaneous detection principle have been conducted in the MPOC configuration. In order to limit the capacitive current to the field-emission current measurement system, a coupling capacitor with only 100 pF has been used. Due to the missing ground connection, the output of the measuring impedance Z_{cc} has been directly processed with a battery powered PD acquisition unit⁴⁷ and the detected events have been analyzed with the associated PD evaluation software⁴⁸. Before each test, the whole detection system was calibrated with 100 pC impulses while the test circuit was set to the operating sequence *recovery*. In the following, two exemplary measurements are shown.

The first one⁴⁹ is given in Abbildung 6.18. Here, the gap distance is 40 mm, the $\{1 - \cos\}$ - shaped RV

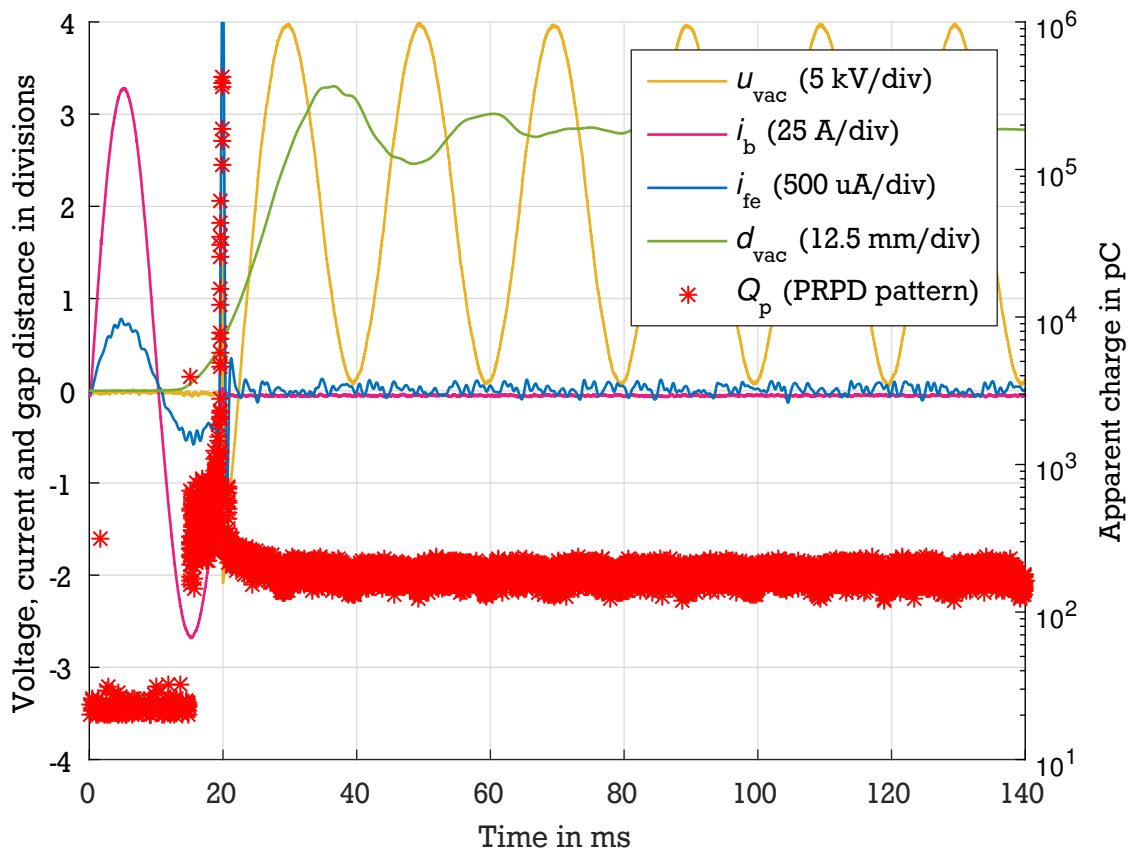


Abbildung 6.18: Simultaneous detection example 1 in MPOC configuration

20 kV, the breaking current up to 80 A and the arcing time 5 ms. The apparent charge threshold was set to 20 pC. In contrast to the voltage, current and gap distance signals, the apparent charge is displayed in a phase-resolved PD (PRPD) pattern. Thus, any detected event is plotted (synchronized to the voltage) as a discrete data point with its associated charge. As can be seen, no detectable field-emission currents occurred⁵⁰ and the results of the apparent charge can be described as follows. Before the breaking arc is ignited, only low noise with a mean value at the threshold level is detected. During the arcing phase, the apparent charge increases until it reaches a maximum at the arc extinction. This is followed by an increased noise level with a mean value around 200 pC. One possible explanation for the increased

⁴⁷ OMICRON MPD 600

⁴⁸ OMICRON Software for MPD and MI, version 1.6.5

⁴⁹ general function test with reduced voltage stress

⁵⁰ This is expected due to the low voltage stress.

noise level might be the disconnection of the large capacitance C_b of the breaking current source's *LRC*-resonance circuit which functions as a low-pass filter. As a consequence for future measurements, the threshold level was set to 100 pC.

A measurement with the improved settings is shown in Abbildung 6.19. Here, the gap distance was

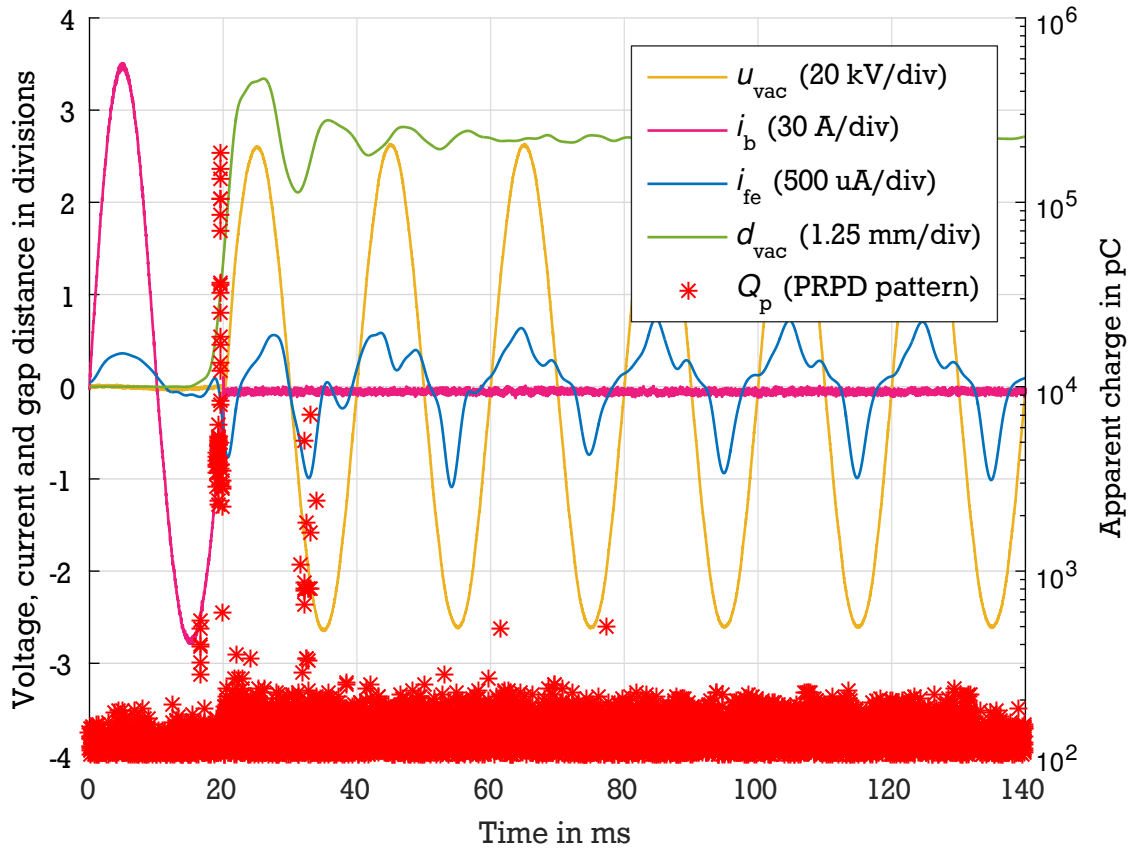


Abbildung 6.19: Simultaneous detection example 2 in MPOC configuration

reduced to 4 mm and the RV has only an AC component with an amplitude of 50 kV to provoke field-emission currents. As can be seen, beside the occurrence of field-emission currents⁵¹, also possible charged micro-particles above the noise level were detected. However, as a result of the MPOC configuration, the charged micro-particles are entirely analyzed with a PD measurement system (acquisition and evaluation). Given the fact that these tools are not designed for this kind of measurement environment, it cannot be excluded that the detected events are after-effects due to arcing based over-loads. Thus, in the following, measurements are conducted in the FEOC configuration.

Simultaneous detection in FEOC configuration

In contrast to the previous measurements, here, the output $u_{hf,cc}$ of the impedance Z_{cc} can be analyzed directly with the oscilloscope. In addition, it is possible to reconfigure the coupling capacitor C_{cc} to its rated capacitance of 1 nF. Based on this configuration, Abbildung 6.20 shows the result of measurement with identical test circuit parameters as used for Abbildung 6.19.

⁵¹ In the first periods the gap distance is not constant. Thus, its capacitance changes. As the capacitive displacement current compensation uses a constant capacitance, the signal of the field-emission current appears to be phase shifted.

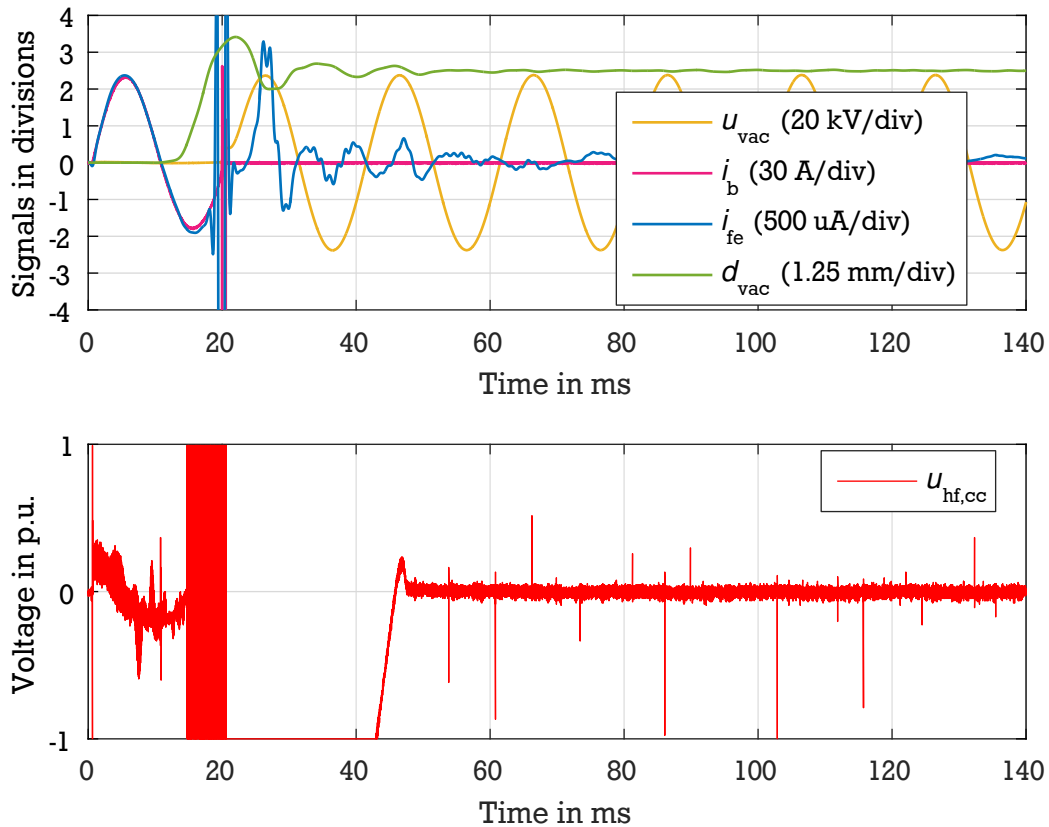


Abbildung 6.20: The first seven periods of an exemplary simultaneous detection in the FEOC configuration

As can be seen, in this particular measurement, during the first 30 ms of the recovery phase the signal $u_{hf,cc}$ is truncated. This is due to its protection system against over-loads. After this time, the system functions normally, and randomly distributed voltage pulses are detected. As micro-particles can be released by mechanical shocks as well, the detected pulses are not necessarily synced with the voltage stress (unlike PD). At the moment, these pulses cannot be analyzed further due to the lack of suitable tools (see Kapitel 7). However, it is possible to determine if high frequency current activity in the VI occurs or not. Within the limited number of experiments⁵², these pulses have been detected, with different statistical patterns, up to 1.4 s into the recovery phase, before they completely disappear. This behavior is exemplary demonstrated in Abbildung 6.21 with the associated complete signal of the measurement above. Additional high frequency current signatures with the same test configuration are located in the Appendix. By eliminating all other high frequency EMIs (see Section 6.3.3), it can be concluded, that these current pulses are caused by charged micro-particles inside the VI.

⁵² less than 100

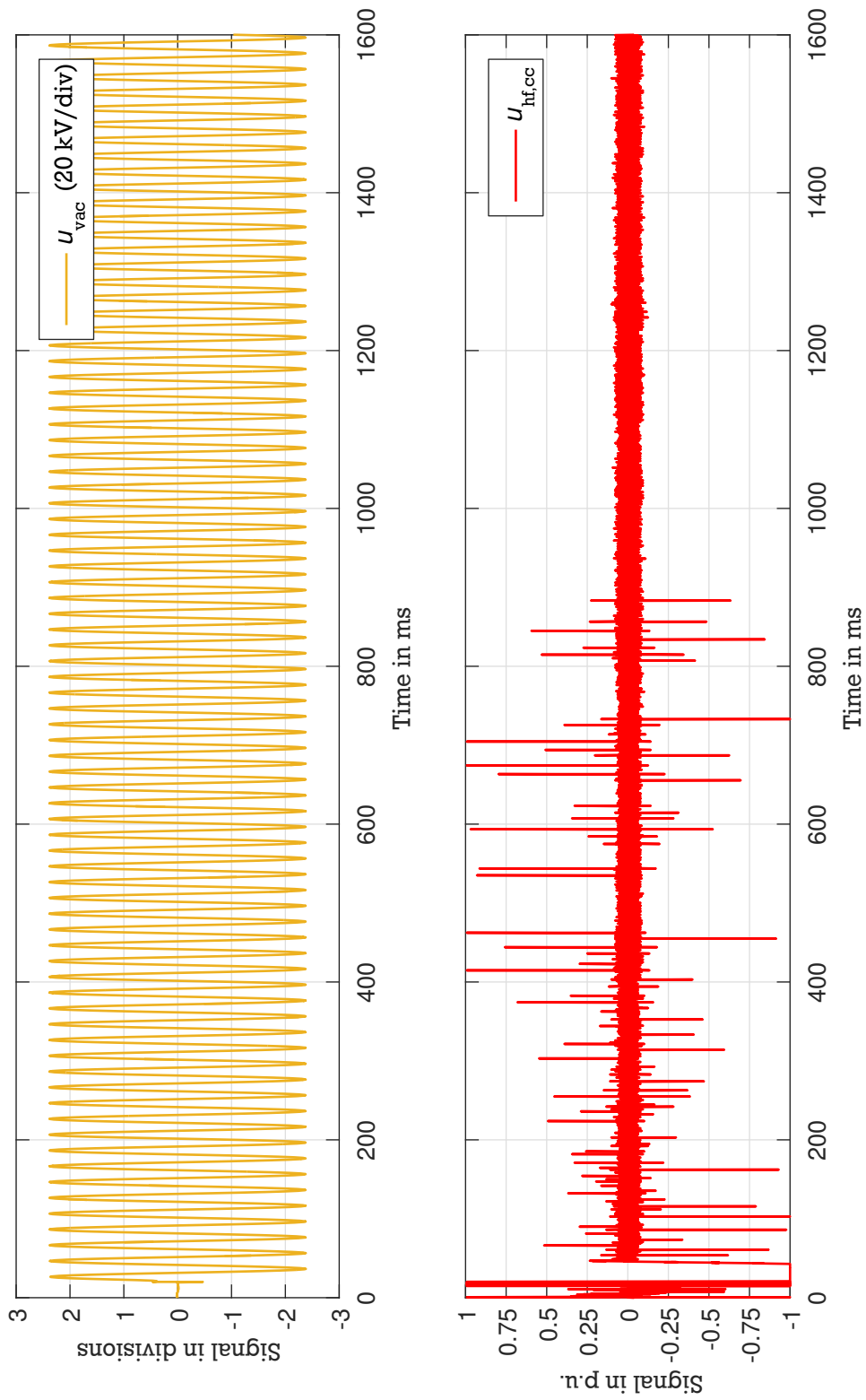


Abbildung 6.21: Complete high frequency current signature

7 Discussion and conclusion

This chapter starts with a review of the possibilities and limitations of the realized test circuit and test object. Afterwards, possible improvements of the field-emission current measurement and the introduction of a charged micro-particle detection system are discussed. In both cases, preliminary results are used to recommend possible steps for further investigations. This chapter ends with a discussion of the simultaneous detection principle of both pre-breakdown phenomena and a recommendation for the most suitable measurement circuitry.

7.1 Summary of the realized test circuit

Within this work, a (low power) synthetic test circuit has been constructed to test 72.5 kV VCBs under the condition of capacitive load switching. Compared to the existing designs used in the medium voltage level, the long-term stability of the RV¹ has been improved. This makes it possible to investigate late-breakdowns even several hundreds of milli-seconds after the beginning of the RV. Furthermore, the RV is switched to the test object less than 100 μs after the natural current zero of the breaking current. This makes it possible to investigate the impact of the VCB's mechanical chain to the occurrence of late-breakdowns. The only drawback of this optimization is the fact that the initial *transient* component of the RV cannot be realized anymore (at least not without additional components). Currently, there are no indications that this period influences the phenomenon of late-breakdowns. Thus, the latter can be investigated more efficiently with this test circuit compared to designs upscaled from the medium voltage level.

In addition, the test circuit and the test object are designed with a sufficient low PD and EMI level to allow sensitive detection of charged micro-particles. Regarding the test circuit, these requirements result in optimized auxiliary systems and additional field grading elements which have no impact on the current-/voltage-characteristic of capacitive switching test. However, the situation is different in case of the test object. Here, in order to ensure a low PD level and to avoid external dielectric breakdowns, in a first step, a customized VCB is used. However, this design (see Abbildung 5.3) differs in two aspects from a usual live-tank VCB (see Abbildung 2.1). First, its floating potentials of the vapor shield and the internal field grading elements are different. This is mainly caused by the use of a liquid insulation medium (dielectric constant 1.90) instead of a gaseous one (dielectric constant nearly one). Second, the test VI is mounted horizontally instead of vertically². This has, among other things, a strong impact on micro-particles. For instance, in a horizontal position, micro-particles can fall off the contact surface due to the earth's gravity field. While this practically designed test object is suitable for initial measurements regarding the charged micro-particle detection, it should be replaced with a regular VCB as soon as enough experience has been gathered.

¹ refers to the reduction of the DC voltage component decay

² due to space limitations

7.2 Discussion of the pre-breakdown current measurement

In the following, the improvements regarding the measurement and analysis of field-emission current as well as the identified detection principle for charged micro-particle detection are discussed. Finally, the simultaneous use of both detection principles is reviewed and recommendations for future measurement are given.

Field-emission current measurement and analysis

In a first step, the a field-emission current measurement system concept from the medium voltage level has been adapted towards a high number of consecutive capacitive switching operations. To achieve this, its passive power diode based protection has been replaced. Instead, a switch based system has been implemented which utilizes a synthetic test's property of a predefined high voltage and high current phase. Based on a comparison measurement between both protection principles, the following conclusion can be made. In a synthetic test environment, there is no need to use a diode based protection. Here, a power diode based protection is a possible source of a systematic measurement error.

In a second step, the FN analysis has been combined with a frequency analysis of the RV to detect mutual interferences between the test circuit and the test object. Such interferences are, for instance, capable of limiting the amplitude and rise time of field-emission currents and can hereby prevent its further development to a dielectric breakdown. However, with a determination of the total harmonic distortion of each period of the RV, these limitations can easily be identified and separated from further analysis.

Micro-particle detection

Within this work, a method to detect micro-particles in a VCB has been presented. It has been shown that charged micro-particles can be detected with this method and that their electrical characteristics are similar to PDs. Therefore, the PD measurement principle can be utilized for their detection. As a consequence, this requires a test environment with a sufficient low PD and EMI level. However, especially the low EMI level is difficult to verify. This is caused by the auxiliary systems needed in a synthetic test circuit to perform, for instance, a breaking operation³. Thus, a suitable EMI absence verification procedure has been introduced.

Based on first measurements, the following recommendations regarding the use of a PD measurement system can be made:

- a coupling capacitor and a PD measuring impedance are suitable to detect the apparent charge of micro-particles. However, the over-load protection of the PD measuring impedance causes a *blindness*⁴ after the breaking arc is extinguished.
- a PD acquisition unit in combination with the associated evaluation software is not suitable. This is due to the fact that these tools are not designed to work immediately after breaking operations. As a results, false apparent charge events might detected.

³ For example, the position sensor switch of the auxiliary breaker snaps into its final position during the recovery phase and is usually operated with 110 V DC.

⁴ up to a few periods of the RV

Thus, in order to estimate the amplitude and frequency range of charged micro-particle events, a PD measuring impedance is well suited. However, as soon as these parameters have been determined, the measurement system has to be improved regarding its *blindness*. For this purpose, a similar bypass switch as in the field-emission current measurement system can be used.

A further challenge is the data acquisition. This is based on the high frequency components in the measuring signal of a charged micro-particle event. As a consequence, a high sampling of at least 100 MS s^{-1} is required which cannot be maintained during the whole duration of the RV (up to seconds)⁵. Instead, a threshold triggered sequential measurement has to be conducted. However, especially due to the effects of the breaking operation, this trigger has to be linked with the test sequence⁶ to prevent false detections. Thus, a customized event based data acquisition is needed.

Based on preliminary results the following can be stated. First, a detection of charged micro-particles in a VCB after a real switching operation is in principle possible. Second, there is an indication that charged micro-particles can be released up to seconds after the current interruption.

Simultaneous detection principle

There are two possible measurement circuits available to detect field-emission currents and charged micro-particles simultaneously. However, in each case, the uncertainty of one measurement remains unchanged⁷ while the other one is decreased. Based on preliminary measurements, the FEOC configuration offers the best compromise due to the following reasons:

- The increase of uncertainty in the charged micro-particle measurement is of secondary importance because the charge Q_p alone⁸ has only a *small* significance. Thus, this measurement is in any case rather a detection to determine the presence and frequency of occurrence of charged micro-particles.
- A field-emission current measurement is not practical in a MPOC configuration due to the higher amplitude of total capacitive current. Here, the *normal* capacitive current of the test object is increased by the current caused by the coupling capacitor. Thus, the value of the measuring resistance has to be decreased to capture the total capacitive current which, in turn, increases the uncertainty of the field-emission current measurement.
- All measurements can be conducted with respect to ground reference.

It is therefore recommended to use the FEOC configuration for further measurements rather than the MPOC.

⁵ Practical data acquisition tools do not have enough memory.

⁶ Without this requirement, the sequenced memory mode of a modern oscilloscope could be used.

⁷ with respect to a single measurement with only this system

⁸ without the knowledge of its mass and shape



Appendix

Additional high frequency current signatures

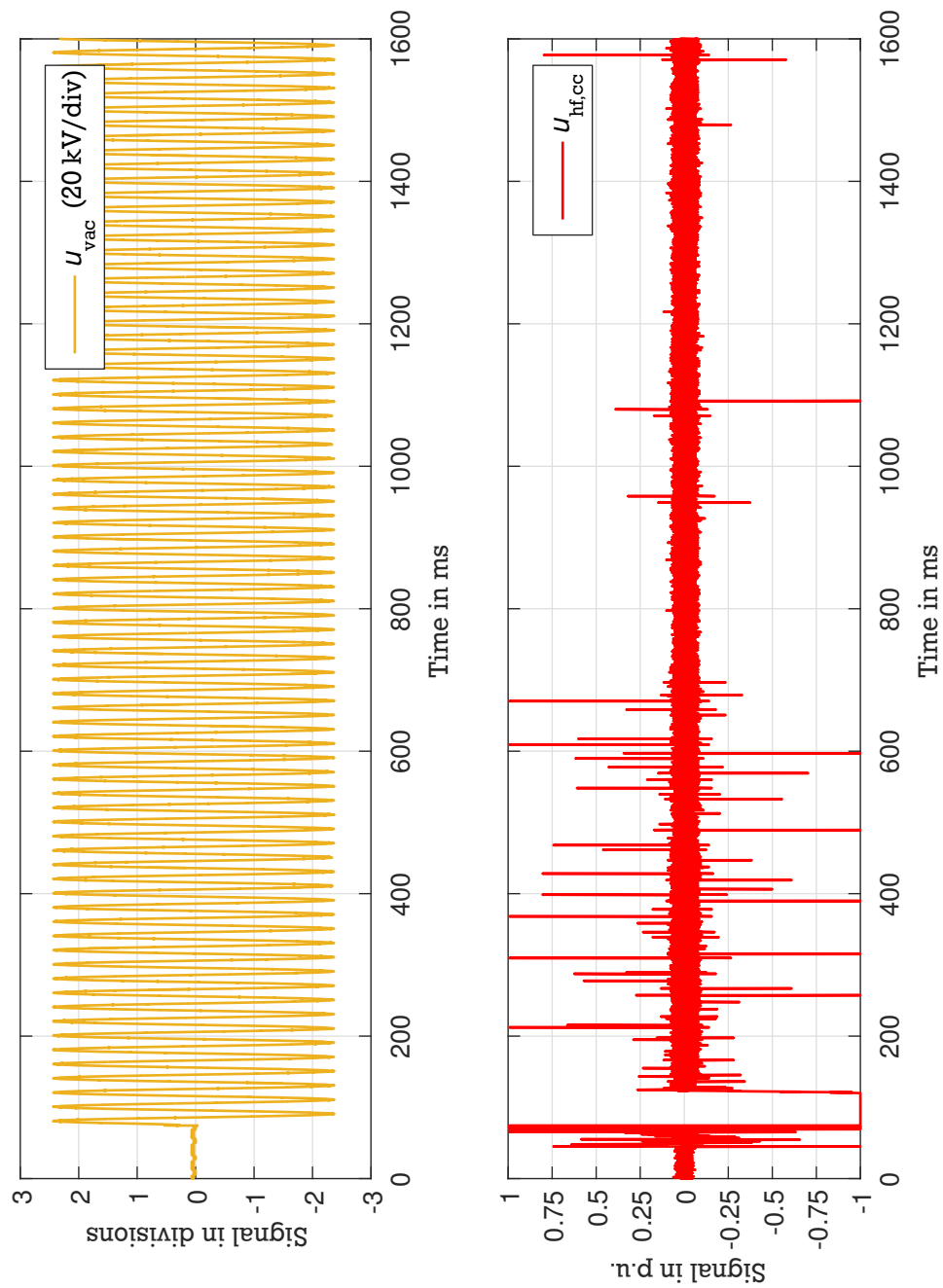


Abbildung 7.1: Additional complete high frequency current signature; same circuit setting as in Abbildung 6.21

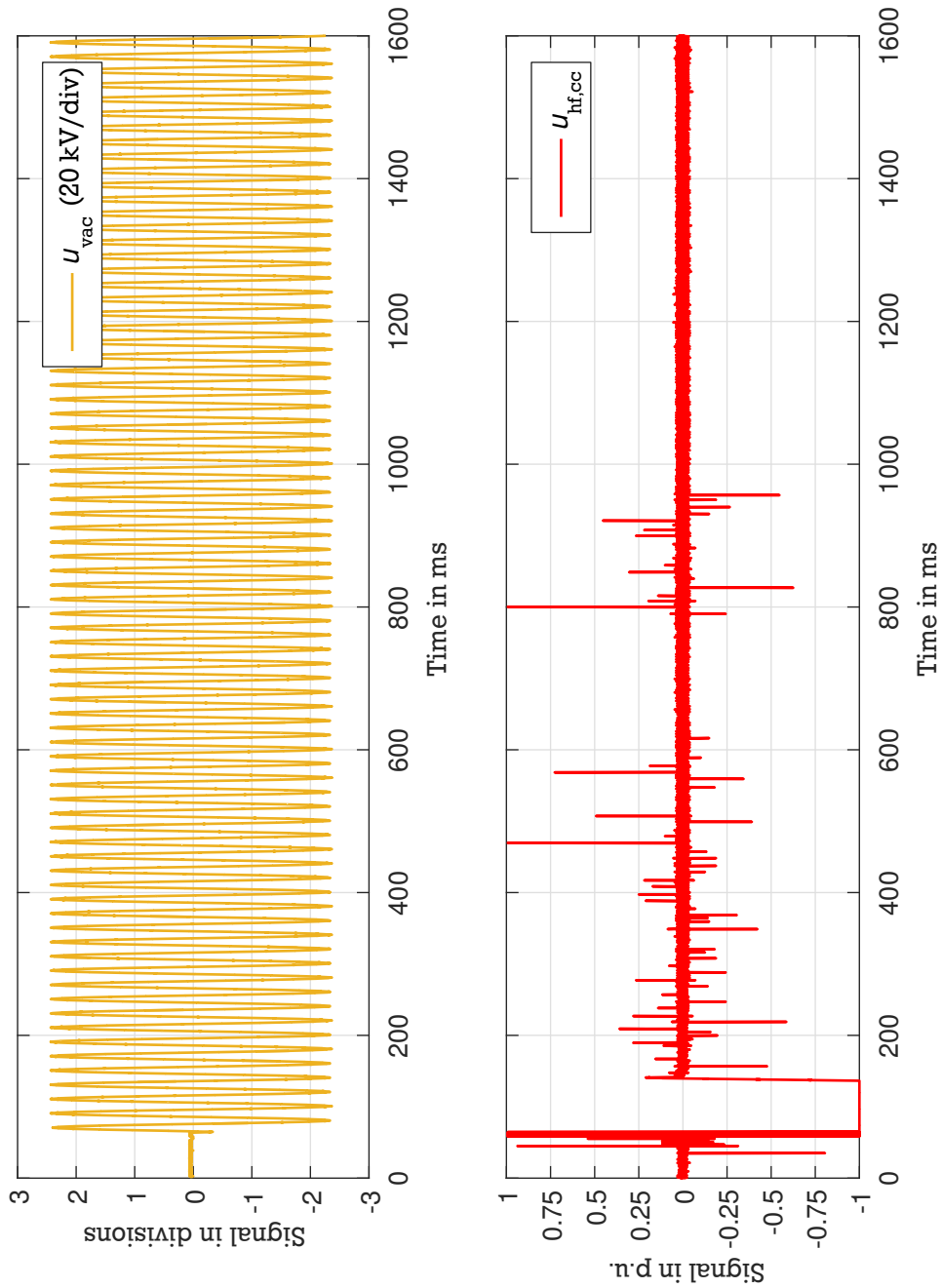


Abbildung 7.2: Additional complete high frequency current signature; same circuit setting as in Abbildung 6.21

Overview of the laboratory

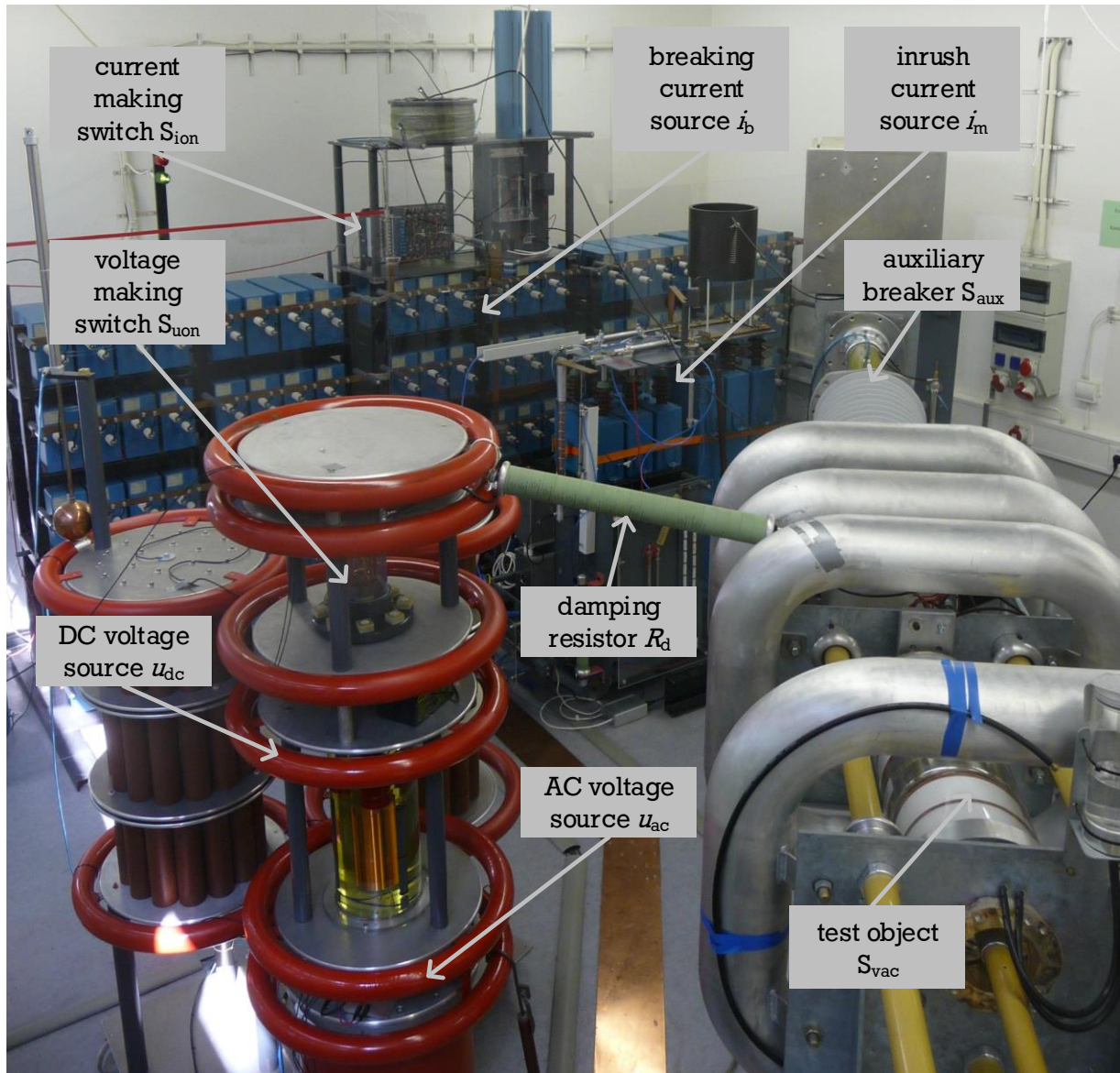


Abbildung 7.3: Overview of the laboratory



Literaturverzeichnis

- [3M99] 3M: *Fluorinert Electronic Liquids: For Electronic Reliability Testing*. 1999
- [ABB13] ABB: *Power Capacitors and Harmonic Filters: Buyer's Guide*. 2013
- [BBMR93] BARRAULT, M. ; BERNARD, G. ; MAFTOUL, J. ; ROWE, S.: Post-arc current measurement down to the ten milliamperes range. In: *IEEE Transactions on Power Delivery* 8 (1993), Nr. 4, S. 1782–1788. <http://dx.doi.org/10.1109/61.248285>. – DOI 10.1109/61.248285. – ISSN 08858977
- [BGW⁺12] BRUCHER, J. ; GIERE, S. ; WATIER, C. ; HESSENMÜLLER, A. ; NIELSEN, PE.: 3AV1FG - 72.5kV Prototype Vacuum Circuit Breaker (Case Study with Pilot Customers). In: CIGRE (Hrsg.): *CIGRE, Paris Session 2012*, 2012, S. n.a.
- [CIG14] CIGRE (Hrsg.): *The Impact of the Application of Vacuum Switchgear at Transmission Voltages: 589*. 2014
- [Cla11] CLAUSERT, Horst: *Gleichstromnetze, Operationsverstärkerschaltungen, elektrische und magnetische Felder*. 11., korrigierte Aufl. München : Oldenbourg, 2011 (Grundgebiete der Elektrotechnik). – ISBN 9783486597196
- [Coo58] COOK, Meluin A.: *Science of high explosives*. [S.l.] : Robert E Krieger, 1958. – ISBN 9780882750101
- [DGK⁺04] DULLNI, E. ; GENTSCH, D. ; KLEBERG, I. ; NIAYESH, K. ; WENKAI SHANG: Switching of capacitive currents. In: ISDEIV (Hrsg.): *21st International Symposium on Discharges and Electrical Insulation in Vacuum*, 2004, S. 407–410
- [DRG10] DELACHAUX, T. ; RAGER, F. ; GENTSCH, D.: Study of vacuum circuit breaker performance and weld formation for different drive closing speeds for switching capacitive current. In: ISDEIV (Hrsg.): *24th International Symposium on Discharges and Electrical Insulation in Vacuum*, 2010, S. 241–244
- [DTSY12] DONEN, Taiki ; TSUKIMA, Mitsuru ; SATO, Shinji ; YOSHIDA, Tomokazu: Investigation of correlation between vacuum breakdown phenomena and field emission current during shunt capacitor switching. In: ISDEIV (Hrsg.): *25th International Symposium on Discharges and Electrical Insulation in Vacuum*, 2012, S. 161–164
- [DWG⁺06] DULLNI, E. ; WENKAI SHANG ; GENTSCH, D. ; KLEBERG, I. ; NIAYESH, K.: Switching of capacitive currents and the correlation of restriking and pre-ignition behavior. In: *IEEE Transactions on Dielectrics and Electrical Insulation* 13 (2006), Nr. 1, S. 65–71. <http://dx.doi.org/10.1109/TDEI.2006.1593402>. – DOI 10.1109/TDEI.2006.1593402. – ISSN 1070–9878

-
- [DVTM14] DONEN, Taiki ; YANO, Tomotaka ; TSUKIMA, Mitsuru ; MIKI, Shinichi: The impact of capacitive switching condition on vacuum breakdown phenomena. In: ISDEIV (Hrsg.): *26th International Symposium on Discharges and Electrical Insulation in Vacuum*, 2014, S. 137–140
- [DZ10] DULLNI, Edgar ; ZHAO, Sean-Feng: Bouncing phenomena of vacuum interrupters. In: ISDEIV (Hrsg.): *24th International Symposium on Discharges and Electrical Insulation in Vacuum*, 2010, S. 463–466
- [EC83] EASTHAM, D. ; CHATTERTON, P: The Detection of Microparticle-Induced Breakdowns Using a Twin-Beam Laser Scattering System. In: *IEEE Transactions on Electrical Insulation* EI-18 (1983), Nr. 3, S. 209–213. <http://dx.doi.org/10.1109/TEI.1983.298601>. – DOI 10.1109/TEI.1983.298601. – ISSN 00189367
- [EE15] ENTSO-E: *ELECTRICITY IN EUROPE 2015*. 2015
- [Fal06] FALKINGHAM, L. T.: Vacuum Interrupter Design for HV and VHV Applications. In: ISDEIV (Hrsg.): *22nd International Symposium on Discharges and Electrical Insulation in Vacuum*, 2006, S. 204–207
- [Far93] FARRALL, G. A.: Electrical breakdown in vacuum interrupters. In: *IEEE Transactions on Electrical Insulation* 28 (1993), Nr. 4, S. 580–591. <http://dx.doi.org/10.1109/14.231541>. – DOI 10.1109/14.231541. – ISSN 00189367
- [Flu82] FLURSCHEIM, Charles H.: *IEE power engineering series*. Bd. 1: *Power circuit breaker theory and design*. Rev. ed. Stevenage : Peregrinus on behalf of the Institution of Electrical Engineers, 1982. – ISBN 978-0-90604-870-2
- [GH93] GEBEL, R. ; HARTMANN, W: Mechanical shocks as cause of late discharges in vacuum circuit breakers. In: *IEEE Transactions on Electrical Insulation* 28 (1993), Nr. 4, S. 468–472. <http://dx.doi.org/10.1109/14.231527>. – DOI 10.1109/14.231527. – ISSN 00189367
- [Gie03] GIERE, Stefan: *Vakuumschalttechnik im Hochspannungseinsatz*. Braunschweig, Technische Universität Carolo-Wilhelmina zu Braunschweig, Dissertation, 2003
- [GPS⁺51] GOUCHER, F. S. ; PEARSON, G. L. ; SPARKS, M. ; TEAL, G. K. ; SHOCKLEY, W: Theory and Experiment for a Germanium p–n Junction. In: *Physical Review* 81 (1951), Nr. 4, S. 637–638. <http://dx.doi.org/10.1103/PhysRev.81.637.2>. – DOI 10.1103/PhysRev.81.637.2. – ISSN 0031-899X
- [Gre11] GREMMEL, Hennig (Hrsg.): *Schaltanlagen Handbuch*. 12., neubearb. Aufl. Berlin : Cornelsen, 2011. – ISBN 9783589241026
- [GRRT12] GIERE, S. ; RENZ, R. ; RICHTER, F. ; TRAPP, N.: Capacitive current switching capability of 72.5 kV high-voltage vacuum interrupters. In: ISDEIV (Hrsg.): *25th International Symposium on Discharges and Electrical Insulation in Vacuum*, 2012, S. 217–220

-
- [Hal13] HALBACH, Patrick: *Einfluss des Prüfkreises auf das Abreißstromverhalten von Vakuumschaltern unter Berücksichtigung spezieller Netzkonfigurationen in der Mittelspannung*. Darmstadt, Technische Universität Darmstadt, Dissertation, 2013
- [Hig04] HIGH-VOLTAGE SWITCHGEAR AND CONTROLGEAR: *Part 100: High-voltage alternating-current circuit-breakers*. 2.0. 2008-04
- [HL14] HAUSCHILD, Wolfgang ; LEMKE, Eberhard: *High-Voltage Test and Measuring Techniques*. Berlin, Heidelberg and s.l. : Springer Berlin Heidelberg, 2014. <http://dx.doi.org/10.1007/978-3-642-45352-6>. <http://dx.doi.org/10.1007/978-3-642-45352-6>. – ISBN 9783642453519
- [Hos88] HOSEMANN, Gerhard: *Elektrische Energietechnik*. 29. Aufl. Berlin and Heidelberg : Springer, 1988. – ISBN 9780387153599
- [HSM07] HERING, Ekbert ; STOHRER, Martin ; MARTIN, Rolf: *Physik für Ingenieure*. 10. neubearb. Aufl. Berlin [u.a.] : Springer, 2007 (Springer-Lehrbuch). – ISBN 3540718567
- [JLD99] JÜTTNER, Burkhard ; LINDMAYER, Manfred ; DÜNING, Gerd: Instabilities of prebreakdown currents in vacuum I: late breakdowns. In: *Journal of Physics D: Applied Physics* 32 (1999), Nr. 19, S. 2537. – ISSN 0022–3727
- [JS81] JÜTTNER, B. ; SIEMROTH, P.: Über den Gleichspannungsdurchschlag im Ultrahochvakuum. In: *Beiträge aus der Plasmaphysik* 21 (1981), Nr. 4, S. 233–245. <http://dx.doi.org/10.1002/ctpp.19810210402>. – DOI 10.1002/ctpp.19810210402. – ISSN 00058025
- [Kap11] KAPETANOVIC, Mirsad: *High voltage circuit breakers*. Bosnia : Sarajevo, 2011
- [KBFO00] KOLYADA, Yu.E. ; BULANCHUK, O. N. ; FEDUN, V. I. ; ONISHCHENKO, I. N.: Aerosol microparticles and emission characteristics of the pulsed high-current vacuum diode in a microsecond range. In: ISDEIV (Hrsg.): *19th International Symposium on Discharge and Electrical Insulation in Vacuum*, 2000, S. 68–71
- [KD04] KIENLE, Paul ; DRANSFELD, Klaus: *Physik: II: Physik II: Elektrodynamik und Spezielle Relativitätstheorie*. 7., 7., aktualisierte Aufl. 2004. <http://dx.doi.org/10.1524/9783486846287>. <http://dx.doi.org/10.1524/9783486846287>. – ISBN 3486585983
- [KE65] KNOLL, Max ; EICHMEIER, Joseph: *Technische Elektronik: Erster Band Grundlagen und Vakuumtechnik*. Berlin, Heidelberg : Springer Berlin Heidelberg, 1965. <http://dx.doi.org/10.1007/978-3-642-92902-1>. <http://dx.doi.org/10.1007/978-3-642-92902-1>. – ISBN 9783642929038
- [KF95] KIND, Dieter ; FESER, Kurt: *Hochspannungs-Versuchstechnik: Mit 211 Bildern und 12 Laborversuchen*. 5., überarb. und erw. Aufl. Braunschweig : Vieweg, 1995 (Studium Technik). – ISBN 3528438053

- [KH89] KONIG, D. ; HEINEMEYER, R.: Prebreakdown currents of vacuum tubes with increased pressure stressed with AC voltage. In: *IEEE Transactions on Electrical Insulation* 24 (1989), Nr. 6, S. 937–941. <http://dx.doi.org/10.1109/14.46316>. – DOI 10.1109/14.46316. – ISSN 00189367
- [KHK10] KOOCHACK ZADEH, M. ; HINRICHSSEN, V. ; KUIVENHOVEN, S.: Measurement of field emission current during switching of capacitive current in vacuum. In: ISDEIV (Hrsg.): *24th International Symposium on Discharges and Electrical Insulation in Vacuum*, 2010, S. 249–252
- [KHSL10] KOOCHACK ZADEH, M. ; HINRICHSSEN, V. ; SMEETS, R. ; LAWALL, A.: The impact of capacitor bank inrush current on field emission current in vacuum. In: ISDEIV (Hrsg.): *24th International Symposium on Discharges and Electrical Insulation in Vacuum*, 2010, S. 210–213
- [KHSL11] KOOCHACK ZADEH, M. ; HINRICHSSEN, V. ; SMEETS, R. ; LAWALL, A.: Field emission currents in vacuum breakers after capacitive switching. In: *IEEE Transactions on Dielectrics and Electrical Insulation* 18 (2011), Nr. 3, S. 910–917. <http://dx.doi.org/10.1109/TDEI.2011.5931080>. – DOI 10.1109/TDEI.2011.5931080. – ISSN 1070–9878
- [KKFN01] KIESSLING, Friedrich ; KAJNTZYK, Ulf ; FISCHER, Reinhard ; NEFZGER, Peter: *Freileitungen: Planung, Berechnung, Ausführung ; mit 163 Tabellen*. 5., vollst. neu bearb. Aufl. Berlin [u.a.] : Springer, 2001. – ISBN 9783540422556
- [KLKG07] KORNER, Florian ; LINDMAYER, Manfred ; KURRAT, Michael ; GENTSCH, Dietmar: Contact behavior in vacuum under capacitive switching duty. In: *IEEE Transactions on Dielectrics and Electrical Insulation* 14 (2007), Nr. 3, S. 643–648. <http://dx.doi.org/10.1109/TDEI.2007.369525>. – DOI 10.1109/TDEI.2007.369525. – ISSN 1070–9878
- [KLKG08] KORNER, Florian ; LINDMAYER, Manfred ; KURRAT, Michael ; GENTSCH, Dietmar: Switching behavior of different contact materials under capacitive switching conditions. In: ISDEIV (Hrsg.): *23rd International Symposium on Discharges and Electrical Insulation in Vacuum*, 2008, S. 202–205
- [KMK⁺14] KIKUCHI, Yuto ; MATSUOKA, Shigeyasu ; KUMADA, Akiko ; HIDAKA, Kunihiko ; DONEN, Taiki ; TSUKIMA, Mitsuru: Motion observation of particles between electrodes and subsequent breakdown phenomena in vacuum. In: ISDEIV (Hrsg.): *26th International Symposium on Discharges and Electrical Insulation in Vacuum*, 2014, S. 133–136
- [Koc02] KOCH, H.: Gasisolierte Übertragungsleitungen der zweiten Generation für das Hochspannungsnetz. In: *e & i Elektrotechnik und Informationstechnik* 119 (2002), Nr. 1, S. 1–5. <http://dx.doi.org/10.1007/BF03161462>. – DOI 10.1007/BF03161462. – ISSN 0932–383X
- [Koo11] KOOCHACK ZADEH, Masoumeh: *Field Emission Current Analysis for the Assessment of Dielectric and Switching Performance of Vacuum Interrupters*. Darmstadt, Technische Universität Darmstadt, Dissertation, 2011

-
- [Kör08] KÖRNER, Florian: *Kontaktverhalten von Vakuumschaltern beim kapazitiven Schalten: Zugl.: Braunschweig, Techn. Univ., Diss., 2008.* 1. Aufl. München : Hut, 2008. – ISBN 9783899639162
- [KSF⁺95] KAMIKAWAJI, T. ; SHIOIRI, T. ; FUNAHASHI, T. ; OKAWA, M. ; KANEKO, E. ; OHSHIMA, I.: Generation of microparticles from copper-chromium contacts in vacuum. In: *IEEE Transactions on Power Delivery* 10 (1995), Nr. 1, S. 286–293. <http://dx.doi.org/10.1109/61.368387>. – DOI 10.1109/61.368387. – ISSN 08858977
- [KSW13] KORIES, Ralf ; SCHMIDT-WALTER, Heinz: *Taschenbuch der Elektrotechnik: Grundlagen und Elektronik.* 10., korrigierte Auflage. Haan-Gruiten : Verlag Europa-Lehrmittel, 2013. – ISBN 9783808556696
- [Kuc07] KUCHLING, Horst: *Taschenbuch der Physik: Mit zahlreichen Tabellen.* 19., aktualisierte Aufl. München : Fachbuchverl. Leipzig im Carl-Hanser-Verl., 2007. – ISBN 978-3446410282
- [Küc09] KÜCHLER, Andreas: *Hochspannungstechnik: Grundlagen - Technologie - Anwendungen.* 3., neu bearb. und erw. Aufl. Dordrecht and New York : Springer, 2009 (VDI-Buch). – ISBN 978-3-540-78412-8
- [Lat95] LATHAM, R. V.: *High voltage vacuum insulation: Basic concepts and technological practice.* London and San Diego : Academic Press, 1995. – ISBN 0-12-437175-2
- [Leu00] LEUSENKAMP, M.B.J.: Nonsustained disruptive discharges in vacuum interrupters. In: IS-DEIV (Hrsg.): *19th International Symposium on Discharge and Electrical Insulation in Vacuum*, 2000, S. 495–498
- [Lip03] LIPPMANN, Hans-Joachim: *Schalten im Vakuum: Physik und Technik der Vakuumschalter.* Berlin and Offenbach : VDE-Verl., 2003. – ISBN 3800723174
- [LWX⁺07] LIU, Zhiyuan ; WANG, Jimei ; XIU, Shixin ; WANG, Zhongyi ; YUAN, Shun ; JIN, Li ; ZHOU, Heming ; YANG, Ren: Development of High-Voltage Vacuum Circuit Breakers in China. In: *IEEE Transactions on Plasma Science* 35 (2007), Nr. 4, S. 856–865. <http://dx.doi.org/10.1109/TPS.2007.896929>. – DOI 10.1109/TPS.2007.896929. – ISSN 00933813
- [Mil15] MILLER, H. C.: Flashover of insulators in vacuum: The last twenty years. In: *IEEE Transactions on Dielectrics and Electrical Insulation* 22 (2015), Nr. 6, S. 3641–3657. <http://dx.doi.org/10.1109/TDEI.2015.004702>. – DOI 10.1109/TDEI.2015.004702. – ISSN 1070-9878
- [MNK⁺75] MURANO, M. ; NISHIKAWA, H. ; KOBAYASHI, A. ; OKAZAKI, T. ; YAMASHITA, S.: Current zero measurement for circuit breaking phenomena. In: *IEEE Transactions on Power Apparatus and Systems* 94 (1975), Nr. 5, S. 1890–1900. <http://dx.doi.org/10.1109/T-PAS.1975.32035>. – DOI 10.1109/T-PAS.1975.32035. – ISSN 0018-9510
- [MS74] MENON, M. M. ; SRIVASTAVA, K. D.: The nature of micro-particles and their role in vacuum breakdown. In: ISDEIV (Hrsg.): *6th International Symposium on Discharges and Electrical Insulation in Vacuum*, 1974, S. 3–10

- [MVG02] MESCHÉDE, Dieter ; VOGEL, Helmut ; GERTHSEN, Christian: *Physik: Mit 92 Tabellen, 109 durchgerechneten Beispielen und 1049 Aufgaben mit vollständigen Lösungswegen ; [die ganze Physik zum 21. Jahrhundert]*. 21., völlig Neubearb. Aufl. Berlin [u.a.] : Springer, 2002 (Springer-Lehrbuch). – ISBN 9783540420248
- [Nat05] NATIONAL INSTRUMENTS: *NI 6122/6123 Specifications*. 2005
- [nkt09] NKT CABLES: *Hochspannung und Offshore - nkt cables*. <http://www.nktcables.com/de/support/download/catalogues-and-brochures/high-voltage-and-offshore/>.
Version: 2009
- [Nor13] NORTH STAR HIGH VOLTAGE, INC.: *Voltage Probe Manual and Data*. 2013
- [Omi16] OMICRON: *MPD 600: High-end measurement and analysis system for partial discharges*. 2016
- [OO04] OEDING, Dietrich ; OSWALD, Bernd R.: *Elektrische Kraftwerke und Netze*. 6. Auflage. Berlin, Heidelberg and s.l. : Springer Berlin Heidelberg, 2004. <http://dx.doi.org/10.1007/978-3-662-06960-8>. <http://dx.doi.org/10.1007/978-3-662-06960-8>. – ISBN 9783662069615
- [RC77] RAVINDRANATH, B. ; CHANDER, M.: *Power system protection and switchgear*. New Delhi : New Age, 1977. – ISBN 9780852267585
- [SBM95] SANDERS, David M. ; BOXMAN, R. L. ; MARTIN, Philip J.: *Handbook of vacuum arc science and technology: Fundamentals and applications*. Park Ridge, N.J., U.S.A. : Noyes Publications, 1995 (Materials science and process technology series. Electronic materials and process technology). – ISBN 0815513755
- [SCG⁺12] SANDOLACHE, G. ; CHAKRABORTY, S. ; GACHES, L. ; SMEETS, R. ; KUIVENHOVEN, S. ; NOVAK, P. ; BEER, P.: An investigation into late breakdown phenomena during capacitor switching performances in relation with vacuum interrupter design and field emission current. In: ISDEIV (Hrsg.): *25th International Symposium on Discharges and Electrical Insulation in Vacuum*, 2012, S. 441–444
- [Sch08] SCHELLEKENS, Hans: Capacitor bank switching with vacuum circuit breakers. In: ISDEIV (Hrsg.): *23rd International Symposium on Discharges and Electrical Insulation in Vacuum*, 2008, S. 157–160
- [SEG⁺10] SANDOLACHE, G. ; ERNST, U. ; GODECHOT, X. ; KANTAS, S. ; HAIROUR, M. ; DALMAZIO, L.: Switching of capacitive current with vacuum interrupters. In: ISDEIV (Hrsg.): *24th International Symposium on Discharges and Electrical Insulation in Vacuum*, 2010, S. 129–132
- [Sie10] SIEMENS AG: *Vakuum-Leistungsschalter 3AH5: Mittelspannungsgeräte Auswahl- und Bestelldaten*. 2010
- [Sie11] SIEMENS AG: *High Voltage Products: The complete portfolio from one source*. 2011

- [Sie12a] SIEMENS AG: *High-Voltage goes Vacuum: Vacuum Circuit Breakers for 72.5kV and 145kV (prototype): Flyer*. 2012
- [Sie12b] SIEMENS AG: *High-Voltage goes Vacuum: Vacuum Circuit Breakers for 72.5kV and 145kV (prototype): Presentation*. 2012
- [SK07] SCHWAB, Adolf J. ; KÜRNER, Wolfgang: *Elektromagnetische Verträglichkeit*. 5., aktualisierte und erg. Aufl. Berlin and New York : Springer, 2007. – ISBN 3540686231
- [SK13] SMEETS, R.P.P. ; KUIVENHOVEN, S.: The impact of switching capacitor banks with very high inrush current on vacuum switchgear. In: ICEPE-ST (Hrsg.): *2nd International Conference on Electric Power Equipment - Switching Technology*, 2013, S. 1–4
- [SKCS12] SMEETS, R. P. P. ; KUIVENHOVEN, S. ; CHAKRABORTY, S. ; SANDOLACHE, G.: Field electron emission current in vacuum interrupters after large inrush current. In: ISDEIV (Hrsg.): *25th International Symposium on Discharges and Electrical Insulation in Vacuum*, 2012, S. 157–160
- [SKF00] SATO, S. ; KOYAMA, K. ; FUJII, H.: Behavior of conductive microparticles under electric field in vacuum and their influence on breakdown characteristics. In: ISDEIV (Hrsg.): *19th International Symposium on Discharge and Electrical Insulation in Vacuum*, 2000, S. 25–28
- [Sla08] SLADE, Paul G.: *The vacuum interrupter: Theory, design, and application*. Boca Raton : CRC Press, 2008. – ISBN 978-0-8493-9091-3
- [SMI97] SMITHSON, PETER A.: Book review: Climate change 1995: the science of climate change. Contribution of working group 1 to the second assessment report of the intergovernmental panel on climate change. J. T. Houghton, L. G. Meira Filho, B. A. Callendar, N. Harris, A. Kattenberg and K. Maskell (eds). Cambridge University Press (Cambridge) 1996. No. of pages: xii+572 pp. Price: £65.00, US\$90.00 ISBN 0-521-56433-6 (hardback); £22.95, US\$34.95 ISBN 0-521-56436-0 (paperback). In: *International Journal of Climatology* 17 (1997), Nr. 8, S. 904–905. [http://dx.doi.org/10.1002/\(SICI\)1097-0088\(19970630\)17:8<904::AID-JOC178>3.0.CO;2-6](http://dx.doi.org/10.1002/(SICI)1097-0088(19970630)17:8<904::AID-JOC178>3.0.CO;2-6). – DOI 10.1002/(SICI)1097-0088(19970630)17:8<904::AID-JOC178>3.0.CO;2-6. – ISSN 08998418
- [Sv08] SCHAVEMAKER, Pieter ; VAN DER SLUIS, Lou: *Electrical power system essentials*. Chichester, England and Hoboken, NJ : Wiley, 2008. – ISBN 0470510277
- [SvK⁺15] SMEETS, Rene Peter P. ; VAN DER SLUIS, LOU ; KAPETANOVIC, Mirsad ; PELO, David F. ; JANSSEN, Anton: *Switching in power transmission and distribution systems*. Chichester, West Sussex, United Kingdom : Wiley, 2015. – ISBN 1118381351
- [SWB⁺12] SMEETS, R.P.P. ; WIGGERS, R. ; BANNINK, H. ; KUIVENHOVEN, S. ; CHAKRABORTY, S. ; SANDOLACHE, G.: The Impact of Switching Capacitor Banks with Very High Inrush Current on Switchgear. In: CIGRE (Hrsg.): *CIGRE, Paris Session 2012*, 2012, S. n.a.
- [TDK15] TDK ; EPCOS AG (Hrsg.): *Surge arrester: 2-electrode arrester*. 2015

-
- [Tel15] TELEDYNE LECROY ; TELEDYNE LECROY (Hrsg.): *WaveSurfer 3000 Oscilloscopes: 200 MHz – 750 MHz*. 2015
- [Toz04] TOZER, E.P.J.: *Broadcast Engineer's Reference Book*. Elsevier/Focal Press, 2004 <https://books.google.de/books?id=DL73f4vFeEwC>. – ISBN 9780240519081
- [TS98] TAKAHASHI, E. ; SONE, M.: Observation of field emission sites and study of heat treatment effects. In: *IEEE Transactions on Dielectrics and Electrical Insulation* 5 (1998), Nr. 6, S. 929–934. <http://dx.doi.org/10.1109/94.740778>. – DOI 10.1109/94.740778. – ISSN 1070–9878
- [WWH01] WIBERG, Egon ; WIBERG, Nils ; HOLLEMAN, A. F.: *Inorganic chemistry*. 1st English ed. / [edited] by Nils Wiberg. San Diego and London : Academic Press, 2001. – ISBN 0123526515
- [XKH⁺15] XU, Shuo ; KUMADA, Akiko ; HIDAKA, Kunihiko ; IKEDA, Hisatoshi ; KANEKO, Eiji: Observation of pre-discharge phenomena with point-to-plane electrodes in vacuum under AC. In: *IEEE Transactions on Dielectrics and Electrical Insulation* 22 (2015), Nr. 6, S. 3633–3640. <http://dx.doi.org/10.1109/TDEI.2015.004684>. – DOI 10.1109/TDEI.2015.004684. – ISSN 1070–9878
- [YGL12] YANG, He ; GENG, Yingsan ; LIU, Zhiyuan: Capacitive current switching of Vacuum Interrupters and inrush currents. In: ISDEIV (Hrsg.): *25th International Symposium on Discharges and Electrical Insulation in Vacuum*, 2012, S. 228–231
- [YGL⁺14] YANG, He ; GENG, Yingsan ; LIU, Zhiyuan ; ZHANG, Yingyao ; WANG, Jianhua: Capacitive switching of vacuum interrupters and inrush currents. In: *IEEE Transactions on Dielectrics and Electrical Insulation* 21 (2014), Nr. 1, S. 159–170. <http://dx.doi.org/10.1109/TDEI.2013.004017>. – DOI 10.1109/TDEI.2013.004017. – ISSN 1070–9878
- [YSM⁺08] YOSHIDA, Tadahiro ; SATO, Shinji ; MIKI, Shinichi ; HARADA, Takakazu ; KOGA, Hiromi: Restrike characteristics on capacitive current breaking in vacuum. In: ISDEIV (Hrsg.): *23rd International Symposium on Discharges and Electrical Insulation in Vacuum*, 2008, S. 210–212
- [YWG⁺16] YAO, Xiaofei ; WANG, Jianhua ; GENG, Yingsan ; YAN, Jing ; LIU, Zhiyuan ; YAO, Jianjun ; LIU, Ping: Development and Type Test of a Single-Break 126-kV/40-kA–2500-A Vacuum Circuit Breaker. In: *IEEE Transactions on Power Delivery* 31 (2016), Nr. 1, S. 182–190. <http://dx.doi.org/10.1109/TPWRD.2015.2456033>. – DOI 10.1109/TPWRD.2015.2456033. – ISSN 08858977
- [YWY⁺14] YU, Yongxiang ; WANG, Jianhua ; YANG, He ; GENG, Yingsan ; LIU, Zhiyuan: The impact of inrush current on field emission current of vacuum interrupters during capacitive current switching. In: ISDEIV (Hrsg.): *26th International Symposium on Discharges and Electrical Insulation in Vacuum*, 2014, S. 145–148

Own publications

1. P. Halbach, B. Baum, V. Hinrichsen, K. Ermeler, J. Teichmann: *Investigations of Current Instabilities before Current Zero for Typical Load Switching Applications*. Proceedings, ISH, August 2011, Hannover/Germany.
2. B. Baum, H. Janssen, V. Hinrichsen: *Dielectric testing of HV vacuum interrupters during capacitive current switching*. Abstract & presentation at 4th ITG International Vacuum Electronics Workshop, October 2014, Bad Honnef/Germany.
3. B. Baum, H. Janssen, M. Holbein: *Ortung von Emissionsstellen in Vakuum-Schaltrohren*. Prior Art Journal, Vol. 21, p. 96, October 2014, Berlin/Germany.
4. B. Baum, B. Surges, V. Hinrichsen: *Dielectric Testing of HV Vacuum Interrupters during Capacitive Current Switching*. Proceedings, ISH, August 2015, Pilsen/Czech Republic.
5. H. Janssen, B. Baum, V. Hinrichsen: *Non-destructive Measuring Method to Locate Inhomogeneities on a Contact Surface of a Vacuum Circuit Breaker*. Proceedings, ISH, August 2015, Pilsen/Czech Republic.



Supervised student research projects and diploma theses

Within this work, the following student theses have been supervised and are part of the presented results:

1. Feilbach, Alexander. *Assembly and start-up of a synthetic test circuit to investigate the dielectric strength of a 72.5 kV vacuum bottle when switching capacitive loads*. Number 1868. Darmstadt, 2011.
2. Schlegel, Barbara. *Development of a measurement system to determine the floating potential of the vapor shields of a 72.5 kV vacuum bottle*. Number 1875. Darmstadt, 2012.
3. Unger, Katja. *Development of an electrical simulation model of a 72.5 kV vacuum bottle*. Number 1876. Darmstadt, 2012.
4. Ranke, Sandra. *Elaboration of a testing procedure to systematically analyze the restriking behavior of high voltage vacuum bottles*. Number 1877. Darmstadt, 2012.
5. Holbein, Markus. *Design and construction of a 200 kV switch for precise switching at the voltage zero crossing*. Darmstadt, 2012.
6. Kaczmarek, David. *Development of a measuring software in Matlab and LabVIEW to analyze test series of a 72.5 kV vacuum bottle*. Number 1844. Darmstadt, 2013.
7. Rodriguez, Julian. *Development of an electrical simulation model of a 72.5 kV vacuum bottle in order to compensate the influence of the test circuit and to optimize the design*. Number 1904. Darmstadt, 2013.
8. Diehl, Lukas. *Determination of the correlation between the restriking behavior of a high voltage vacuum circuit breaker and its kinematic drive chain*. Number 1910. Darmstadt, 2013.
9. Holbein, Markus. *Start-up of a synthetic test circuit to investigate the dielectric strength of a 72.5 kV vacuum interrupter when switching capacitive loads*. Number 1905. Darmstadt, 2013.
10. Ullrich, Alexandra. *Investigation into the effect of magnetic fields on the dielectric strength and the emission currents of electrode arrangements in vacuum*. Number 1918. Darmstadt, 2013.
11. Janssen, Henning. *Design of an electromagnet at high voltage potential to influence the trajectory of electrons in vacuum tubes*. Number 1919. Darmstadt, 2013.
12. Surges, Benjamin. *Investigation of the dielectric strength of medium voltage vacuum interrupters when switching capacitive loads*. Number 1937. Darmstadt, 2014.



Curriculum Vitae

Benjamin Baum

born on 21.04.1985 in Wetzlar, Germany

Work Experience

since 04/2017	Innovation Engineer KEMA Laboratories DNV GL, Arnhem, The Netherlands
11/2015 - 04/2016	Guest Researcher at State Key Laboratory of Electrical Insulation and Power Equipment Xi'an Jiaotong University, China
05/2011 - 10/2016	Scientific Assistant at High Voltage Laboratories Technische Universität Darmstadt, Germany
05/2009 - 09/2009	Industry Internship SEW-Eurodrive GmbH, Bruchsal, Germany
02/2006 - 04/2006	Industry Internship Bosch Thermotechnik GmbH, Lollar, Germany

Education

08/2008 - 03/2009	Study of Electrical Power Engineering Norwegian University of Science and Technology, Norway
10/2005 - 04/2011	Study of Electrical Power Engineering Technische Universität Darmstadt, Germany Degree: Diplom
10/2004 - 09/2005	Study of Physics Technische Universität Darmstadt, Germany
06/2004	University Entry Qualifications Werner-von-Siemens Schule, Garbenheim, Germany Degree: Abitur